LATERAL MODULATION, DIVISIVE INHIBITION, AND NEURAL MECHANISM OF PERCEPTUAL FILLING-IN

Yih-Shiuan Lin

aus Taipei, Taiwan

2022

Gutachter (Betreuer): Prof. Dr. Mark W. Greenlee

Gutachterin: Prof. Dr. Angelika Lingnau

PREFACE

The aim of this thesis, "Lateral modulation in center-surround sinusoidal gratings: divisive inhibition and neural mechanism of perceptual filling-in", is to investigate the underlying mechanisms of lateral modulation in visual phenomena such as perceptual filling-in by means of psychophysics, computational modeling, and neuroimaging techniques. The thesis is composed of five chapters: Chapter 1 contains the General Introduction with an in-depth literature review, Chapter 2 to 4 incorporate the three main studies and Chapter 5 captures Concluding Remarks that contains summaries of the above-mentioned studies as well as a general discussion.

Two articles based on the first two studies have been published in Journal of Vision (impact factor > 1.5) on September 4th 2020 and February 22nd 2022, whereas the manuscript of the third study has been submitted to Scientific Reports (impact factor > 1.5) and was accepted on September 15th, 2022. Chapter 2 to 4 include the pre-print versions of the first two published studies and the accepted version of the third study. The manuscripts of all studies have been formatted according to the APA (American Psychological Association) 7th Edition guidelines. Figure, Table, and Equation numbers have been listed in ascending order. All references are merged into one bibliography following Chapter 5. Supplementary files and figures have been merged and ordered accordingly in the Appendix at the end of the thesis. The raw data and model results are provided as supplementary materials in Excel format and can be accessed online (Study 1: https://doi.org/10.1167/jov.20.9.5; Study 2: https://doi.org/10.1167/jov.22.2.13) are not included in the current thesis. No further changes have been made to the text of the published articles.

All studies mentioned in the thesis were in collaboration with Professor Chien-Chung Chen, Department of Psychology, National Taiwan University, Taipei, Taiwan. The author contributions are listed on Page 12 to 14.

ACKNOWLEDGEMENT

The past five and a half years of doing a PhD is by far the longest journey I have set up my mind to experience. I have learned a great deal that has brought me closer and closer to my goal of becoming a competent visual neuroscientist. Finishing my PhD does not signify an end, rather a beginning of a further academic pursuit. Along the way, I have received generous and unconditional supports from many. These people are the key reasons how I have come so far. I would like to express my most sincere gratitude to them here. However, going through all their names would take another volume of thesis. I could therefore only name a few who cross path to my PhD work most closely.

First of all, I would like to thank my supervisor, Prof. Mark Greenlee, for helping me with every step of my study over the years. Be it developing research proposals, applying for fundings, accommodating in Regensburg, proceeding with my projects, revising papers, and many more, he is always there to provide help, supervision, and insight. I am also grateful for him supporting my research trips back in Taiwan, especially during the peak of the COVID-19 pandemic, so I could continue with my project without hindrance. Mark, thank you for giving me the freedom, flexibility, and trust to carry out my research in the best suited manners. You have been the best role model of an accomplished scientist.

The next person to thank is Prof. Chien-Chung Chen in National Taiwan University, who plays a major role in my PhD project. Without the constant consulting with Prof. Chen about the data collection, analyses, and statistics in my research, I believe it would have taken me way longer to achieve the level of expertise I have today. I am forever grateful for his support, encouragement, and mentoring that started in my master's years. During his last sabbatical stay in Regensburg, we spend numerous hours improving my PhD work and coming up with future

5

research ideas. I am really looking forward to working on our future research projects together in the following years.

I would also like to mention my gratitude towards Prof. Lothar Spillmann, who inspired this PhD project during his stay in Taipei back in 2016. Through many fruitful exchanges, we came up with an exciting proposal that became the backbone of my PhD thesis. I will always remember how excited Lothar looked when he was talking about the fascinating nature of filling-in. I am sure Lothar will be glad that I inherited his passion for human vision and that I intend to carry on his legacy of filling-in research.

I would also like to mention my lovely colleagues in Mark's lab, including Dr. Maka Malania, my secondary supervisor. Without their support in research and in life, my stay in Regensburg would not have been so easy. I am also grateful for Prof. Angelika Lingnau accepting to evaluate my thesis. I have learned a lot from Prof. Lingnau's and Prof. Jens Schwarzbach's groups during the past years through the courses and exchanges with the lab members. I'm forever thankful for knowing the fellow graduate students in these labs. Some of them have become my life-long friends and I cannot wait to continue my journey with them as peers inside or outside of academia.

This PhD journey is not short of challenges, both academic and personal. I am extremely lucky to have lived and worked in an environment in which mental health problems are not seen

as taboo and people are there for you to lend you a helping hand. During my darkest hours, my supervisors, colleagues, friends, and family have built up the most secure support system that kept me afloat and going. Having experienced the mental health crisis in academia at first hand, I found my way to the WIN center (Zentrum zur Förderung des wissenschaftlichen Nachwuchses) for early career researchers in the University of Regensburg, where my ideas of mental health project were welcomed with open arms. I thank Dr. Angela Weil-Jung and her team for the extraordinary support. I am proud to say that our work in WIN center has been fruitful and gained the potential to bring long-term changes.

Last but not least, a big thank you goes to all my friends back in Taiwan and here in Germany. They never gave up on me whenever I felt like I am losing ground. Thank you for always seeing the best in me when my sight is blinded by my own shadow. Thank you for reminding me that there are more important things in life than work. Thank you for laughing and crying with me and bringing me joy in the cloudiest days. And of course, Mom, Dad, and Bro, thank you for being my biggest and warmest supporters at all times. You let me realize no matter what happens, your love for me would never change, just like my love for you would never falter. You are my haven whenever I feel lost. 最愛你們了。

Sincerely yours,

Yih-Shiuan Lin 林易萱

TABLE OF CONTENTS

ABSTRACT

Lateral modulation refers to the phenomenon that the percept of a test stimulus can be modified by a surrounding pattern. Lateral modulation is ubiquitous throughout the visual system. Thus, understanding the underlying mechanism of lateral modulation can not only unveil the fundamental properties of visual system but also have the potential to increase our understanding of how eye diseases such as macular degeneration that leads to scotoma impact on visual perception. The purpose of this project is to study lateral modulation by investigating visual phenomena such as perceptual filling-in and orientation-specific lateral inhibition by means of psychophysics, computational modeling, and neuroimaging techniques. To address the missing pieces of this puzzling phenomenon, this project defines three goals: 1) To study multiple lateral modulation effects such as center-surround interaction and perceptual filling-in with new paradigms; 2) to analyze the observed lateral modulation effects with a computational model; and 3) to understand the neural mechanism underlying perceptual filling-in.

Three studies have been conducted. Within the first two studies, we established an orientation adaption paradigm in which center-surround sinusoidal gratings are used as adapters to estimate the amount of tilt-aftereffect (TAE) induced onto the percept of the subsequent target. In Study 1, we selectively adapted the center, the surround, and both the center and surround regions and measured the tilt-aftereffect on the subsequently presented target. The TAE was the strongest in the center-only condition, intermediate in the center plus surround condition, and the weakest in the surround only condition. The difference between the center and both center and surround conditions indicated a lateral inhibition effect from the surround. Perceptual filling-in arose in the surround-only condition thus allowed us to investigate the filling-in effect. The TAE occurred even when no physical stimulus was presented at the target location during adaptation,

and the TAE was more pronounced when filling-in was reported. In Study 2, we independently

manipulated the adapter center and surround orientations and measured the TAE. We discovered

that the lateral inhibition we found in Study 1 was orientation specific. We developed a divisive

inhibition model that could explain both the adaptation effect and the lateral modulation effects in

the empirical data of Study 1 and 2. In the third study, we implemented functional magnetic

resonance imaging to study lateral modulation by presenting radial sinusoidal gratings that

activates either the center, the surround, or both the center and surround regions in both left and

right visual fields. When the surround pattern was added to the central pattern, the blood-oxygen

level-dependent signal decreased in V1 to V3 regions, suggesting a lateral inhibition effect. The

multivariate pattern analysis revealed that trained linear classifiers could differentiate between

filling-in and non-filling-in trials, indicating that the neural activation pattern was different

between the two percepts although the stimuli were the same.

The current PhD project demonstrated effective paradigms that provided new evidence in

lateral modulation in human vision. Our computational model captured both the adaptation and

lateral modulation aspects in the data. The empirical findings and modeling results provide new

evidence in the neural mechanism of perceptual filling-in. These paradigms and model have the

potential to improve the understanding of how the brain adapts to eye diseases that could

potentially lead to better detection techniques and rehabilitation programs.

CONTRIBUTIONS

Study 1	Lateral Modulation of Orientation Perception in Center-Surround Sinusoidal Stimuli: Divisive Inhibition in Perceptual Filling-In
Authors	Yih-Shiuan Lin[1], Chien-Chung Chen[2,3], and Mark W. Greenlee[1*]
Author Contributions	Y.S.L. designed and conducted the experiment, analyzed, and interpreted the data, wrote, and revised the article. C.C.C. and M.W.G. provided materials, designed the experiment, interpreted the data, proofread, and revised the article.
Study supervision	MWG
Acknowledgement	Y.S.L. was supported by the German Academic Exchange Service (DAAD, Bonn Germany) in the form of a research grant for doctoral candidates. C.C.C. was supported by 106-2410-H-002-074-MY2. M.W.G. was supported by DFG grant number GR988 25-1. We would like to express our gratitude to Professor Joshua A. Solomon, who was the editor of the current paper, for providing extremely insightful and helpful editorial recommendations regarding data analysis as well as the model architecture.
Commercial relationships/conflict of interests	None
Declaration of Helsinki	Yes
Clinical trial	No
Journal (Impact Factor)	Journal of Vision (2021 Impact Factor: 2.004)
Publication status	Submitted December 13, 2019; Accepted July 30, 2020; Published September 4, 2020

Study 2	The role of lateral modulation in orientation-specific adaptation effect
Authors	Yih-Shiuan Lin[1], Chien-Chung Chen[2,3], and Mark W. Greenlee[1*]
Author Contributions	Y.S.L. designed and conducted the experiment, analyzed, and interpreted the data, wrote, and revised the article. C.C.C. and M.W.G. provided materials, designed the experiment, interpreted the data, proofread, and revised the article.
Study supervision	M.W.G.
Acknowledgement	Y.S.L. was supported by the German Academic Exchange Service (DAAD, Bonn Germany) and MOST (TOP Grants, Taiwan) in the form of a research grant for doctoral candidates. C.C.C. was supported by MOST(Taiwan) 109-603 2410-H-002-086-MY4. M.W.G. was supported by DFG grant number GR988-27-1.
Commercial relationships/conflict of interests	None
Declaration of Helsinki	Yes
Clinical trial	No
Journal (Impact Factor)	Journal of Vision (2021 Impact Factor: 2.004)
Publication status	Submitted October 18, 2021; Accepted January 27, 2022; Published February 22, 2022.

Study 3	Neural correlates of lateral modulation and perceptual filling-in in center-surround radial sinusoidal gratings: an fMRI study
Authors	Yih-Shiuan Lin[1], Chien-Chung Chen[2,3], and Mark W. Greenlee[1*]
Author Contributions	Y.S.L. designed and conducted the experiment, analyzed, and interpreted the data, wrote, and revised the article. C.C.C. and

	M.W.G. provided materials, designed the experiment, interpreted the data, proofread, and revised the article.
Study supervision	M.W.G.
Acknowledgement	Y.S.L. was supported by the DAAD (German Academic Exchange Service, Bonn Germany) and the MOST (TOP Grants, Taiwan) in the form of doctoral candidate research grant. C.C.C. was supported by MOST(Taiwan) 109- 603 2410-H-002-086-MY4 and Hans Vielberth Foundation of the University of Regensburg. M.W.G. was supported by DFG grant number GR988-27-1.
Commercial relationships/conflict of interests	None
Declaration of Helsinki	Yes
Clinical trial	No
Journal (Impact Factor)	Scientific Reports (2-year impact factor (2021): 4.996; 5-year impact factor (2021): 5.516)
Publication status	Submitted May 18, 2022; Accepted September 15, 2022. In press.

[1]Institute of Experimental Psychology, University of Regensburg, Regensburg, Germany

[2]Department of Psychology, National Taiwan University, Taipei, Taiwan

[3]Neurobiology and Cognitive Science Center, National Taiwan University, Taipei, Taiwan

*Corresponding author: Mark W. Greenlee; postal address: Universität Regensburg, Universitätsstraße 31, 93053 Regensburg, Germany; Tel: +49 (0)941 943 3281; E-mail: mark.greenlee@ur.de

ABBREVIATIONS

2AFC	Two-alternative forced-choice
CRF	Classical receptive field
CW	Clockwise
F	F value
FA	Flip angle
fMRI	Functional magnetic resonance imaging
FOV	Field-of-view
GLM	General linear model
Hz	Hertz
ISI	Inter-stimulus-interval
LGN	Lateral geniculate nucleus
LIBSVM	Library for support vector machines
LOC	Lateral occipital cortex
mm	Millimeter
MPRAGE	Magnetization Prepared - rapid Gradient Echo
ms	Millisecond
MSE	Mean standard error
MVPA	Multivariate pattern analysis
p	P-value
PF	Psychometric function
rs	Pearson's correlation coefficient
R^2	R squared (goodness of fit)
RF	Receptive field
RMSE	Root-mean-square error
ROI	Region of interest
s	Second
SE	Standard error
SVM	Support vector machine
t	T-value
T1	Longitudinal relaxation time
T2	Transverse relaxation time
TAE	Tilt-aftereffect
TE	Echo time
TR	Repetition time
ρ	Pearson's correlation coefficient
Ψ	Psi method

1. CHAPTER 1: INTRODUCTION

1.1 Research Background

Humans are visual creatures. In other words, we rely heavily on our visual system. Its function is to analyze and understand the images entering our eyes to help us navigate the world around us. To accomplish this, the visual system must process the inputs and recognize individual elements within the visual field. Doing so requires a hierarchical processing starting from the retina, subcortical regions such as the lateral geniculate nucleus, primary visual cortex, to other higher visual areas. In the natural world, a visual element rarely appears on its own. And it is well-known that the percept of one element can be drastically altered by the presence of nearby elements. Many visual phenomena such as tilt illusion (Figure 1.1A), in which the perceived orientation of the center is tilted away from the surround orientation (Blakemore et al., 1970; Gibson, 1937a), Ebbinghaus illusion (Figure 1.1B), where the perceived size of the center disk depends on the size of the surround inducers (Ebbinghaus, 1902; Roberts et al., 2005; Wundt, 1898), and visual crowding (Figure 1.1C), in which the center target detection or recognition is deteriorated in the presence of surround flankers (Andriessen & Bouma, 1976; Levi, 2008), directly result from the interaction between the center and its surround elements. Perceptual filling-in (Figure 1.1D), in which the visual system compensates the missing information within the center by interpolating information from the surround, is yet another example of this interaction process (Pessoa & De Weerd, 2003). This center-surround interaction is often termed lateral modulation. Lateral modulation reveals that neurons responding to different visual field regions interact with each other to determine the final percept. Unraveling how this long-range interaction is achieved remains one of the fundamental challenges for visual neuroscientists.

Figure 1.1

Visual phenomena resulting from lateral modulation
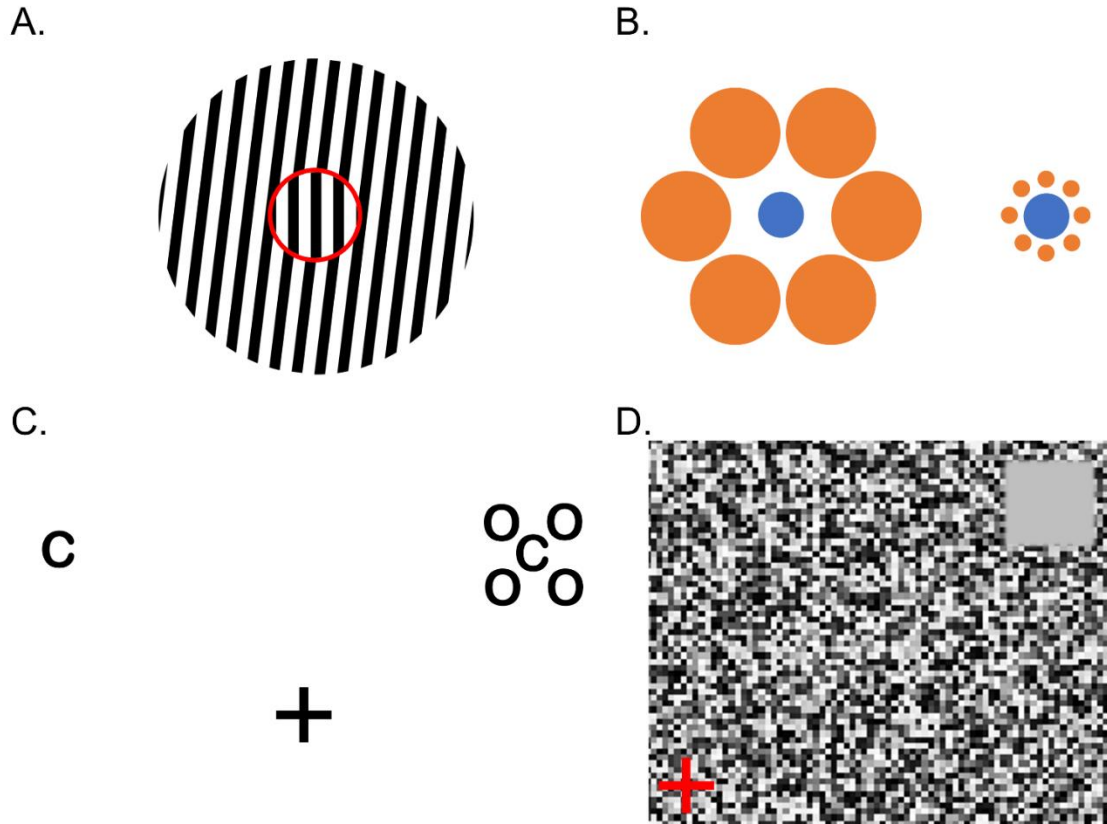
Note. This figure demonstrates four different kinds of visual phenomena that are the consequences of the interaction between center and surround visual elements. **A.** Tilt illusion. The center grating circled by the contour is physically vertical but perceived as tilted to the counterclockwise direction due to the presents of the clockwise surround. **B.** Ebbinghuas illusion. The two blue disks in the center on the left and right are identical. However, the left center disk is perceived as smaller than the right one when we place larger surround disks on the left and smaller ones on the right. **C.** Visual crowding (adapted from the stimuli used in Malania, Pawellek, Plank and Greenlee (2020)). When we fixate the black fixation cross below, it is easy to detect the opening of the Landolt C on the left side, but more difficult on the right side due to the crowding effect from the four surrounding flankers. **D.** Perceptual filling-in. With steady prolonged fixation on the lower left red cross, the gray square, an artificial scotoma, on the upper right corner would disappear and be replaced by the background noise texture. The effect is enhanced with flickering dynamic background.

Over the past decades, vision scientists have put their research interests in revealing the underlying mechanisms of lateral modulation with numerous paradigms and methodologies. Evidence has shown that the lateral modulation effect can be either excitatory or inhibitory depending on the image features such as luminance contrast and orientation. Many have studied the lateral modulation mechanisms with orientation gratings with varied contrast and orientation. However, it is still unclear how the central orientation percept can be modified as a function of the surround orientation, especially during visual adaptation. Additionally, whether it is lateral excitation or inhibition from the surround that contributes to perceptual filling-in is still under debate.

In this thesis, we address some key issues of lateral modulation that remain unsolved with psychophysics, computational modeling, and neuroimaging approaches. Our main objective is to first pinpoint how lateral excitation and inhibition are involved to determine the percept given our experimental manipulations of stimuli orientation. We can then further investigate the underlying mechanism of the observed lateral modulation effects with the help of a divisive inhibition model and fMRI experiment. In the following sections of Chapter 1, I first review the literature of three major topics: lateral modulation, divisive inhibition, and perceptual filling-in. We evaluate the most relevant evidence and research paradigms to emphasize the remaining unknowns in the field and the potential approaches to address these issues. Following the literature review, we describe the research questions that remain pending and discuss how we intend to answer them with the subsequent studies. Chapter 2 to 4 present these three studies. I then summarize the empirical findings and model fitting results in Chapter 5. I further examine the extend of which our findings address the research questions and which issues remain for future investigations.

1.2 Literature Review

1.2.1 Lateral modulation in vision

The influence of the surround pattern on the visual processing of a central stimulus has been the subject of many investigations (Gilbert & Wiesel, 1990; Pessoa & De Weerd, 2003). Such lateral modulation is observed in numerous visual phenomena such as visual crowding, tilt illusion, and perceptual filling-in (Clifford, 2014; Komatsu, 2006; Schwartz et al., 2007, 2009; Solomon et al., 2004; Spillmann & Werner, 1996). Nevertheless, the underlying neural mechanisms remain elusive.

Evidence of lateral modulation can be found from early to late stages along the visual system hierarchy. For instance, horizontal cells (HCs) in the retina provide the first lateral projection in the retina (Baylor et al., 1971). Each HC receives synaptic signals from photoreceptors located centrally and transmits feedback signals back to those photoreceptors. HCs also collect signals from a larger group of photoreceptors surrounding the center photoreceptors. The activated surround photoreceptors send excitatory signals to the HCs and the HCs send inhibitory feedback to the center photoreceptors, mediating the response of the nearby bipolar cells and creating the typical center-surround/excitatory-inhibitory receptive fields (RFs) of the ganglion cells. This circular-symmetric shape of RFs can also be found in the neurons of the lateral geniculate nucleus (LGN). In the primary visual cortex, RFs become selective to more visual properties such as orientation, motion direction, luminance contrast, and even stimulus size (Hubel & Wiesel, 1962).

At the cortical level, lateral modulation occurs beyond the range of the classical receptive field (CRF). The neuronal response can even be modulated by a stimulus placed outside of its neuron's CRF. Stimuli presented in such nonclassical, or long-range, surround region alone do

not activate the neuron. However, such a long-range surround stimulus can nevertheless suppress or facilitate the CRF response when the recorded neuron is activated by a central stimulus, suggesting a long-range lateral modulation effect (Cavanaugh et al., 2002a, 2002b; C.-C. Chen et al., 2001; Maffei & Fiorentini, 1976). Many studies have studied the orientation and spatial frequency tuning of the center-surround modulation and found that it has similar feature selection as those of the CRF, suggesting that the lateral modulation is feature specific (Blakemore & Tobin, 1972; Cavanaugh et al., 2002b; C.-C. Chen et al., 2001; DeAngelis et al., 1994; Gilbert & Wiesel, 1990; Ozeki et al., 2004; Sillito et al., 1995). Some groups presented an expanding patch or annulus beyond the CRF and discovered two surround areas (near and far surrounds) that affect the CRF response differently depending on the contrast used (Angelucci & Bressloff, 2006; Ichida et al., 2007; Sengpiel et al., 1997; Shushruth et al., 2009).

Another common strategy to study lateral modulation is using the lateral masking paradigm, in which a Gabor target, or a sinusoidal grating windowed by with a two-dimensional Gaussian function, is presented with Gabor flankers (Polat & Sagi, 1993; Zenger & Sagi, 1996). Psychophysics studies reported that when the target and flankers were collinear and of parallel orientation, the target detection threshold was reduced, suggesting a facilitation effect, whereas when the flanker and target were orthogonal to each other, no facilitation was found. Solomon and colleagues (1999) examined such collinear facilitation flanker effect by using flankers of the same or opposite-sign contrast and discovered that the opposite-sign flankers created weaker facilitation than the same-sign flankers. Chen and Tyler (2001, 2002) employed a dual-mask paradigm to investigate the flanker effect by adding a pedestal of various contrast levels occupying the same spatial location as the target. Without the flankers, the target threshold first decreased (facilitation) then increased (suppression) as the pedestal contrast increased. The collinear flankers produced facilitation at low pedestal contrast and suppression at high pedestal

21

contrast. The orthogonal flankers did not produce the facilitation and only contributed

suppression at high pedestal contrast. The authors concluded that two flanker modulation effects

were involved: one narrowly tuned to and the other broadly tuned to flanker orientation. A

contrast gain control model was used to explain their data, suggesting that the observed lateral

modulation was subject to a divisive inhibition process. In a single cell recording study, Chen and

colleagues (2001) measured the contrast response functions of neurons in cat visual cortex and

reported various types of flanker effects in different types of cells depending on the stimulus

contrast and orientation in agreement with psychophysics studies in humans (C.-C. Chen &

Tyler, 2001, 2002). In a later fMRI experiment, Chen (2014) explored the neural correlates

corresponding to these two inhibitory components.

The tilt illusion in combination with its temporal counterpart, tilt-aftereffect (TAE), are

two visual phenomena frequently studied in human vision that are related to lateral modulation

effect (Clifford, 2014). The tilt illusion, first reported by Gibson (1937a), describes how an

oriented pattern surround could affect the perceived orientation of a central pattern. When two

orientations are close to each other the central orientation is perceived tilted away from the

surround. This effect is often termed repulsion. In contrast, when the two orientations are farther

away, the perceived central orientation is closer to the surround. This effect is instead termed

attraction or assimilation. Solomon and colleagues (2004) presented a vertical Gabor target

alongside with two Gabor flankers of various orientations in the parafoveal region and examined

the induced tilt illusion perceived for the target. The results were described in terms of the bias

and sensitivity estimated from the target orientation response psychometric function. They

reported a small assimilation effect with flankers of small orientation deviations from the target

(within 5°) and a large repulsion effect with the oblique flankers (22.5° or 45° way from the

target), indicating an orientation-specific flanker effect on the target bias. In addition, the

presence of flankers reduced the target sensitivity. In general, the flanker orientation that induced most bias also reduced target sensitivity the most except for the vertical and horizontal flankers. The vertical and horizontal flankers induced little bias but decreased a fair amount of target sensitivity. Solomon and Morgan (2006) presented targets and flankers to their observers' foveal area and reported similar results. Different from the parafovea, they found little to no target sensitivity loss when the target and flankers were parallel to each other. The authors therefore suggested that the lateral modulation effect in the tilt illusion in the fovea and parafovea might involve different processes.

The TAE, on the other hand, describes the phenomenon that when we first adapt the visual system to one orientation, a subsequently presented stimulus is seen tilted away from the adapting orientation (Gibson, 1937b; Gibson & Radner, 1937). Researchers have reported interesting results when tilt-illusion and TAE are combined. For example, Magnussen and Kurtenbach (1980) discovered that when a second orientation pattern was added to the first adapting pattern, the TAE decreased, indicating a lateral inhibition effect between the two adapting patterns. A similar effect was reported by Kurtenbach and Magnussen (1981). Later, Greenlee and Magnussen (Greenlee & Magnussen, 1987, 1988) presented two alternating orientation patterns with varied spatial frequencies and orientations during the adaptation period. When the two adapting patterns were of the same spatial frequency or orientation, the contrast threshold of the following contrast increased, suggesting an inhibitory effect. On the contrary, as the two adapting patterns became dissimilar to each other, the target threshold decreased even below the baseline condition where one adapter was interleaved with a blank (zero contrast) screen, suggesting the existence of disinhibition. The motion aftereffect (MAE), an adaptation effect closely related to TAE, describes that a drifting adapting grating could make a subsequently viewed static grating appear moving in the opposite direction (Anstis et al., 1998;

Mather & Harris, 1998). Falkenberg and Bex (2007) investigated the lateral modulation effect in

MAE by adding surround adapting pattern that varied in its orientation and drift direction, spatial

frequency, and temporal frequency. They discovered a lateral inhibition effect that reduced the

MAE when a drifting surround was added. The lateral inhibition effect was strongest when the

adapter surround shared the same features of the adapter center, suggesting an orientation-

specific lateral modulation effect.

Others have presented sinusoidal gratings in the center and surround regions of the visual

field and measured the center target contrast detection and discrimination thresholds. For

example, Cannon and Fullenkamp (1991) reported suppressive surround modulation effect on the

target perceived contrast when they presented a high-contrast annular surround pattern along with

the target. The surround suppression increased as the width of the surround annulus increased and

decreased as the space between the center and surround increased. The center and surround

gratings in Cannon and Fullenkamp (1991) were always of the same orientation, i.e. iso-oriented.

In a similar contrast perception paradigm, Yu and colleagues (2001) manipulated the surround

contrast and orientation and measured the surround effect on the center target perceived contrast.

They found that, at all surround contrasts, iso-oriented surround suppressed the perceived target

contrast. Interestingly, the cross-orientation surround, a grating with an orientation orthogonal to

that of the target, increased the target perceived contrast, especially at higher surround contrast,

suggesting instead a facilitative surround effect. The iso-orientation suppression sustained and

decreased slowly as the center-surround gap increased, whereas the cross-orientation facilitation

decreased more rapidly with increased gap. Meese et al. (2007) presented annular and

superimposed masks with varied sizes to study how different cross-oriented patterns affect the

center target contrast detection and discrimination thresholds. At low spatial frequency, they

found evidence of cross-orientation facilitation in the annular mask, at intermediate mask contrast

and cross-orientation suppression in the superimposed mask, as mask contrast increased. At

higher spatial frequency, both mask types induced surround facilitation at intermediate mask

contrast, indicating that the cross-orientation lateral effects depended highly on the stimulus

contrast and spatial frequency. In a later study, Meese and colleagues (2009) compared the cross-

orientation effects in the fovea and periphery with these two mask types. In the periphery, either

mask induced suppressive effect as mask contrast increased, with the parallel annular mask

creating a saturation effect. In the fovea, the overall target threshold decreased compared to the

periphery, the cross-oriented and parallel annular masks induced little suppression, whereas the

cross-oriented superimposed mask showed a similar pattern of results in the fovea and periphery.

In a fMRI study, Brouwer and Heeger (2011) showed evidence of such a cross-orientation

suppression in human V1. They presented a vertical target grating and a superimposed horizontal

mask grating with various luminance contrast levels and measured the BOLD (blood-oxygen

level-dependent) activation during the stimulus presentation. They identified orientation channels

corresponding to subpopulations of neurons with a forward model (Brouwer & Heeger, 2009)

and reported that the channels tuned to the target orientation showed decreased activation as

mask contrast increased. In contrast the channels tuning to the mask orientation exhibited a

reduction in activation as target contrast increased. Along with the tilt illusion and orientation

adaptation, these studies demonstrate the power of manipulating the orientations of the center and

surround gratings and how this cross-orientation paradigm could provide insights into how the

center and surround regions interact with each other at different eccentricity and center-surround

configurations.

Perceptual filling-in is another visual phenomenon that closely related to lateral

modulation. Filling-in, or perceptual completion, is the perceptual tendency of observers to

perceive an illusionary visual pattern in a central intermittent blank region that matches the

surround texture. Such a completion process suggests the existence of an interaction between the center and the surround regions in a way that the visual system interpolates the information provided by the surround pattern, filling in the missing information. Filling-in can be observed in the area of the blind spot (Komatsu et al., 2000; Ramachandran, 1992). The blind spot is the part of the visual field that corresponds to the region (optic disk) on the retina lacking photoreceptors where the optic nerve exits the eye. Even though there are no photoreceptors in the optic disk on the retina, we rarely experience the percept of a blank spot in daily life even with monocular viewing. Instead, we perceive a continuous and uninterrupted visual world. Matsumoto and Komatsu (2005) presented a bar stimulus in the blind spot of macaque monkeys and human participants with one end of the bar fixed at a location outside of the blind spot and the other end changing position. When the changing end of the bar exceeded the blind spot, human participants reported that perceptual completion occurred, and a complete bar was seen crossing through the blind spot. Similarly, in a human study, Spillmann and colleagues (2006) presented frames of color and texture of different width around the contour of the blind spot and determined that a frame width as narrow as 0.05° visual angle was enough for color and 0.2° for texture to be filled-in within the blind spot.

Filling-in can also be induced in the regions outside the blind spot in healthy observers. Ramachandran and Gregory (1991) found that a blank region absent of stimuli, i.e. an artificial scotoma, in the periphery surrounded by a dynamic random dot pattern would fade away and be perceived as being replaced by the surrounding pattern after prolonged steady fixation. Such artificial scotoma paradigm is an ideal tool to study perceptual filling since it has a definite and measurable onset time, easily controllable size and location, and can be reproduced across observers (De Weerd et al., 1995, 1998; Morgan et al., 2007; Spillmann & Kurtenbach, 1992). Evidence showing that filling-in induced in one eye can be transferred to the other eye suggesting

that such filling-in has a cortical origin (Paradiso & Nakayama, 1991). Such slow filling-in can be sped up by briefly adapting the scotoma contour (Anstis, 2013; Anstis & Greenlee, 2014), indicating that the stimulus border plays an crucial role during the filling-in process.

Filling-in can also occur in the retinal scotoma, the visual field area where vision is lost due to damages of the visual pathways in patients suffering from macular degeneration. Such filling-in could cause the patients to become unaware of or to underestimate the scotoma size (Crossland & Rubin, 2007; Pessoa & De Weerd, 2003; Zur & Ullman, 2003). Zur and Ullman (2003) measured the filling-in in central scotoma caused by age-related macular degeneration. Such filling-in is associated with central vision loss resulting from macular atrophy and it can lead to cortical reorganization to some extent. A computational model that simulated cortical reorganization was proposed to explain the filling-in of the retinal scotoma (McManus et al., 2008). In the paper of Zur and Ullman (2003), the authors reported that the perceptual completion happening in the retinal scotoma had a larger scale than that recorded in the artificial scotoma in the periphery. In addition, the retinal scotoma filling-in happened instantaneously, contrary to the artificial scotoma filling-in which required prolonged fixation time to occur. These findings suggest that these two different types of perceptual filling-in might involve very different neural mechanisms.

Filling-in can also be induced instantly in some visual illusions such as the Craik–O'Brien–Cornsweet illusion (Cornsweet, 1970), where the perceived lightness of a gray region is enhanced or reduced by the edges of a central border, resulting in a "spreading out" of the border luminance contrast. Similarly, in the watercolor illusion effect, the color of the border on one side can appear to spread out throughout an uniform region until it reaches the border on the opposite side of the object (Pinna et al., 2001, 2003). The neon color spreading illusion describes the

situation when the illusory color appears to spread out but to be contained within an illusory

border of a disk (Bressan et al., 1997). Another visual illusion related to filling-in is Kanizsa

triangle, in which inward facing Pac-man inducers can create an illusory surface provided with

the appropriate configuration (S. Chen et al., 2018; Grossberg & Mingolla, 1985; Kanizsa, 1979,

1987). These fast filling-in effects demonstrate again the importance of the border during the

process.

1.2.2 Divisive inhibition and lateral modulation

Divisive inhibition, also termed contrast gain control or normalization, describes the

nonlinear neural response as an excitation component computed by a linear operator being raised

by a power then divided by an inhibitory component plus a normalizing constant (Carandini &

Heeger, 2012; Foley, 1994; Heeger, 1992). Such a normalization process has been proposed to

explain the neural responses in the retina (Boynton & Whitten, 1970), LGN (Bonin et al., 2005),

and the primary visual cortex (Albrecht & Geisler, 1991; Heeger, 1991, 1992). Many authors

have proposed divisive inhibition models to explain visual phenomena such as pattern masking

(Brouwer & Heeger, 2011; Foley, 1994; Meese & Holmes, 2002; Watson & Solomon, 1997), tilt

illusion (Solomon et al., 2004), lateral masking (C.-C. Chen et al., 2001; C.-C. Chen & Tyler,

2002), and adaptation effect (Foley & Chen, 1997; Ross & Speed, 1991; Wilson & Humanski,

1993).

To explain the tilt illusion, Blakemore et al. (1970) proposed a pooling model. In this

model, the neural response of one orientation detector in the visual cortex of a hypercolumn is

determined by an excitation that is narrowly tuned to a specific orientation range and a broad-

band inhibition. The final orientation percept of an oriented stimulus depends on the population

response of all orientation detectors, with the detector tuned to the stimulus orientation being

optimally excited and those tuning to other orientations inhibited. When two closely placed

oriented gratings have similar orientations, the two response distributions of detector neurons

from two hypercolumns would inhibit each other and bias each population response away from

their original orientation percept. The inhibitory response of one orientation detector could

decrease the response of another detector when the two orientations were close to each other,

therefore pushing the actual perceived orientation away from its physical orientation, resulting in

the repulsion effect in the tilt illusion. However, such a pooling model failed to explain the data

in Solomon and colleagues (2004), where the author reported a large repulsion effect with

distractors of target deviations and a small assimilation effect with distractors of small deviations.

The pooling model would instead predict that the assimilation effect to be larger than the

repulsion effect. Solomon et al. (2004) proposed an alternative divisive inhibition model in which

sensitivity modulation was considered. The author further processed an opponent process in

which each neuron tuned to an orientation is paired to another neuron tuned to the opposite

orientation with respect to a reference (e.g., vertical orientation). The orientation percept of the

system is determined by the neuron pair of the greatest response difference. When this opponent

process was considered in the model, their model could also explain the loss of sensitivity that

was related to visual crowding in the presence of flankers. Such a model could better capture the

tilt illusion data in the parafovea (Solomon et al., 2004) and the tilt illusion data in the fovea

(Solomon & Morgan, 2006). Divisive inhibition has also been implemented to explain the lateral

modulation effect in the lateral masking paradigm (Snowden & Hammett, 1998; Solomon et al.,

1999). In a single cell recording study, Chen and colleagues (2001) measured the contrast

response functions of neurons in cat visual cortex. They presented a target Gabor inside the

neuron CRF and flankers outside of the CRF. The authors reported four types of flanker effects in

different types of cells depending on the stimuli contrast and orientation: 1) a flanker effect that

increased the response to a low contrast target but suppressed the response to a high contrast target, 2) an expansive facilitative flanker effect that increased the target response when the target was of high contrast without suppression at low target contrast, 3) an expansive suppressive flanker effect at higher target contrast and no facilitation at low target contrast, and 4), the exact opposite of the first type, a flanker effect that increased high contrast target response and decreased low contrast target response. Such results demonstrated the multifaceted nature of the long-range modulation effect that depends on the stimulus features. In a psychophysics set up, Chen and Tyler (2001) presented two flankers above and below the target and pedestal and measured the target discrimination threshold under different pedestal contrast. Without the flankers, the target contrast first decreased (facilitation) then increased (suppression) as the pedestal contrast increased, demonstrating the typical dipper TvC (threshold vs. contrast) function. With the flankers, the target threshold decreased at low pedestal contrast, suggesting a facilitative flanker effect, whereas the target threshold increased at higher pedestal contrast, indicating a suppressive effect. Later in 2002, Chen and Tyler manipulated the orientation of the flanker and found that the facilitative flanker effect at low pedestal contrast was narrowly tuned to the flanker orientation and decreased as the flanker orientation deviated from the target and pedestal orientation. On the other hand, the pedestal masking enhancement effect at higher pedestal contrast remained mostly the same regardless of the flanker orientation. Altogether, when the flanker was present, the TvC function had a horizontal shift to the lower pedestal contrast direction.

Such a long-range flanker modulation effect cannot be fully captured by the traditional divisive inhibition model, which assumes that the flanker influence on the target is additive. The model predicts that the flanker effect would become neglectable at higher pedestal contrast (Morgan & Dresp, 1995; Snowden & Hammett, 1998; Solomon et al., 1999). Therefore, to

account for all aspects of the flanker effect, Chen and colleagues proposed a lateral sensitivity modulation model which captures the lateral interaction between neighboring cells that modulate the target cell sensitivity in terms of excitation and inhibition (for similar models, see Xing and Heeger (2001) as well as Cavanaugh, Bair and Movshon (2002a)). The model implemented two multiplicative sensitivity modulating parameters, one in the nominator and the other in the denominator, of the response function. These two multiplicative parameters represent the long-range flanker effect and could fully capture the changes in target response when flankers were added to the target. Similar models has successfully explained modulation effect on target threshold in the dual masking paradigm in Chen and Tyler (2001, 2002).

Most of these models focused on explaining the lateral modulation effect in contrast detection and discrimination. Only a few studies have explored models that apply divisive inhibition in the orientation domain, especially in the tilt aftereffect. Even fewer studies have approached perceptual filling-in with normalization models to understand the underlying mechanism. Therefore, a major goal of this thesis is to develop a divisive inhibition model that can capture the lateral modulation effects, including perceptual filling-in, on the perceived orientation of the central stimulus.

1.2.3 Neural Mechanism of Perceptual Filling-in

The abundance of filling-in evidence has led to two major theories of the underlying mechanism (Komatsu, 2006). The first is the symbolic, or the cognitive, theory which proposes that the scotoma region due to lack of visual input is being represented by the surround pattern in higher-level areas along the visual hierarchy (Pessoa et al., 1998; von der Heydt et al., 2003). Such a theory suggests that filling-in simply involves a passive process, in which the higher-level visual system simply ignores the missing information from entering consciousness. The symbolic

theory would therefore predict invariant cortical activities regardless of whether filling-in is

perceived or not. The second is the isomorphic theory which implies that filling-in involves an

active process enabling the reconstruction of the missing information in the filled-in region based

on the surrounding pattern (De Weerd et al., 1995; Meng et al., 2005). Contrary to the prediction

of the symbolic theory, the isomorphic theory would predict changes of neural responses in the

early visual cortex reflecting lateral interactions during filling-in. Recent neural evidence favors

the isomorphic theory. That is, filling-in results from the lateral interaction between the central

filled-in region and the surround. For example, Matsumoto and Komatsu (2005) reported an

increase of neural activities in macaque V1 when the bar stimulus was filled-in at the blind spot.

Such a finding has later led to a computational theory explaining the underlying neural

mechanism of filling-in at the blind spot (Satoh & Usui, 2008). In human V1, Sasaki and

Watanabe (Sasaki & Watanabe, 2004) found that the BOLD signal increased in the blank region

where neon color spreading occurred, suggesting a feedback process from higher-level visual

areas. Similarly, Weil and colleagues (2007) reported that magnetoencephalographic (MEG)

responses in the filled-in areas were correlated with the subjective percept of filling-in. These

research results support the notion that an active processing is involved when the unstimulated

area is filled in by the surround pattern.

In theory, there are two non-exclusive ways such an active process during filling-in can be

achieved. The first is the excitatory lateral processing. As suggested by Ramachandran &

Gregory (1991), it implies that the neurons with RFs corresponding to the surrounding stimulated

region send excitatory inputs to the neurons with RFs covering the unstimulated region. As a

result, the neurons responsible for the unstimulated region would be activated as if a visual

stimulus was present. Komatsu (2006) proposed a computational model that captures such

excitatory lateral interaction. The second is the inhibitory lateral processing, which theorizes that

filling-in is a product of the broadly tuned inhibitory mechanisms with widespread scope encompassing the blank region. Behavioral studies have shown evidence supporting involvement of lateral inhibition during filling-in. Evidence for inhibitory processing being involved during filling-in comes from the twinkle aftereffect, which describes the twinkling white noise percept commonly experienced in the unstimulated artificial scotoma region after the surround filling-in inducing pattern was turned off (Hardage & Tyler, 1995; Morgan et al., 2007). Such active twinkling sensation only happens after the inducer offset, hinting that it is the result of a rebound mechanism that is suppressed during the stimulation period when filling-in is perceived. Since the aftereffect always appears like white noise regardless of inducing pattern feature, such inhibition effect is likely to be extremely broadly tuned. Mihaylov and colleagues (2007) also reported that the detection threshold of Gabor patches presented in an artificial scotoma was elevated by surrounding dynamic noise.

Similarly, in neuroimaging, researchers have presented evidence of lateral inhibition related to filling-in percept. Chen and colleagues (2005) presented high-contrast flickering pinwheel pattern with four 45° wedges separated by 45° blank regions. The authors found that the BOLD signal in the unstimulated inter-wedge regions of the human striate cortex decreased when the neighboring regions were stimulated, leading to the conclusion that the surround neurons sent inhibitory signals to the central neurons during filling-in process. In a later fMRI experiment in which a lateral masking paradigm was adapted, Chen (2014) further differentiated two inhibitory components in such lateral suppression: a general inhibition whenever the flankers were present and a feature-specific inhibition that occurred only when the target and flankers were collinear, i.e. when they had the same orientation. Mendola and colleagues (2006) reported reduced neural activity was found in lower-tier visual cortex (V1 and V2), whereas increased activity in higher-tier regions (V3 and V4) was evident when a disk stimulus was filled-in with the mean luminance

background. The study Weil et al. (2007) reported reduced MEG power at target frequency when filling-in was perceived, adding further neuroimaging evidence of the involvement of lateral inhibition processing. In another line of work, De Weerd and associates (Peters et al., 2010; van de Ven et al., 2011) found an anti-phase modulation of BOLD signal in an area of constant luminance while the luminance of the surround changed.

The fact that both lateral excitation and inhibition evidence has been reported reveals the possibility that both mechanisms are present during perceptual filling-in. One possible explanation is that filling-in involves a narrowly tuned excitation from the surround that leads to similar activation of the surround pattern in the unstimulated region as well as a broadly tuned inhibition which causes a rebound mechanism after stimulation offset resulting in the twinkle aftereffect.

1.3 Research questions and hypotheses

Previous research has contributed to a better understanding of how neurons with different receptive fields interact with each other. Nonetheless, we are far from grasping the whole picture of lateral modulation and its role in perceptual phenomena like filling-in.

Tilt illusion and tilt aftereffect demonstrate how oriented patterns separated in space and time can alter the orientation percept (Greenlee & Magnussen, 1987, 1988; Magnussen & Kurtenbach, 1980; Solomon et al., 2004; Solomon & Morgan, 2006). In the tilt illusion, we observe how the surround orientation changes the orientation percept of the central stimulus. However, we do not know how such a tilted percept resulting from the lateral modulation could affect a subsequently presented oriented pattern. The TAE, in contrast, offers information about how adapted orientation detectors in the brain respond to a subsequently presented oriented target, but not how the adaptation effect would change in the presence of surround pattern during

the adaptation phase. To combine the merits and compensate for the shortcomings of each paradigm, one could include a surround pattern during the adaptation period to investigate how the surround features affects the central percept.

Masking paradigms with lateral flankers and cross-oriented patterns show evidence of how surround and superimposed masks change the contrast detection and discrimination threshold of the central target (Cannon & Fullenkamp, 1991; C.-C. Chen et al., 2001; C.-C. Chen & Tyler, 2001, 2002; Meese et al., 2007; Yu et al., 2001). However, these masking paradigms that focused on the target contrast percept or discrimination did not provide information about how the target orientation percept would change as a function of the surround orientation. As many neurons in visual cortex are selective for stimulus orientation, it is important to understand how lateral modulation affects our orientation percept. One way to consider the orientation-specific lateral modulation effect on the orientation percept is to measure how the central target percept changed with varied surround orientation.

The literature on perceptual filling-in, on the other hand, reveals how the brain remaps sensory inputs when faced with central missing information by interpolating the surround information into the blank regions. However, the underlying neural mechanism remains elusive. In addition, many filling-in experiments used dynamic random noise or texture with small elements as background to study how the artificial scotoma was filled in (De Weerd et al., 1995; Ramachandran & Gregory, 1991) or homogeneous luminance or colored objects to investigate the object fading process (Mendola et al., 2006). These types of background pattern do not provide information about how surround orientation specifically affect the filling-in process. To address this issue, Sakaguchi (2001, 2006) presented an oriented surround grating to his observers and noted how much time required for the central oriented target to be filled-in varied

35

with surround orientation. The results showed that, as the surround orientation increasingly deviated from the center target, the time needed for filling-in increased, indicating that the filling-in process depends on the stimulus orientation. Further studies are needed to fully capture to what extend filling-in varies as a function of the stimulus orientation of the center and surround stimuli.

In the current project, we aim to bridge these gaps in the literature on lateral modulation effects including perceptual filling-in with paradigms using center-surround orientation gratings and discuss the underlying neural mechanisms with the help of computational modeling and neuroimaging techniques. Therefore, we defined three main research goals in the thesis:

Goal 1: Establish Paradigms to Investigate Orientation-Specific Lateral Modulation Effects

The key focus of the thesis is to understand of the neural mechanism of lateral modulation. We therefore presented orientation gratings with different center and surround orientations and measured how the manipulation affects the orientation percept. The paradigms we develop should a) capture the orientation effect in lateral modulation, b) provide information about the impact of surround modulated percept on a subsequently presented stimulus, and c) allow for the estimation of perceptual filling-in. Paradigms employing a center-surround grating with varied orientations best suit our objectives. With respect to psychophysics, we established a TAE paradigm that selectively adapted different regions of the visual field. The reason of choosing an adaptation paradigm is two-fold: 1) by selectively adapting different parts of the visual field with different patterns we can observe how the center and surround mechanisms interact with each other to determine the percept of a subsequently presented target. By comparing, for example,

the condition when both the center and surround are adapted with the condition when only the center is adapted, we can infer whether adding the surround increases or decreases the adaptation effect. An increase in the adaptation effect suggests an excitatory lateral modulation effect, whereas a decrease of the adaptation effect indicates an inhibitory lateral modulation effect. In addition, by varying the adapter surround and center orientations independently, we can infer how the lateral modulation changes as a function of the stimulus orientation. 2) The prolonged fixation period in the adaptation phase allows perceptual filling-in to be induced in the surround-only adapter, enabling us to estimate how the filled-in percept impacts the percept of a subsequently presented target. The presentation of the target provides a more objective and quantitative measurement of perceptual filling-in than simply relying on the subjective reports of observers when filling-in occurs. If perceptual filling-in in the unstimulated center involves an active lateral modulation process from the stimulated surround, we expect to detect an adaptation effect induced on the following target even when there is no physical overlap between the target and the adapter. Furthermore, we can predict how the filling-in induced TAE depends on the surround orientation based on previous evidence of orientation-specific lateral modulation effect.

With respect to neuroimaging, we presented center-surround gratings and record the brain activation during stimulus presentation in the MRI scanner. As the eccentricity increases, the cortical magnification factor that determines how many neurons will respond to the visual field region decreases (Harvey & Dumoulin, 2011; Wandell et al., 2007). Therefore, we modified and increased the size of the oriented gratings to maximize the brain activation that can be recorded with fMRI. We presented radial sinusoidal patterns that activated different regions in the visual field and measured the BOLD signals

by means of functional magnetic resonance imaging. By comparing how early visual areas

respond to different center-surround stimuli we could examine the neural correlates of the

lateral modulation effects observed already at the behavioral level. As ample evidence has

shown that surround pattern could inhibit the center, we expect to observe inhibitory

effect in the target brain regions when the surround pattern is added to the stimulus center.

We also expect to find a difference in BOLD activation between trials when our

participants report filling-in compared to trials when they do not.

Goal 2: Explain Lateral Modulation Effects with a Divisive Inhibition Model.

After establishing the empirical paradigm that capture different lateral modulation

effects, we define a computational model that allows us to quantitatively examine the

underlying mechanisms with model parameters that represent the lateral interaction

between the center and surround during the adaptation phase. In terms of candidate

mechanism models to explain the lateral modulation effect, some studies have proposed

that lateral modulation is subject to a normalization process that can be depicted by

divisive inhibition models (C.-C. Chen et al., 2001; C.-C. Chen & Tyler, 2001; Solomon

et al., 2004; Xing & Heeger, 2001). For instance, Chen and colleagues (2001) revealed

that their sensitivity modulation model could explain the long-range lateral effect on the

target response function when flankers were present. We then incorporate the merits of

previous models and develop a variant of the divisive inhibition model to explain the

observed lateral modulation effects including perceptual filling-in and cross-orientation

center-surround interaction. Our model should 1) reflect the population coding that

underlies the target orientation percept by considering the inputs of multiple orientation

detectors, comparable to the way these signals are processed in the visual cortex (Deneve

et al., 1999; M A Paradiso, 1988; Pouget et al., 2000), 2) capture the adaptation effect induced in the percept of the target, and 3) contain sensitivity modulation parameters that vary with the surround orientation.

Goal 3: Understand the Underlying Neural Mechanism of Perceptual Filling-in

The underlying mechanism of perceptual filling-in is still under debate. Some researchers proposed that filling-in involves a passive process; that is, the higher-level visual areas simply ignore the lack of visual input and represent the blank region with the surround features (Pessoa et al., 1998; von der Heydt et al., 2003). Therefore, no active neural responses are needed in the filled-in region. Others postulate that filling-in involves an active processing from the surround to the center; evidence supporting an excitatory (Matsumoto & Komatsu, 2005; Ramachandran & Gregory, 1991) and inhibitory (C.-C. Chen et al., 2005) active process has been reported, revealing the possibility that filling-in cannot be explain by a single process. Therefore, the last focus of the current project is to investigate the neural mechanism of filling-in with our new paradigms and proposed computational model in the hope of reconciling the seemingly conflicting results in the literature. Our adaptation paradigm reveals how the filled-in percept influences the percept of the subsequently viewed target. With careful examination of the computational modeling results of our proposed divisive inhibition model, we gain new insights into the underlying neural mechanisms. The fMRI experiment could provide evidence of neural correlates when filling-in is perceived compared to when it is not perceived.

To fulfill these major goals, we conducted three main studies within the current thesis: In Study 1, we selectively adapted the center, the surround and both regions with sinusoidal grating adapters and observed how the orientation percept of the following target changed with different

CHAPTER 1: INTRODUCTION

adapter types (see Chapter 2). The surround-only adapter could induce perceptual filling-in in the center blank region, allowing us to study the effect of filled-in orientation percept on the target. Comparing the TAE results between different adapter type conditions should reveal how the adapted neurons respond to different visual field regions thereby contributing to the target percept. In Study 2, we manipulated the adapter center and surround orientation to examine how the lateral modulation effect varied as a function of the surround feature (see Chapter 3). We developed a divisive inhibition model that could explain the TAE for different adapter types and adapter orientations with sensitivity modulation parameters. Our model provided insights into how lateral excitation and inhibition were involved during the adaptation phase. In the final study, we stimulated again center, surround, or both regions simultaneously in the visual field and examine how BOLD activation changed in visual cortical areas (see Chapter 4). We conducted both univariate and multivariate analyses to understand the neural correlates of the lateral modulation effects including perceptual filling-in.

In the following chapters, we first focus on each of the studies by presenting three manuscripts, two published and one accepted by leading international journals, in Chapter 2 to 4. Then, in Chapter 5, within the Concluding Remarks, we reformulate the main goals and summarize the major findings of the three studies. Moreover, we discuss the contributions and scientific significance as well as the limitations of these results followed by possible future directions.

2. CHAPTER 2: STUDY 1 "LATERAL MODULATION OF ORIENTATION PERCEPTION IN CENTER-SURROUND SINUSOIDAL STIMULI: DIVISIVE INHIBITION IN PERCEPTUAL FILLING-IN"

This study has been published after peer-review on September 4th 2020 in Journal of Vision (JOV), an open access journal. DOI: 10.1167/jov.20.9.5. The supplementary files that are not included in the thesis (Supplementary File S1, S3, and S4) can be downloaded from the JOV page: https://jov.arvojournals.org/article.aspx?articleid=2770759.

2.1 Abstract

The perception of a target stimulus may be altered by its context. Perceptual filling-in is thought to be one example of lateral modulation, in which the percept of a central blank area is replaced by that of the surround. We investigated the mechanisms in eccentric vision underlying filling-in by selectively adapting the center (pedestal adapter), surround (annulus adapter), or both (disk adapter) in a sinusoidal grating and observed how the adaptation influences the orientation percept of a subsequently presented Gabor target, located at the same position as the adapter center. In a binary choice task, observers were to judge the orientation (clockwise or counterclockwise) of the target after adaptation. The tilt aftereffect (TAE), corresponding to an illusory tilt of a physically vertical Gabor target, depended both on the adapter orientation and the adapter type. The TAE, peaked between 10 degrees and 20 degrees adapter orientation, was strongest in the pedestal, followed by the disk, and weakest in the annulus adapter conditions. The difference between the disk and pedestal conditions implies lateral inhibition from the surround. Lacking physical overlap with the target, the annulus adapter nonetheless induced a small but significant TAE in the central area. The effect of filling-in on the TAE was estimated by comparing the results from trials with and without subjectively reported filling-in during adaptation to the annulus adapter. The TAE was greater when filling-in occurred during adaptation, suggesting a stronger lateral modulation effect on trials where filling-in was induced. The data were fit by a variant of a divisive inhibition model, in which the adaptation effect is captured by the increase of an additive constant in the denominator of the response function, whereas the surround modulation in the adapter is modeled by an excitatory sensitivity in the numerator.

Keywords: surround modulation, perceptual filling-in, lateral inhibition, orientation

selectivity, spatial vision.

2.2 Introduction

The effect of context on a centrally located target stimulus has long been recognized in visual sciences (Gilbert & Wiesel, 1990; Pessoa & De Weerd, 2003). At the retinal level, horizontal cells (HCs) carry out the first lateral projection in the retina (Baylor et al., 1971). Every HC receives synaptic signals from several photoreceptors and the former transmits feedback signals back to the photoreceptors to alter their neurotransmitter release. This HC feedback is mostly inhibitory. A group of photoreceptors, which send synaptic signals directly to a bipolar cell, forms the receptive field center of that bipolar cell. Meanwhile, HCs collect signals from a larger group of photoreceptors surrounding the centrally located photoreceptors and these form the receptive field surround. When the surround photoreceptors are activated, they send excitatory signals to the HCs, the HCs in turn send inhibitory feedback to the centrally located photoreceptors, mediating the response of the bipolar cell. This creates the typical center-surround/excitatory-inhibitory receptive fields (RFs) often observed in bipolar cells. This simple circular-symmetric shape of RFs can be found up in the retinal ganglion cells and neurons in the lateral geniculate nucleus (LGN). Owing to their symmetrical shape, these RFs are non-selective to stimulus orientation. In the primary visual cortex, or V1, RFs become more selective to the orientation, motion direction, contrast, and size of the stimulus (Hubel & Wiesel, 1962). From here onward, lateral interactions between regions in the visual field form a complex network with both feedforward and feedback circuits.

At the cortical level, lateral modulation occurs also beyond the center-surround classical receptive field (CRF). One example is the surround suppression observed when a neuron's receptive field is stimulated with an oriented grating stimulus. The surround stimuli themselves

43

do not induce any neural activity in the recorded neuron, but can nevertheless suppress (predominantly) or facilitate the CRF response activated by a central stimulus (Barlow, 1953; Cavanaugh et al., 2002a, 2002b; Hubel & Wiesel, 1959; Maffei & Fiorentini, 1976). This surround modulation requires long-range integration of information across multiple CRFs. Many studies show that the surrounding area beyond the CRF can have similar orientation and spatial frequency tuning as those of the CRF, suggesting that this form of lateral inhibition is feature-specific (Blakemore & Tobin, 1972; Cavanaugh et al., 2002b; DeAngelis et al., 1994; Gilbert & Wiesel, 1990; Nelson & Frost, 1978; Ozeki et al., 2004; Sillito et al., 1995). Different paradigms have been suggested to study this long-range lateral inhibition. Using the method consisting of an expanding patch or an expanding annulus to study the surround beyond the CRF, various groups discovered two surround areas (near and far surrounds) that contribute different contrast-dependent effects on the CRF (Angelucci & Bressloff, 2006; Ichida et al., 2007; Sengpiel et al., 1997; Shushruth et al., 2009).

Another common way to investigate lateral modulation is through a psychophysical lateral masking paradigm, in which target detection threshold is estimated in the presence of surround flankers on either side of the target (Polat & Sagi, 1993, 1994; Zenger & Sagi, 1996). These authors reported that the flanker effect depended on the relative orientation between the flankers and the target. When the target and flankers were collinear, the target detection threshold was significantly reduced. On the other hand, when the flankers were orthogonal to the target, no target facilitation was found. Solomon, Watson, and Morgan (1999) further investigated such collinear facilitation flanker effects by using flankers of the same or opposite-sign contrast as the target and found that the opposite-sign flankers created a much weaker facilitation on the target than the same-sign flankers. Later, the same authors discovered that adding non-collinear flankers surrounding the central target cancelled such facilitation effects (Solomon & Morgan, 2000).

44

Chen and Tyler (2001, 2002) used a dual-mask paradigm to investigate the flanker effect. They added a pedestal, which occupied the same spatial location with the same spatio-temporal properties of the target. Without the flankers, the target detection threshold first decreased (facilitation) then increased (suppression) with the pedestal contrast (i.e. the well-known dipper effect). The collinear flankers reduced the target threshold when no pedestal was presented and increased the target threshold at high pedestal contrast. The orthogonal flankers did not produce the facilitation effect, but instead led to a suppression effect at high pedestal contrast. They concluded that there are two flanker effects, one narrowly and the other broadly tuned to flanker orientation. They proposed a divisive inhibition model to explain the data, suggesting that the observed lateral modulation is subject to a normalization process. In a later functional magnetic resonance imaging (fMRI) experiment, (C.-C. Chen, 2014) explored the neural correlates corresponding to these two inhibitory components. Two effects were evident in his results: first a general inhibition that reduced the target BOLD signal in the presence of the flankers, and second, a flanker-specific inhibition that was stronger when the flanker shared the target orientation (collinear flanker effect). In another line of work, Meese and colleagues (Meese et al., 2007; Meese & Holmes, 2007) used either annular or superimposed masks of various sizes to investigate how different cross-oriented surrounds can affect the contrast detection and discrimination thresholds of a Gabor target. They reported cross-orientation facilitation as well as cross-orientation suppression from both types of mask. The observed lateral modulation effect varied with spatial and temporal frequencies and masking area.

It is suggested that perceptual filling-in is a visual phenomenon that results directly from center-surround modulation (Anstis & Greenlee, 2014; Pessoa & De Weerd, 2003; Ramachandran & Gregory, 1991). Filling-in describes the effect when the visual system integrates surround features to compensate for occluded or absent information in the center.

Filling-in can be experienced in the blind spot, with retinal scotoma, or for artificial scotoma. The blind spot is the part of the visual field corresponding to a region on the retina where the optic nerve exits the eye, thus lacking photoreceptors to detect variations in light. Humans do not experience a dark hole corresponding to the blind spot (even with monocular viewing) because the visual system interpolates and fills in the blank by extracting information at the edge or surround regions (Ramachandran, 1992). Neurophysiological studies reported active neural response in early visual cortex in the projection zone corresponding to the blind spot (Fiorani Júnior et al., 1992; Komatsu et al., 2000, 2002; Matsumoto & Komatsu, 2005) or to that evoked by artificial scotoma (De Weerd et al., 1995; Sasaki & Watanabe, 2004), indicating that the central filled-in regions were modulated by the surround neurons that receive visual input. Such perceptual completion has been observed in the retinal scotoma of macular degeneration patients (Zur & Ullman, 2003). Furthermore, scotoma can be induced artificially with the help of strict central fixation or gaze-contingent displays. Ramachandran and Gregory (1991) placed a gray-homogeneous square (the artificial scotoma) in a twinkling noise background. After prolonged steady fixation, the gray square was filled in by the noise background. Morgan, McEwan and Solomon (2007) presented a dynamic noise pattern with two artificial scotomata on the left and right visual fields as the adapter. When the field was switched off (after participants reported the scotomata being filled-in) and replaced by a mean luminance background, flickering phantasms were perceived. To estimate the effect of such phantasms, the authors presented two small noise patches in the scotoma regions after adaptation, one containing both the target and the pedestal, and the other only the pedestal. Participants were to choose the patch with the target. The target contrast threshold increased after adaptation. In addition, when the adapting field was presented to only one eye, the target threshold increased on both eyes, suggesting a cortical origin of such an adaptation effect.

46

The functional role of lateral modulation during filling-in remains unclear. Although some studies reported increased neural activities in the filled-in regions, suggesting that lateral excitation is involved (De Weerd et al., 1995; Komatsu, 2006; Matsumoto & Komatsu, 2005; Roe et al., 2005; Sasaki & Watanabe, 2004), others proposed that lateral inhibition from the surround might also play a role. Tong and Engel (2001) conducted a binocular rivalry fMRI experiment and measured the activity of the cortical area corresponding to the eccentric visual field location of the blind spot of one eye. When the stimuli were presented, the BOLD signals increased when the ipsilateral-eye image was dominant and decreased when the blind-spot eye image was dominant. This finding suggested a monocular lateral inhibition in V1 neurons when stimulus was presenting at the blind spot. In an magnetoencephalography (MEG) experiment when a uniformly illuminated target disappeared and was replaced by the dynamic background texture, the MEG power at the target frequency was reduced (Weil et al., 2007). Such power reduction suggests a decreased neural representation of the invisible (filled-in) stimuli in visual cortex. The same group later applied the same filling-in paradigm in an fMRI study and reported again BOLD signal reduction in the V1 and V2 area representing the filled-in target (Weil et al., 2008). These seemingly contradicting results lead to the possibility that the underlying mechanism of filling-in could be complex involving multiple processes that include both lateral excitation and inhibition.

Although many groups have investigated the lateral modulation in vision with various paradigms such as lateral masking and visual crowding, few have studied the lateral modulation by selectively adapting the central and/or surround mechanism and observed the effect on the central percept.

To understand more about lateral modulation in human vision, we designed an adaptation paradigm in which we estimated the target Gabor percept after adapting to sinusoidal-grating adapters. Prolonged viewing of one grating (the adapter) leads to a perceptual tilt in a subsequently presented grating (the target) in a direction opposite of the adapting orientation (the orientation shift). This tilt aftereffect (or TAE) was first termed by Gibson and Radner (1937) and widely discussed in the literature (see (Clifford, 2014) for a recent review). To be perceived as vertical, the target must be oriented more in the direction of the adapter, which indicates a perceptual shift in the opposite direction.

In the first experiment of the present study, we compared the estimated TAE (orientation shift) observed in the target under different adapter conditions. We used three different oriented grating conditions: the pedestal adapter (center-only), the annulus adapter (surround-only), and the disk adapter (center and surround) presented in the upper right visual quadrant. By comparing the estimated orientation shift between the pedestal and the disk conditions, we can infer whether the lateral modulation from the surround is inhibitory or excitatory. In an attempt to link the magnitude of the TAE to filling-in, we asked observers to report their experience of filling-in during the surround-only adaptation (the annulus condition). A positive correlation between the magnitude of the TAE and filling-in would be supportive of a common underlying mechanism. In the second experiment, we focused only on the effects of the annulus adapter to understand more about the nature of the lateral modulation effect during perceptual filling-in. We separated the trials into those with reports of the filling-in percept and those without and estimated the orientation shift respectively. We can thus compare the TAE on trials where filling-in is perceived during adaptation to trials where it was not. We then constructed a model that incorporated divisive inhibition models for adaptation (Foley & Chen, 1997) and lateral interaction (Chen & Tyler, 2001) to account for the data.

2.3 Methods

Participants

Nine observers (six women) participated in the study, aged between 20 and 38 years, including one of the authors (YSL) and 8 naïve participants (P1 to P8). All observers participated in experiment 1, whereas three of them (YSL, P1 and P3) also took part in experiment 2 and the fixation stability test. All have normal or corrected-to-normal vision. Informed consent was received from each individual before participation. The study protocols were approved by the University of Regensburg ethics committee (application number: 19-1591-101) and all experiments were performed according to the Declaration of Helsinki on human experimentation. Participants received monetary compensation or class credits as rewards. Observers first performed a short practice session before the formal experiment to become acquainted with the stimuli and the task.

Apparatus

Four participants viewed stimuli on a 24-inch Sony Trinitron FW900 CRT monitor with 1024×768 resolution, the rest on a Dell S2417DG 24-inch LED monitor with 2560×1440 resolution. Both monitors had 120 Hz refresh rate and were calibrated and gamma-corrected using a spot photometer (MINOLTA CS-100). Mean luminance was 37.8 cd/m^2 for the CRT monitor, and 73.8 cd/m^2 for the LED monitor. Viewing distance and stimuli size were kept constant across the two viewing setups with the help of a chinrest. No significant difference in orientation shift estimation was found when we tested one observer on the two monitors; thus, we collapsed data across both settings for the analysis. The main experiment was carried out in a dimly lit room.

To determine if there was a difference in fixation stability across different adapter conditions, a fixation stability test was conducted in another dimly lit room with the video Eyetrace 3.20 eye tracker controlled by the video Eyetrace toolbox 3.250 (Cambridge Research Systems Ltd). The stimuli were presented on a 60 Hz Dell 1908FP monitor with a resolution of 1024×768 and a viewing distance of 60 cm. The mean luminance was 30.3 cd/m^2.

Stimuli

Three sinusoidal grating adapters were used in the current study (see Figure 2.1). A) one with the same spatial extent of the target, labeled pedestal adapter, B) an annulus adapter with no spatial overlap with the target, and C) a continuous disk adapter the same size as the annulus adapter (with no central gap). Both the pedestal adapter and the target Gabor were defined by the following equations:
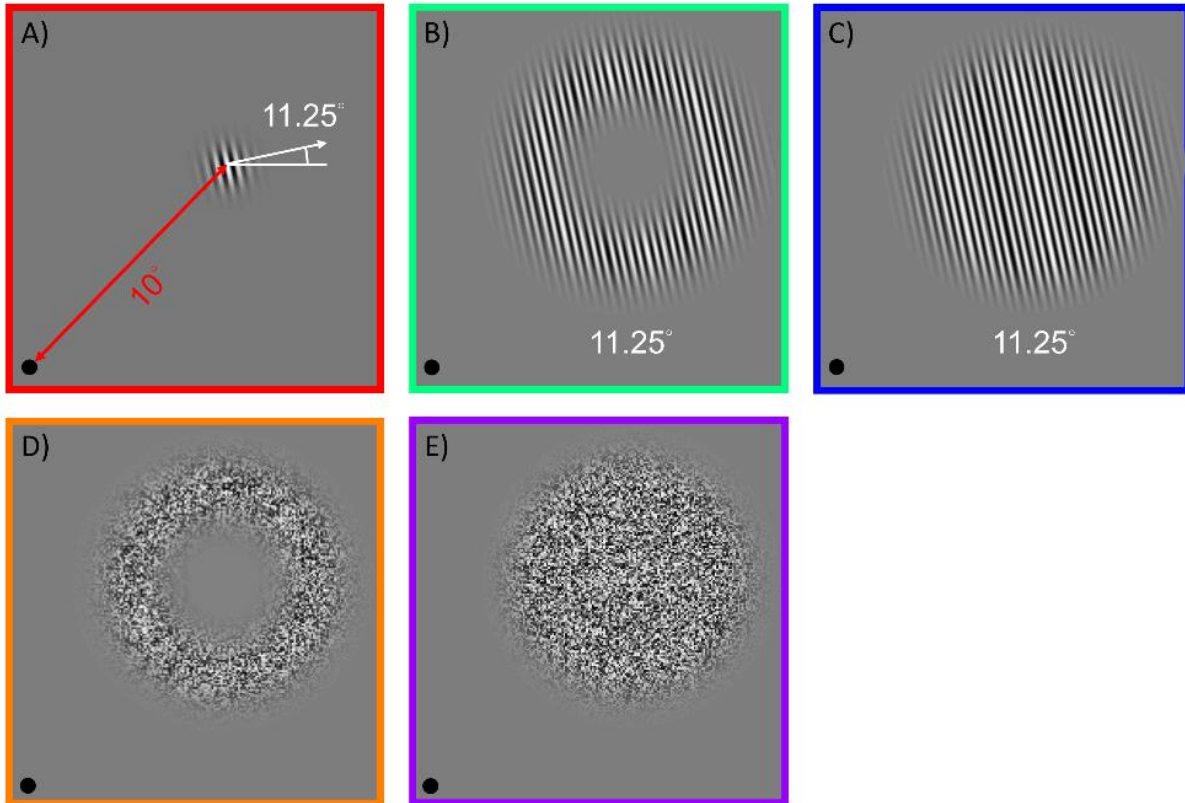
$$G(x, y) = B + BC\cos(2\pi f x')e^{\left(\frac{-x'^2 - (y' - u_y)^2}{2\sigma^2}\right)},$$

as well as

$$x' = x\cos\theta + y\sin\theta,$$

$$y' = -x\sin\theta + y\cos\theta,$$

where B was the mean luminance, while C the pattern contrast, f the spatial frequency, θ the pattern orientation, μ_y the vertical displacement of the pattern, and σ the scale parameter. The pedestal adapter and Gabor target had a scale parameter (σ) of 0.3 degrees.

Figure 2.1

Examples of the Adapters Used in the Current Study

Note. A) Demonstrates the 11.25 degrees pedestal adapter, which was placed 10 degrees away from the fixation point, indicated by the black dot on the lower left corner. B) Shows the 11.25 degrees annulus adapter, C) the 11.25 degrees continuous disk adapter, D) the noise annulus adapter and E) the noise disk adapter. The target Gabor was of the same size as the pedestal adapter in A). We blurred both edges (inner and outer) of the annulus in B) by multiplying the sinusoidal grating with a Gaussian function centering at 3.5 degrees eccentricity from the adapter center (10 degrees from the centrally located fixation point, depicted in the lower left corner in panels A through E). The Gaussian function had a scaling factor (σ) of 0.9 degrees along the inwards and outwards radial directions. To avoid physical overlap between the annulus and the target, we added a mean luminance disk with the radius that was 10' larger than the Gabor target. The border color matches that used in the Figure 2.2 (psychophysics data and model fitting results) for sake of illustration only and was not present in the experiments.

The annulus adapter was created by generating a sinusoidal grating multiplied by a Gabor envelope in polar coordinates, centered at 3.5 degrees eccentricity with a scale parameter (σ) of 0.9 degrees. In the center of the annulus, was a disk of a mean luminance resembling an artificial scotoma). The radius of the disk was 10' larger than the target Gabor to avoid any spatial overlap between the target and the annulus. The spatial extent of the Gabor was defined as the point when the envelope amplitude decreased below 0.5% of maximum amplitude. The disk adapter had the same outer radius as the annulus. All adapting patterns were at -1 dB (89.13%) luminance contrast and had 3 cycles per degree (cpd) spatial frequency. The stimulus orientation was defined by the direction of the luminance contrast variation; thus, the vertical grating was assigned the value of 0 degrees. The sinusoidal grating adapters were presented in one of five orientations (0 degrees, 11.25 degrees, 22.5 degrees, 45 degrees and 90 degrees), three of which were tilted counterclockwise (CCW) from vertical and one is horizontal.

In addition to adapters with orientation information, we added three control adapter conditions without orientation information: a noise annulus (D) in Figure 2.1), a noise disk (E) in Figure 2.1), and a gray control condition in which a blank field (no adapter) was presented during the adaptation phase. We created the noise annulus and disk by randomly assigning luminance value to every 2-by-2 pixel square, resulting in a salt-and-pepper type of noise pattern (see Figure 2.1 E). The luminance of each square was determined by $B \times \left(1 + C \times U(x, y)\right)$, in which B is the mean luminance, C the contrast parameter set to 89.13%, or -1dB, and $U(x, y)$ a uniform distribution with a range of -1 to 1. The gray control blank-field/no adapter condition was included (not shown in Fig. 2.1) to estimate any baseline orientation shift without prior adaptation.

All stimuli were presented 10 degrees eccentric from the central fixation on the upper right quadrant of the visual display (7.07 degrees from fixation in *x* and *y* direction). The visual stimuli were all generated using Matlab (Mathworks, Inc., Natick, MA, USA) with PsychToolbox (http://psychtoolbox.org/).

Procedure

Experiment 1

We used a single interval binary-choice task to estimate the target orientation shifts after adaptation to the adapting stimuli. On each trial, one of the three above-mentioned adapters were displayed for 8 seconds, with a 5 Hz counterphase flickering frequency to minimize after-image formation. The target was presented for 200 ms after the adapter, with an 83.3 ms inter-stimulus interval (ISI) between the two stimuli. Participants were asked to judge whether the target was tilted in the CCW or clockwise (CW) direction relative to vertical by pressing corresponding keyboard buttons. An auditory feedback was given to the participant after his/her response in each trial. The next trial began after the participant gave a response. We used the Ψ threshold-and-slope-seeking staircase (Kontsevich & Tyler, 1999) to determine the orientation of the next target and estimated the orientation when the observer judged the target orientation as appearing to be in the same direction as its physical appearance at an 86% rate for both CCW and CW trials. We measured the CCW and CW orientation shifts using two independent interleaved staircases with random trial sequences. When the participant judged the target orientation as the same as its physical orientation in a previous trial of the same sequence, the target orientation in the next trial in the same sequence decreased (i.e. toward the vertical orientation). Otherwise, the target orientation increased.

All 18 conditions (3 adapter types × 5 orientations plus 3 control conditions – no noise, annulus noise, full disk noise) were repeated at least three times, resulting in a total of 54 blocks, each containing 72 trials including 2 practice trials at the beginning of each block. In a random order, half of the trials contained CCW-oriented targets, the other half CW-oriented ones. A 7-point Likert-type query appeared after every 10 trials in every condition requesting the observer to retrospectively report their filling-in experience during adaptation. During the annulus adapting condition, participants pressed 1 when they experienced no perceptual filling-in on the last trial, and 7 when the central aperture was perceived as completely filled-in by the surround pattern during adaptation. They were asked to always press 1 in the pedestal and control conditions, 7 in disk conditions, when the query to do so appeared.

To make sure participants exhibited steady fixation, we included a central color detection task, in which they were asked to press the space bar whenever the fixation cross turned red during the adaptation period. All participants were trained to obtain a high fixation task accuracy (over 95% performance on the fixation task) before real data collection began.

Experiment 2

Provided the possibility that not all trials in the annulus condition of Experiment 1 induced filling-in, the orientation shift estimated might be a mixed effect from filling-in and non-filling-in trials. To further examine the effect of perceptual filling-in, we designed a complementary filling-in experiment. In Experiment 2, only the annulus adapters with five orientations were used. The task in Experiment 2 was identical to that of experiment 1 except that a Yes/No filling-in query was prompted after every trial, and

that the program stopped only when all four conditions (CCW/CW orientations × with filling-in/without filling-in) reached at least 35 trials each (not including the practice trials). We estimated the orientation shift necessary to null the TAE in each of the four conditions based on the target orientation presented and the observer binary-choice response in each trial using the same threshold-and-slope estimation algorithm as the Ψ procedure implemented in our experiment (Kontsevich & Tyler, 1999). We took the data in the first 35 trials of each condition so that the amount of trials used to estimate the perceived orientation shift was kept the same across all conditions. By doing so, we can separately examine the adaptation effect on the target with and without reports of perceptual filling-in.

Fixation stability test

To make sure that the difference in TAE between different adapter conditions did not result from differences in how well the participants fixated, we conducted a control experiment with an eye tracker to estimate the potential effects of fixation stability on the results. We recruited three observers who participated in both experiments 1 and 2 (including one author). Each participant performed one run of the following four conditions: the pedestal adapter, the annulus adapter, and the disk adapter in experiment 1, and the annulus adapter in experiment 2. Participants completed the four conditions in random sequence. The experimental procedure was exactly the same as that in experiment 1 and 2 respectively except that an eye tracking calibration was performed at the beginning of each run.

2.4 Results

In the following sections, we will focus our discussion on the averaged data across all observers in experiment 1 and 2. The estimated values of Ψ procedure of each participant in each run in the two experiments are shown in Supplementary File S1 (with observer LYS referred to as P0) in .xlsx (Excel; Microsoft, Redmond, WA) format. The orientation shift of both CCW and CW target is expressed in degree away from vertical, whereas the unit of the slope is $d'/\log\theta$, detectability per log target orientation (in degree). In experiment 1, we estimated the target orientation shift necessary to null the TAE under different adapter conditions. We had three oriented grating adapters: the pedestal adapter (center-only), the annulus adapter (surround-only), plus the disk adapter (center and surround). In addition, we included three control adapters that contain no orientation information: the noise annulus adapter, the noise disk adapter, and the gray control condition (no adapter during the adaptation period). The averaged data of nine observers in experiment 1 are shown in Figure 2.2 (for individual-subject data, see Supplementary Figure A.1 in Appendix A). Two types of target were presented in random sequence after the adapter: a counterclockwise (CCW) rotated target or a clockwise (CW) rotated target. We estimated how much orientation shift away from vertical of each type of target was needed to cancel the TAE induced by the adapter. The perceived orientation shifts of the CCW target are plotted against adapter orientation in Figure 2.2a, whereas that of the CW target are shown in Figure 2.2b. The CCW orientation shift varied with adapter type and adapter orientation, whereas the CW orientation shift remained mostly unchanged. This was expected because most of our adapters were oriented in the CCW direction and created a CW TAE that led to a robust perceived CCW orientation shift that was captured best by the CCW targets. The CW-oriented targets were included in the experiment as catch trials to make sure the observers were following task instructions. Thus, the data demonstrated in Figure 2.2b can be seen as the orientation shift in a

control condition when no significant TAE was induced. In the following sections, we focus only

on the CCW orientation shift results of the CCW target.

Figure 2.2

The Averaged Data of Estimated Perceived Orientation Shifts in Experiment 1
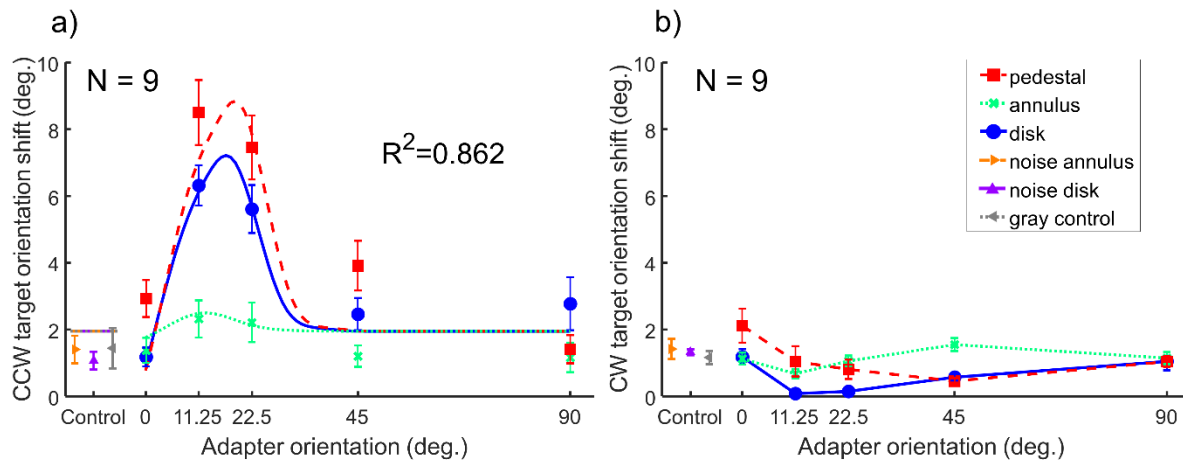
Note. Two types of targets were presented after adaptation: a CCW-oriented target (**a**) and a CW-oriented target (**b**).

We estimated how much orientation shift of each type of target was needed to cancel the TAE induced by the

adapter. In the current study, all adapters were of CCW orientation relative to the vertical orientation. In both CCW **a**

and CW target **b**, the three curves show results of oriented grating adapters (red-dashed curve: pedestal adapter;

green-dotted curve: annulus adapter; blue-solid curve: disk adapter), with five orientation levels indicated on the x-

axis. The three triangle markers present data points from the three control conditions (orange right-pointing triangle:

noise annulus adapter; purple up-pointing triangle: noise disk adapter; gray left-pointing triangle: gray control/no

adapter condition). The error bars are ±1 standard error of measurement. In a, the smooth curves are the best fits of

our computational model. The short-dashed lines close to the three control data represent model fits of the control

conditions (see Model part in Results).

For the oriented grating adapters, the amplitude of perceived orientation shift (compared to the gray control baseline) was highest in the pedestal condition (red-dashed curve), intermediate in the disk condition (blue-solid curve), and smallest in the annulus condition (green-dotted curve). We performed paired t-tests between the peaks (at 11.25 degrees) of oriented grating adapter conditions and the gray control condition and found that all three perceived orientation shifts were significantly higher than the baseline. The $t(8)$ was 7.53 for the pedestal, 7.44 for the disk, and 3.07 for annulus conditions with a Bonferroni-corrected p-value of $< .001$ for pedestal and disk (effect size Cohen's $d = 2.91$ and 2.69 respectively) and .024 for the annulus (Cohen's $d = 0.50$) conditions.

For the noise annulus and noise disk adapters, no orientation shift variation was found compared with baseline. The t-tests between the noise stimuli and the gray control were not significant ($t(8) = $ -0.91 for noise disk, -0.16 for noise annulus, n.s.). This suggests that when the adapter carried no coherent orientation information, the target orientation percept remained unchanged after adaptation. These results suggest that the observed adaptation effect was orientation specific. In the following, we will focus mainly on the effects of the oriented grating adapters.

In Kontsevich and Tyler (1999), the authors performed Monte-Carlo simulations to examine how the threshold and slope estimated by the Ψ method would converge after a certain amount of trials. Figure 1 of their paper shows that the estimated threshold reached a precision of 2dB after about 30 trials, whereas the estimated slope required about 300 trials to reach the same precision level. In the current study, only 35 trials were presented in each adapter condition, which was sufficient for threshold convergence but not for slope convergence. As a result, the estimated slope values stayed around the initial value two, which was the middle point of the

slope range, set from 1 to 4 in our study (for the Ψ method slope values, see File S1). Thus, we will not discuss the Ψ slope values below.

The Ψ method was chosen as a placement method in the current study, allowing us to use an adaptive staircase method to determine which test orientation to be used based on the observer previous response. However, the Ψ staircase method was initially developed to estimate the threshold and slope in a 2AFC task, not in a binary-choice task used here. In addition, the Ψ method assumed that at the lowest stimulus level, the correct probability corresponds to 0.5. Such assumption might not hold in our case (especially after adaptation), resulting in deviation of estimated parameters from the actual response probability. To examine whether the estimated orientation shift reflects the 86% CCW responding rate, we fitted a cumulative normal psychometric function (PF) to the raw data (the CCW trials) for each participant with the Matlab-based Palamedes toolbox (Prins & Kingdom, 2018). We then examined the relationship between the estimates of the PF fitting results and the ones from the PSI method. The estimated orientation shift required to reach the 86% CCW responding of the two methods were found to be quite comparable within each participant. To examine whether there was a systematic relationship between the orientation shift and the slope (a possible confound between the bias and unreliability in the data), we calculated the Pearson correlation coefficient between the estimated 86% CCW responding rate and the fitted slope (beta) value in the PF fitting results of all conditions for each participant. Results showed that the orientation shift was negatively correlated with the slope in two out of the nine participants (rs(14) = -0.51 and rs(14) = -0.50, p = 0.021 and 0.024), suggesting that in the data of these two observers, the bias and unreliability were proportional to each other, but not in the data of the remaining seven observers. Details of the PF fitting methods, the comparison between two methods, as well as the correlation between

the PF fitting parameters can be found in Supplementary materials (File S2 online, or Appendix A in the current thesis).

Another way of examining the data in the current study is by combining both CW and CCW trials of the same adapter condition together and fitting one PF function to the combined data set. The procedure and results of such data reanalysis is included in the Supplementary File S2 (included in Appendix A of the current thesis), whereas the raw trial data used to fit the PF functions are shown in Supplementary File S3. The results show a very similar pattern as presented in Figure 2.2a (the estimated orientation shift by the Ψ method). Thus, in the remaining sections of this paper, we will focus our discussion on the Ψ method threshold estimate (the orientation shift).

Lateral modulation can express itself either as lateral excitation or as lateral inhibition. If the adapter surround induced lateral excitation effect on the adapter center, then after adaptation we should expect an increased adaptation effect. On the other hand, if the adapter surround imposed lateral inhibition instead, we should observe a decrease of the adaptation effect on the target. Our results showed that the CCW orientation shift in the full disk condition was lower than for the pedestal condition, suggesting that lateral inhibition arose when the surround was stimulated during adaptation.

To evaluate the association between the filling-in percept during adaptation and the perceived orientation shift during test, we calculated the non-parametric Spearman's rank correlation coefficient between the filling-in reports (see Methods for details) and the perceived orientation shift of the annulus condition at its peak (11.25 degrees). The result (shown in Figure 2.3a) showed a positive correlation coefficient that was significant ($rs(7) = 0.69$ $p = 0.022$),

indicating that across all observers the stronger the perceptual filling-in perceived by the

observer, the stronger the adaptation effect induced for the target.

Figure 2.3

The Relationship between the Perceptual Filling-in (Occurring in the Annulus Adapter

Condition) and the Orientation Shift (TAE)
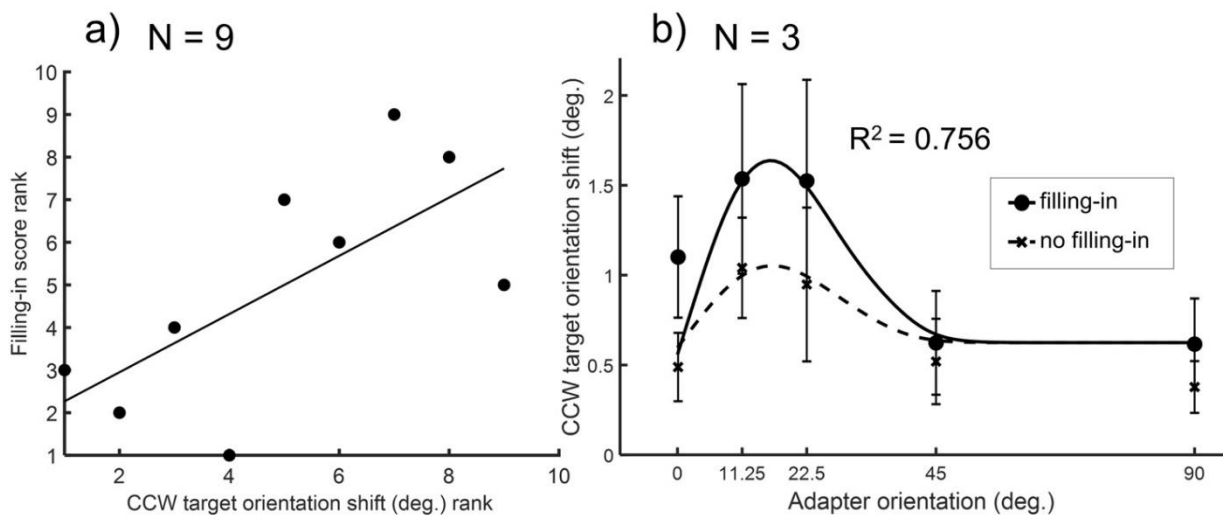
Note. (**a**) The scatter plot of the correlation between the rank of the CCW target orientation shift and the rank of the

filling-in score of the annulus condition of each participant (N = 9) in experiment 1. The solid line represents the

least-squares fitted regression line, *rs*(7) = 0.69. (**b**) The averaged data of estimated perceived orientation shifts of

CCW target in experiment 2 (in which only the annulus adapter was used). The symbols (disk: with filling-in; cross:

without filling-in) represent the behavioral data while the smooth curves (solid curve: with filling-in; dotted curve:

without filling-in) the best fits of the model (see Results). The error bars are ±1 standard error of measurement.

In experiment 1, we did not monitor the subjective perceptual filling-in experienced by

the observers on a trial-by-trial basis. Instead, the query was only prompted once every 10 trials.

As a result, we could only access the averaged filling-in percept in the whole block and the

estimated orientation shift might not entirely reflect the effect when filling-in occurred. Given

that the central area could undergo a different amount of adaptation effect with or without filling-in, in experiment 2, we asked the participants to report whether they experienced perceptual filling-in during adaptation in the annulus condition immediately after each trial. This way, we could separately estimate the adaptation effect for filling-in and non-filling-in trials.

The data of three observers in experiment 2 are presented in Figure 2.3b (individual-subject data in Supplementary Figure A.2 in Appendix A). Compared with the data when filling-in was not reported, the orientation shift was larger when filling-in occurred. A 2-way repeated measure ANOVA was conducted on the averaged data across the three observers to compare the main effects of filling-in and five adapter orientations, as well as the interaction between these two factors. The filling-in main effect was significant ($F(1, 18) = 15.11$, $p < 0.01$, $\hat{f} = 0.69$), suggesting that the TAE was stronger when filling-in was perceived during adaptation. The main effect of adapter orientation was also significant ($F(4, 18) = 9.99$, $p < 0.01$, $\hat{f} = 1.09$), suggesting that the TAE varied across different adapter orientations. The interaction between filling-in and adapter orientation was not significant ($F(4, 18) = 0.92$, $p = 0.48$) suggesting that the orientation-tuning of the aftereffect was not altered by filling-in. The results agree well with the positive correlation across different subjects between the filling-in score and target orientation shift observed in experiment 1 (see Figure 2.3a).

To verify whether the observer's fixation differed across different adapter condition, we estimated the fixation stability of the three participants with an eye tracker. The video device records the horizontal and vertical eye positions during the stimuli presentation on each trial in the following four conditions: the pedestal adapter, the annulus adapter, and the disk adapter in experiment 1, and the annulus adapter in experiment 2 (in which results are sorted into filling-in and no filling-in trials based on the subjectively reported filling-in percept during adaptation). All

adapters used in the fixation stability test had the same (11.25 degrees) orientation. We preprocessed the raw eye tracking data by removing timepoints with missing data (e.g. when observer blinked during the stimulus presentation) and ruling out eye positions that surpass 3.3 degrees in amplitude (10 times the normal range of microsaccade, which is usually less than 20' (Carpenter, 1988)) in radius to exclude outliers and potential recording artifacts.

We estimated the fixation stability of each trial by calculating the bivariate normal ellipse area (BCEA) value in each trial defined by the following equation (Castet & Crossland, 2012; Schönbach et al., 2017),

$$BCEA = 2k\pi\sigma_H\sigma_V(1 - \rho^2)^{0.5},$$

where σ_H and σ_V are the standard deviations of the horizontal and the vertical fixation positions, and ρ the Pearson's correlation coefficient between the two fixation positions. k is a constant determining the probability area as in

$$P = 1 - e^{-k},$$

in which e is the base of the natural logarithm and P the probability area. We used a k value of 3.079 which leads to a P of 0.954. Figure 2.4 demonstrates the averaged orientation shift of the CCW target and the BCEA value across the three participants in different adapter conditions.

Figure 2.4

The Averaged CCW Target Orientation Shifts (TAE) and BCEA Values Across Three

Participants in Different Adapter Conditions
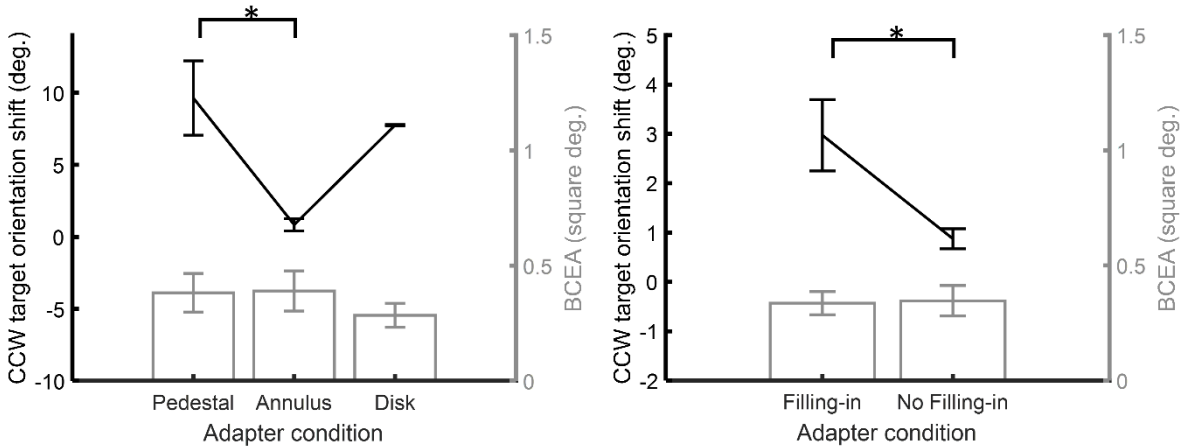
Note. In both panels, the line represents the orientation shift plotted against the adapter condition with value and unit

corresponding to the left y-axis, while the bars represent the BCEA plotted against the adapter condition with

reference to the right y-axis. The left panel shows the three conditions in experiment 1: the pedestal, the annulus and

the disk adapters. The right panel shows the two conditions in experiment 2: the filling-in and no filling-in conditions

(both with the annulus adapter). The error bars depict ±1 standard error of measurement. The asterisk symbol

demonstrates which two conditions/trial-types are significantly different (p < 0.05).

One-way repeated measure ANOVAs on the orientation shifts and the BCEAs in

experiment 1 data were conducted. The one-way ANOVA conducted on the mean orientation

shift shows that there is a difference between different adapter types ($F(2, 4) = 10.93, p < 0.05, \hat{f}$

$= 0.62$). The pairwise post-hoc Tukey HSD (honestly significant difference) multiple comparison

test indicates that the pairwise contrast between the pedestal and the annulus ($qT(3,6) = 6.28, p <$

0.05) exceeds the critical difference, whereas the contrast between the pedestal and the disk

($qT(3,6) = 1.34$, $p = 0.64$) as well as the contrast between the disk and the annulus ($qT(3,6) =$ 4.93, $p = 0.05$) did not. In contrast, the one-way ANOVA computed for the BCEA values revealed no significant difference between the adapter types ($F(2, 4) = 4.40$, $p = 0.10$). Again, the paired t-test done on the perceived target orientation shifts of the two conditions in experiment 2 shows that there is a difference between the two ($t(2) = 3.95$, $p < 0.05$), whereas the t-test on the BCEA values when filling-in was compared with when it was not reported failed to show a significant difference ($t(2) = -2.16$, $p = 0.16$). These statistics suggest that there was no significant difference between the fixation stability across different adapter types, although they induced different magnitudes of the TAE. Nor did we find evidence for differences in fixation stability on trials where subjects perceived filling-in compared to when they did not.

Model

Model architecture

Contrast gain control or divisive inhibition has been proposed to explain a wide range of visual phenomena and can be observed as early as the processing stage of the retina. This normalization process has also been identified in areas such as in LGN (Bonin et al., 2005) and primary visual cortex (Albrecht & Geisler, 1991; Gardner et al., 2005; Heeger, 1992; Müller et al., 2003; Ohzawa et al., 1985). Wilson and Humanski (Wilson & Humanski, 1993) used a contrast gain control model to explain the contrast threshold elevation after adaptation to cosine gratings of selected spatial frequencies. Their model could account for the TAE data from Campbell and Maffei (1971). Similarly, Foley and Chen (1997) proposed a two-process divisive inhibition model, in which the adaptation affected up to two parameters in the denominator, to interpret the pattern adaptation effect on target contrast threshold. Meese and Holmes (2002) proposed an alternative gain

control model (where one adaptation factor was introduced in the denominator) to explain their own masking data and the adaptation data of Foley and Chen (1997).

We used a variant of divisive inhibition (or contrast normalization) model to fit our TAE data. Our model is inspired from both Foley and Chen (1997), in which the adaptation effect was captured by increases in the parameters in the denominator, and Chen and Tyler (2001), in which the lateral modulation effect from the flankers was represented by multiplicative parameters. Figure 2.5 demonstrates a schematic diagram of the current model. In the current model, we assumed multiple orientation channels (as local mechanisms in one hypercolumn) with preferred orientations distributed evenly from -90 degrees to 90 degrees (with CW orientation assigned negative values, and CCW positive values) degrees at intervals of 11.25 degrees. The tuning bandwidth (full width at half maximum, or FWHM) of all channels was set at 22.5 degrees. The response of each oriented channel towards the target first goes through a receptive field-like linear operator (the linear filter in Figure 2.5) then a nonlinear operator. The final response predicted by the model is determined by the excitatory component divided by the inhibitory component and an additive constant.

Figure 2.5

The Schematic Diagram of the Model Used in the Current Study
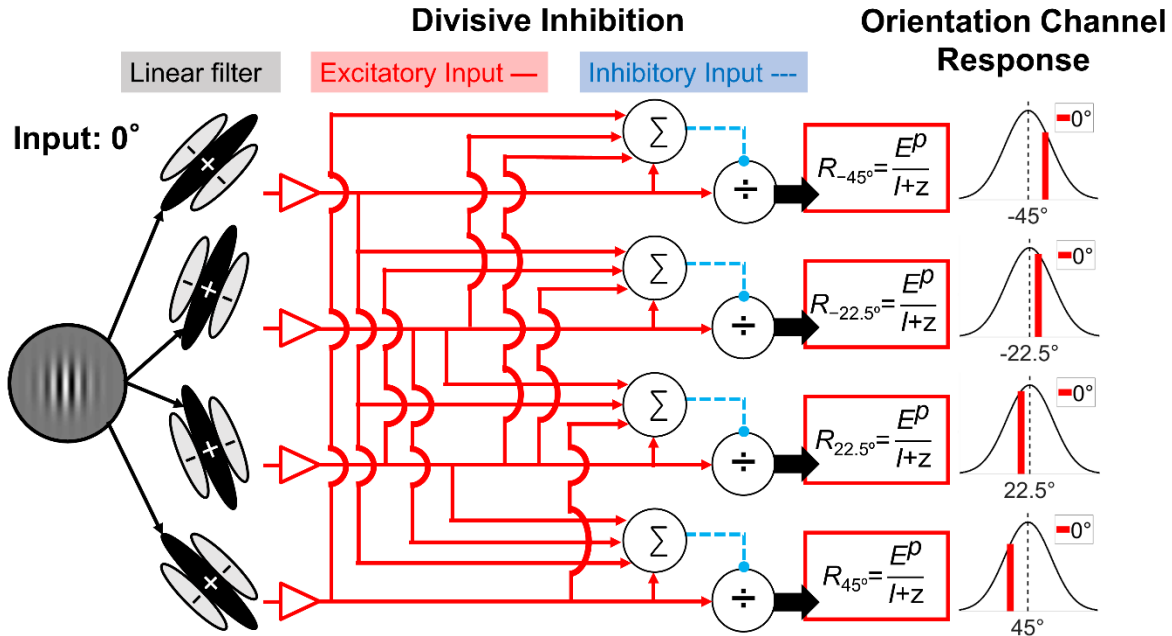
Note. The orientation channel response to the target is determined by an excitatory component (E) raised by a power (p) then divided by an inhibitory component (I) plus a constant (z). See text for detailed description.

The excitation of the linear operator in channel j towards the target is determined by the product of the sensitivity profile of the linear operator and the input image (C.-C. Chen et al., 2000; Foley & Chen, 1999; Phillips & Wilson, 1984). Here we assume the profile to be a Gabor function and the input image to be also a Gabor pattern (see section *Stimuli* in Method). The input image could be either the target or the adapter. The product of the Gabor function and the Gabor pattern, integrated over space can be factored into the following components: (1) Because the input contrast, C_i of the ith image component (such as the target, or one of the adapters), is independent of the spatial structure, it can be taken out as an individual term. (2) The orientation dependent component that can be captured by an orientation tuning function, O_j. And (3) The orientation independent part of product

that can be taken as a constant in our experiment. We called this constant the sensitivity

parameter, Se_i. The excitation of the jth channel to the ith image component can thus be

defined as,

$$E'_{ij} = Se_i \cdot C_i \cdot O_j(\theta_i). \tag{2.1}$$

The orientation tuning function, in our case, is assumed to be a Gaussian function, as has

been implemented in studies modeling neuron tuning curves and psychophysics data

(Deneve et al., 1999; M A Paradiso, 1988; Pouget et al., 1998, 2000; Schwartz et al.,

2007; Westrick et al., 2016; Wilson & Humanski, 1993). That is,

$$E'_{ij} = Se_i \cdot C_i \cdot e^{-\frac{(\theta_i - \theta_j)^2}{\sigma^2}}, \tag{2.2}$$

where the θ_j is the channel preferred orientation and σ^2 the channel variance which

determines the channel bandwidth.

The linear operator excitation in Equation 2.2 is then halfwave-rectified (C.-C.

Chen & Tyler, 2001, 2002; Foley, 1994; Foley & Chen, 1997, 1999) into

$$E_{ij} = max\ (E'_{ij}, 0), \tag{2.3}$$

where max represents the operation to select the larger to the two numbers. Without

adaptation, the channel response to the ith input image is computed by the rectified

excitation raised by the power p then divided by the inhibitory component I_{ij} as well as

the normalization constant z. That is,

$$R_{ij} = \frac{E_{ij}{}^p}{I_{ij} + z}. \tag{2.4}$$

The inhibitory component is the summation of all relevant mechanisms (in our case, N

channels), given by

$$I_{ij} = Si_1 \cdot (E_{ij})^q,\tag{2.5}$$

where Si_1 is the inhibition sensitivity of the jth channel (self-inhibition).

The perceived orientation is determined by a population coding operation, which is

the preferred orientation of each channel, θ_j, weighed by the response of that channel, R_{ij},

divided by the sum of responses of all channels (Clifford et al., 2001; Deneve et al., 1999;

Jin et al., 2005; Mély et al., 2018; Pouget et al., 1998; Westrick et al., 2016) and the

adjusted by an internal bias parameter, m. That is

$$P_i = \frac{\sum_{j=1}^{N} R_{ij} \cdot \theta_j}{\sum_{j=1}^{N} R_{ij}} + m.\tag{2.6}$$

The internal bias parameter is needed because the observers might make a CW or CCW

match to the target even in the control conditions void of experimental manipulation.

Modeling implementation

In our experiment, each trial started with prolonged exposure to an adapter. In

adaptation, the visual system adjusts its response characteristics to accommodate the

current visual environment (Barlow, 1972; Barlow & Földiák, 1989). Indeed, the dynamic

range of the contrast response function of V1 neurons can be changed following a prolong

exposure to a stimulus (Albrecht et al., 1984; Anderson et al., 1997; Gardner et al., 2005;

Sclar et al., 1989). Such dynamic range shift can be modelled with a change in the semi-

saturation parameter of a Naka-Rushton (Naka & Rushton, 1966) type model of contrast

response function. In our model, a shift of the dynamic range can be achieved by a change in parameter z in Equation 2.4.

In psychophysics, Foley and Chen (1997) found that, in addition to the additive constant (z in Eq. 4), the sensitivity of the target mechanism to the inhibitory signals from the mechanisms that tune to the orthogonal orientation also increased after adapting to a Gabor pattern. The cross-orientation inhibition can be captured by a term in the inhibition part which is the summation of the excitations across channels. The experiments of Foley & Chen (1997) systematically varied the contrast of the cross-orientation components of the image and thus the cross-orientation inhibition to the response function. In our experiment, all the stimuli had the same contrast. As a result, the sum of the responses across orientation channels, and in turn the cross-orientation inhibition, would be similar for targets of any orientation and thus can be absorbed by the additive constant, z. Therefore, for the current experiment, we only need to consider the change of the additive constant z following the adaptation. That is, after adaptation, the response function in Equation 2.5 becomes,

$$R_{ij} = \frac{E_{ij}{}^p}{I_{ij}+z'_j} = \frac{E_{ij}{}^p}{I_{ij}+z\cdot a_j}, \tag{2.7}$$

and

$$a_j = (1 + R_{kj}),$$

in which R_{kj} is the response of channel j to the kth adapting stimulus, which can be computed in the same way as the response with Equations 2.1-2.5. Notice that, there were different types of adapter in our experiment. Thus, we allowed the excitatory sensitivity to each type of adapter, Se_i, to be a free parameter.

We fitted the model to the group averaged data (as shown in Figure 2.2 and 2.3) with a Powell's algorithm (Press et al., 1988) to search for the parameter values that minimize the sum of the squared differences between the measured and predicted TAE reported for the target, or sum of squared error (*SSE*). The set of the best fit parameters is shown in Table 2.1. The smooth curves in Figures 2.2 and 2.3 represent the fits.

For experiment 1, the model can explain up to 86.2% of the variance in the averaged data. The root mean square error (*RMSE*) was 0.90, slightly larger than the mean standard error of measurement, which was 0.56. For experiment 2, the model can explain 75.6% of the variation in the averaged CCW data. The *RMSE* was 0.20, compatible with the mean standard error of measurement, which was 0.32.

Table 2.1 shows the best-fitting parameters for both experiment 1 and experiment 2 (the best-fitting parameters of individual-subject data can be found in Supplementary File S4, a Microsoft Excel file in which each sheet contains data of all participants of one experiment). Except for p, q, Si_1, m, and Se in the annulus and the disk conditions in experiment 1 as well as the Se in the no filling-in trials in experiment 2, all parameters were fixed (6 free parameters in total), because the goodness of fit (R^2) did not change empirically if they were free parameters or fixed. For the same reason, parameter z can be fixed as 0.50.

Table 2.1

List of Fitting Parameters and R^2 for the Averaged CCW Orientation Shifts of Orientation-Grating Stimuli and the Gray Control/No Adapter Condition.

PARAMETER		
Se		
	Target	**100.00**
	Pedestal	**100.00**
	Annulus	1.01
	Disk	38.7900
	Control[*]	**0.00**
	Filling-in	**10.00**
	No filling-in	1.22
Si_1	Exp 1	0.38
	Exp 2	0.74
p	Exp 1	1.26
	Exp 2	0.77
q	Exp 1	0.35
	Exp 2	0.41
z		**0.50**
σ		**9.56**
m	Exp 1	-1.92
	Exp 2	-0.63
R^2	Exp 1	0.862
	Exp 2	0.756
RMSE	Exp 1	0.90
	Exp 2	0.20

Note. Fixed parameters are marked with bold font. [*]The same set of parameters were used to fit the three control conditions (the noise annulus, the noise disk and the gray control) in experiment 1. Six free parameters were used to fit the data of experiment 1 (*Se* in the annulus and the disk conditions, Si_1, p, q, and m) and 2 (*Se* in the filling-in and no filling-in conditions, Si_1, p, q, and m).

The parameter *Se* reflects the channel sensitivity to the adapter *center*, which has the same spatial profile as the target. Thus, changes in *Se* represents the amount of lateral modulation introduced from the adapter surround to the adapter center. For comparison purposes, we fixed the *Se* value in the pedestal condition at 100 as the baseline in experiment 1 to compare between the lateral modulation effect in different adapter conditions. Values above 100 represent a stronger adaptation effect, whereas those below 100 a weaker effect. The lateral modulation effect induced from the adapter surround can be either excitatory or inhibitory. If the modulation effect is excitatory, then after adaptation, such lateral excitation should enhance the adaptation effect on the adapter center. If, on the other hand, the adapter surround induces an inhibitory effect, then when the surround was introduced during adaptation this lateral inhibition should lead to a decrease in the TAE. In our case, when the surround was present in the disk condition, *Se* value decreased to below 40, suggesting a significant decrement of the adaptation effect. The model fitting result agrees well with the empirical finding that the target orientation shift was less in the disk condition than in the pedestal condition, indicating a lateral inhibition effect from the surround.

To examine whether different *Se* values in the model produces a better fit, we also conducted a model comparison between (a) the full model (the current model, in which *Se* is free parameter except for the pedestal condition, leading to six free parameters) and (b) the reduced mode (when all *Se* are fixed as 100.00, thus only four free parameters left). The coefficient of determination R^2 was reduced substantially from 0.861 to 0.56 in the fitted results of the reduced model. An F-test between the two models showed that the full model can explain significantly more variance than the reduced model ($F(2, 12) = 12.09$, $p = 0.0013$). Such results suggested that the amount of lateral modulation from the surround to the center varied across different adapters.

To test whether the filling-in and no filling-in trials demonstrate different characteristics in model fitting, we fitted the same aforementioned model to the experiment 2 data. Here for the purpose of comparison across conditions, we fixed the *Se* for the filling-in condition at a value of 10 and allowed the *Se* for the non-filling-in condition to be a free parameter. The best fits (as shown in Table 2.1) *Se* for the non-filling-in condition was much lower than that for the filling-in condition, suggesting that the adaptation effect was weaker when perceptual filling-in was not perceived.

2.5 Discussion

To understand how the adapter stimulus affects the central target percept, we used sinusoidal adapters either covering the center, the surround, or both stimulus regions. Our results in the experiment 1 showed that the adaptation effect on the Gabor target, reflected by the TAE that shifted the perceived target orientation in a direction opposite to that of the adapter, was greatest in center-only (pedestal), intermediate in center-surround (disk), and smallest in surround-only (annulus) condition (see Figure 2.2a). The difference between the pedestal and the disk condition suggests that adding a surround decreases the adaptation effect of the center, indicating an inhibitory lateral modulation from the surround. Although there was no spatial overlap between the adapter and the target in the annulus condition, a significant TAE was still induced after adaptation. This finding suggests that during adaptation, the adapter surround induced the TAE at the adapter center that was vacant of physical stimulus, thereby leading to a perceived shift in target orientation. We also found a positive correlation between the self-reported strength of perceptual filling-in during adaptation and the TAE magnitude across observers. This result can be taken as evidence for adapter surround contribution to both perceptual filling-in and the adaptation effect. To better discuss the nature of the TAE and its

relationship to perceptual filling-in, we turn to the results of the second experiment. In experiment 2, we estimated the orientation shift on trials when perceptual filling-in was reported and when no filling-in was reported and found that the orientation shift was larger when perceptual filling-in was experienced in the annulus adapter. Our results indicate that the perceived filling-in during adaptation reflects the strength of the subsequent TAE. These findings suggest that exposure to the adapter surround acts to alter contrast gain in the central target region during the adaptation period and this effect is more pronounced when observers experienced filling in. To account for the underlying mechanism of the adaptation effect, we propose a computational model.

The adaptation effect was modelled in the same way as Foley and Chen (1997), who suggested that the additive constant in the denominator of the response function increased after adaptation. We thus implemented the adaptation effect in a mechanism by multiplying the additive constant, z, in the denominator of the response function by an adaptation factor (Equation 2.7), which in turn was determined by its response to the adapter. The stronger a mechanism responded to an adapter, the more adaptation effect it exhibited.

The effect of different adapters was manifested as a change of just one parameter Se (the excitatory sensitivity). We found that Se was smaller in the disk condition than in the pedestal condition (see Table 2.1). Notice that the disk adapter had a larger size and thus potentially greater overlap with the receptive fields of the target channels than the pedestal adapter. Such reduction of sensitivity is not consistent with the effect of spatial summation (C.-C. Chen et al., 2019). Instead, it implies that the extra area of the disk provides an inhibitory signal to the target channels and makes it less sensitive to the input stimuli.

The *Se* value for the annulus condition reflects the effect from the surround in the absence of the adapter center. In the experiment 2, where only annulus adapter was used, the change of parameter *Se* reflected the TAE induced from the surround, which corresponded in magnitude to the subjective filling-in percept of the observers. Thus, our model captured the effect of the surround region that simulated both the perceived orientation shift and the perceived filling-in. However, the current model provides no direct indication as to the cause or underlying mechanism of filling-in. One possibility is that the surround region actively modulates the center filled-in region through lateral interactions (C.-C. Chen et al., 2005; Komatsu, 2006; Komatsu et al., 2002). Because the empirical data reported in the literature, including neuroimaging results, show evidence supporting both lateral inhibition and lateral excitation during perceptual filling-in, it could be that filling-in percept results of an interplay between the excitatory and inhibitory lateral interaction from the surround feature to the central blank regions. Alternatively, it is also suggested that the center region is filled-in due to sensitivity loss at the boundary between the blank area and the surrounding context, that is, the isomorphic theory (Cohen & Grossberg, 1984; Gerrits & Vendrik, 1970; Kinoshita & Komatsu, 2001; Neumann et al., 2001). Yet, another possibility is related to the idea that the brain simply "ignores" the missing information and assumes a complete surface, or the symbolic or cognitive theory (Pessoa et al., 1998; von der Heydt et al., 2003). The limitation of the current study is that although the adaptation paradigm is useful for revealing the effect of different adaptors, it is difficult to pinpoint the exact neural activation or neural mechanism during perceptual filling-in even with the help of a model. In our current model, the value of parameter *Se*, excitatory sensitivity to the adapter center, reflects the strength of TAE, and perceived filling-in induced by the annulus adapter. However, the fact that the variation in *Se* could be the result of many possible factors, such as differences in lateral interaction, different levels of induction from mechanism sensitive both to the center and

surround, changes in boundary sensitivity and even some top-down influences from higher brain regions, we could not determine the source of the filling-in perceived by observers in the current study. Such a limitation could be overcome by implementing neuroimaging methods, such as fMRI in future studies.

To make sure that the difference in TAE between different adapter conditions did not originate from differences in how well the participants maintained their fixation, we conducted a control experiment to estimate the fixation stability in each condition with an eye tracker (see section on Fixation Stability Test in Method). We calculated the BCEA (bivariate normal ellipse area) values considering the fixation variability in the vertical and the horizontal directions. We found that neither the BCEA values among the pedestal, the annulus, and the disk adapter conditions differ (Figure 2.4 left panel) nor did they vary with the self-reported filling-in percept (Figure 2.4 right panel), even when the orientation shifts in different conditions were significantly different in both cases. Such results suggested that the TAE magnitude changes observed in experiments 1 and 2 cannot be explained by differences in fixation stability during adaptation.

2.6 Conclusions

In experiment 1, we used three different adapters that occupied the center, the surround, and both the center and surround regions to induce TAE which resulted in a perceived orientation shift of the target Gabor viewed in eccentric vision. Regardless of the adapter type, the orientation shift first increased then decreased as the adapter orientation moved further away from the target orientation, peaking between 10 degrees to 20 degrees, suggesting that the adaptation effect was orientation specific. The adaptation effect was strongest when the adapting stimulus had the same spatial extent as the target (pedestal condition, center-only). The adaptation effect decreased when the adapter surround was introduced (disk condition, center and

surround), indicating an inhibitory modulation from the surround to the center. This suggests that the surround induced lateral inhibition in the central region. The adaptation effect was smallest, but still significant, in the annulus (surround-only) condition when the adapter had no physical overlap with the target. In addition, observers who perceived stronger filling-in during the annulus adapter condition also perceived a stronger TAE.

In experiment 2, we used only the annulus adapter and recorded the subjectively reported filling-in percept after every trial to estimate the orientation shift separately for filling-in and non-filling-in trials. We discovered that the orientation shift was larger when filling-in occurred. Control measurements in a subgroup of participants indicated that our findings cannot be explained by differences in fixation stability across the different adaptation conditions. Together with the finding of a positive correlation between the strength of filling-in and the magnitude of the TAE in experiment 1, we conclude that the filling-in percept is associated with a stronger adaptation effect.

We adapted a divisive inhibition model to account for our results. In the model, we assumed that the observed adaptation effect was the result of an increase in the additive constant, z, in the denominator, leading to a reduction of the channel response after adaptation, as was observed in the literature (Foley & Chen, 1997). The magnitude of the adaptation effect is decided by the response of the local mechanism to the adapter, which is determined by the excitatory sensitivity parameter, Se, in the numerator. This sensitivity modulation has been shown to be crucial for surround modulation in other studies (C.-C. Chen et al., 2001; C.-C. Chen & Tyler, 2002).

3. CHAPTER 3: STUDY 2 "THE ROLE OF LATERAL MODULATION IN ORIENTATION-SPECIFIC ADAPTATION EFFECT"

Author-produced version of an article published after peer-review on February 22nd 2022 in Journal of Vision, an open access journal. DOI: 10.1167/jov.20.9.5. The supplementary files that are not included in the thesis (Supplementary File S1 and S2) can be downloaded from the JOV page: https://jov.arvojournals.org/article.aspx?articleid=2778591.

3.1 Abstract

Center-surround modulation in visual processing reflects a normalization process of contrast gain control in the responsive neurons. Prior adaptation to a clockwise (CW) tilted grating, for example, leads to the percept of counterclockwise tilt in a vertical grating, referred to as the tilt-aftereffect (TAE). We previously reported that the magnitude of the TAE is modulated by adding a same-orientation annular surround to an adapter, suggesting inhibitory lateral modulation. To further examine the property of this lateral modulation effect on the perception of a central target, we here used center-surround sinusoidal patterns as adapters and varied the adapter surround and center orientations independently. The target had the same spatial extent as the adapter center with no physical overlap with the adapter surround. Participants were asked to judge the target orientation as tilted either CW or counterclockwise from vertical after adaptation. Results showed that, when the surround orientation was held constant, the TAE magnitude was determined by the adapter center, peaking between 10° and 20° of tilt. More important, the adapter surround orientation modulated the adaptation effect such that the TAE magnitude first decreased and then increased as the surround orientation became increasingly more different from that of the center, suggesting that the surround modulation effect was indeed orientation specific. Our data can be accounted for by a divisive inhibition model, in which (1) the adaptation effect is represented by increasing the normalizing constant and (2) the surround modulation is captured by two multiplicative sensitivity parameters determined by the adapter surround orientation.

Keywords: lateral modulation, surround inhibition, tilt-aftereffect, spatial vision, divisive inhibition

3.2 Introduction

The concept of lateral modulation describes how the visual percept of a central stimulus can be affected by the presence of a surround pattern. Such lateral modulation of the stimulus surround on sensitivity to the stimulus center has long been recognized (De Weerd & Pessoa, 2003; Gilbert & Wiesel, 1990). Examples of the lateral modulation effect includes visual crowding, perceptual grouping, figure-ground segregation, tilt-illusion, and perceptual filling-in (Clifford, 2014; Komatsu, 2006; Schwartz et al., 2007, 2009; Solomon et al., 2004; Spillmann & Werner, 1996). At the cortical level, it is shown that even if a stimulus presented to a region outside the classical receptive field (CRF) does not elicit neural activity, it can modulate the neuronal response to a central stimulus, suggesting that such lateral modulation effects extend beyond the typical classical receptive field (Barlow, 1953; Bringuier et al., 1999; Cavanaugh et al., 2002a, 2002b; C.-C. Chen et al., 2001; Hubel & Wiesel, 1959; Maffei & Fiorentini, 1976). This long-range lateral modulation effect suggests that neurons responding to the center and surround regions of the visual field do not work in isolation but rather interact and integrate the activity of nearby neurons.

The lateral modulation effect has been the focus of numerous studies that implement various paradigms to investigate the observed phenomena. For example, in psychophysical experiments, the perceived contrast of a central stimulus can be decreased or enhanced by a surrounding pattern, and such a lateral modulation is tuned to the surround features such as luminance contrast, spatial frequency, size, and orientation (Cannon & Fullenkamp, 1991; Chubb et al., 1989; Meese et al., 2007, 2009; Petrov et al., 2005; Petrov & McKee, 2006; Polat & Sagi, 1993; Snowden & Hammett, 1998; Solomon et al., 1993, 1999; Yu et al., 2001, 2002). For example, Yu, Klein and Levi (2001) reported that the perceived contrast of the stimulus center

was suppressed when the center and surround patterns were of the same orientation, whereas it was enhanced when the center and surround orientations were orthogonal. Such lateral modulation can differ in foveal and peripheral vision. The lateral modulation effect was found to be both facilitative and suppressive in the fovea, but was only suppressive in the periphery (Xing & Heeger, 2000). In a dual-masking paradigm, in which a Gabor target is presented with a superimposed pedestal grating of various contrast level while surrounded by flankers, Chen and Tyler (2001, 2002) showed that colinear flankers produced a facilitative effect on the target threshold at low pedestal contrasts while they induced a suppressive effect at high contrasts. In comparison, orthogonal flankers could only produce suppressive effects on the central target threshold (also see Meese, Summers, Homes, and Wallis, 2007; Meese et al., 2009; Solomon and Morgan, 2000; Chen and Tyler, 2002, 2008).

In addition to psychophysical experiments, single cell recording studies also provide insights into the lateral modulation effect and its properties. Many studies showed that lateral modulation from the surround depends on the spatial configuration and luminance contrast of the center and surround stimuli (Blakemore & Tobin, 1972; Kapadia et al., 1999; Levitt & Lund, 2002; Nelson & Frost, 1978, 1985; Sengpiel et al., 1998; M. A. Smith et al., 2006). Among them, Polat and colleagues (1998) manipulated the contrast of the target that was presented within the cell's receptive field of the cat as well as the contrast and orientation of two lateral flankers located outside of the receptive field. They discovered that high-contrast collinear flankers facilitated the response of the neurons to the low-contrast target and suppressed the response to high-contrast targets, whereas orthogonal flankers showed mostly a suppressive effect on the target response. In a later study, Chen and colleagues (2001) reported four types of contrast-dependent lateral modulation effects and proposed a sensitivity modulation model to explained the single-neuron recording data. Some researchers used gratings in different sizes and contrasts

to estimate the summation receptive fields of neurons in macaque V1 and discovered that the summation receptive field measured at a low contrast was larger than that measured at high contrast (Li & Li, 1994; Sceniak et al., 1999; Sengpiel et al., 1997; Shushruth et al., 2009). Thus, the effect of the surround on the neuronal activity is contrast dependent, that is, it is suppressive at high contrast and facilitative at low contrast.

Neuroimaging studies have also revealed possible neural correlates of the lateral modulation effect. In one functional magnetic resonance imaging study, Williams and colleagues (2003) reported that adding a surround grating to the central pattern reduced the blood-oxygen level-dependent signal in early visual areas and that a parallel surround grating produced a stronger signal decrease, suggesting an orientation-specific lateral suppression effect. Similarly, another study (C.-C. Chen et al., 2005) showed in a functional magnetic resonance imaging experiment, where a flickering pinwheel pattern was presented, that the unstimulated interwedge regions was associated with a decreased blood-oxygen level-dependent signal, indicating a lateral inhibition effect from the surrounding areas. In another functional magnetic resonance imaging study involving a lateral masking paradigm (a central grating is surrounded by collinear and noncollinear flankers), Chen (2014) further partitioned the lateral suppression effect into a more general inhibition effect insensitive to spatial features of the surround as well as a more specific effect tuned to the surround spatial configuration.

Several computational models have been proposed to account for the lateral modulation effect. Chen and Tyler (2001, 2002) proposed a divisive inhibition (or contrast gain control) model using multiplicative sensitivity parameters to explain the flanker effect observed in their dual masking experiments. Xing and Heeger (2001) put forth a variant of the contrast gain control model to explain the center-surround modulation under different surround configurations

by including weights that represent surround facilitation and suppression. Schwabe and colleagues (2006) proposed a recurrent network model that considers the top-down feedback connections in the visual cortex to account for the near- and far-surround modulation. Their model successfully predicts the contrast-dependent lateral modulation subsequently observed in macaques (Schwabe et al., 2010). In a later review, Angelucci et al. (2017) proposed a theoretical model that involved feedforward, feedback, and horizontal connections to explain the surround modulation effects.

Previous studies of center-surround modulation focused more on how the lateral interaction influences the target contrast discrimination (C.-C. Chen & Tyler, 2002; Meese et al., 2007; Xing & Heeger, 2000) or perceived contrast (Cannon & Fullenkamp, 1991; Yu et al., 2001, 2002) and less on how the target orientation percept can be affected by an adapter modulated by surround features. Many neurons in the visual cortex are tuned to stimulus orientation and neurons tuning to neighboring orientations can inhibit each other (Blakemore et al., 1970; Blakemore & Tobin, 1972; Carpenter & Blakemore, 1973; Hubel & Wiesel, 1962, 1968); thus, it is also important to explore the effect of lateral modulation in the orientation percept.

The tilt illusion and the tilt-aftereffect (TAE) are two visual phenomena commonly studied to understand the orientation domain of human vision (Clifford, 2014; Gibson & Radner, 1937). The tilt illusion describes the situation when a surround oriented-grating alters the perceived orientation of a center grating to the opposite direction of the surround orientation, whereas the TAE demonstrates that the perceived orientation of a target grating can be tilted away from a preceding oriented adapter. In both cases, the effect is the strongest when the surround pattern or the adapter has orientation close to (10°–20° away from) the center stimulus or the target, indicating that neurons tuned to similar orientations inhibit each other, which results

in the visual illusion and aftereffect of a tilt adaptation. Magnussen and Kurtenbach (1980)

reported that adding a second adapting pattern ranging from 6° to 60° clockwise (CW) to a 15°

CW adapter decreased the TAE on the subsequently presented vertical target. The authors

concluded that a lateral inhibition process was involved because the inhibitory effect from

neurons inhibiting the vertical (and near vertical) orientation channels cause by the first adapter

was inhibited by the second adapter (see also Kurtenbach and Magnussen, 1981). Similarly,

Greenlee and Magnussen (1987, 1988) implemented a method of sequential adaptation in which

two adapting patterns were alternating in time during the adaptation phase and estimated the

contrast threshold of a following target grating. Their results showed that, when the two adapting

gratings were of the same spatial frequency or orientation, the target threshold increased,

suggesting a suppressive effect. In contrast, the contrast threshold decreased as the second

adapting grating deviated from the first in spatial frequency and orientation and even went below

the level when only one adapter was presented, indicating an inhibitory effect between the two

adapting patterns. Adaptation effects involving patterns with multiple oriented components

provided further insights in how gratings interact with each other. For example, the plaid pattern

composed of two oblique sinusoidal gratings can be perceived as a blurred checkerboard of

horizontal and vertical edges. Such compound checkerboards became distorted after adaptation to

one oblique grating, suggesting that the adaptation process interfered with the combination and

interaction between responses to the two oblique gratings resulting from combining responses of

two orientation filters (Georgeson, 1992; Georgeson & Meese, 1996). Later, Meese and

Georgeson (1996a, 1996b) used plaids and gratings varied in orientation and contrast as adapters

and recorded whether the participants perceived the test plaid as a compound pattern or

individual components. They found that the adapter plaid with a 45° rotation from the test plaid,

but of the same spatial frequency decreased the percentage of the compound response, whereas

CHAPTER 3: STUDY 2

the aligned adapter plaid, that is, having the same orientation but with a spatial frequency that was three times higher, increased the percentage of the compound response. These results show that the filter combination process after adaptation depends on the difference in spatial configuration between the adapter and the test stimulus. In addition, adaptation to a vertical and horizontal grating made the test plaid look stretched horizontally and vertically, indicating the presence of a TAE in the compound percept. These studies demonstrated the power of the adaptation paradigm in revealing how two patterns overlapping spatially interact with each other. Here, our study focused instead on the interactions between patterns not overlapping in space; that is, how the surround pattern affects the neural response to the center pattern. Thus, we adapted the TAE paradigm to further investigate how the center and surround regions of the adapter could interact with each other and inferred the lateral modulation effect during the adaptation phase.

In a previous study (Lin et al., 2020), we selectively adapted the center, the surround, and both the center and the surround regions using a center-surround sinusoidal grating as an adapter in the periphery and estimated the magnitude of the TAE on the target. We used three types of adapters: a center adapter that had the same spatial extent as the target, a disk adapter that covered both the center and surround regions, and an annulus adapter that was located in the surround region without physical overlap with the target. We found that the TAE was most pronounced for the center adapter, intermediate for the disk adapter, and weakest for the annulus adapter. The decrease in the TAE magnitude of the disk condition compared with the center condition indicated an inhibitory lateral modulation effect from the adapter surround. The limitation of the previous study is that in the disk condition, the adapter surround always had the same orientation as the adapter center. Therefore, we could not capture how the lateral

modulation effect on the adapter center would change if the adapter surround was of a different orientation, which now is the focus of the current study.

Studying the effect of the adapter surround orientation on the adapter center allows us to observe how the TAE changed quantitatively with varying surround orientations, leading us to investigate the cross-orientation interaction of the lateral modulation effect in the orientation domain. Therefore, to further investigate the property of such a lateral modulation effect here, we manipulated the surround and center orientations independently. By doing so, we can observe how much the lateral modulation effect from the adapter surround was induced on the adapter center by measuring the changes in TAE on the subsequently presented target. In an adaptation paradigm, a center-surround adapter was presented followed by a target Gabor, about which participants were to make an orientation judgement. We measured how the TAE induced on the target depended on the adapter center and surround orientations. Because many earlier studies have shown that such lateral modulation depends on the surround features, we expect to observe an orientation-specific modulation on the TAE as the surround orientation is varied. A contrast gain control (or divisive inhibition) model has been shown to be able to explain the lateral modulation effect reported in psychophysics experiments (C.-C. Chen & Tyler, 2001, 2002; Clifford, 2014; Goddard et al., 2008; Meese et al., 2007; Schwartz et al., 2009; Xing & Heeger, 2001) Therefore, we fitted a modified divisive inhibition model inspired by the previous studies (C.-C. Chen & Tyler, 2001, 2002; Foley & Chen, 1997; Lin et al., 2020) to our data and examined how the model parameters capturing the lateral modulation effect varied with changes in the surround orientation. If the lateral modulation effect is independent of the surround orientation, then the TAE magnitude should remain constant regardless of the variation in the surround orientation. In contrast, if the lateral modulation effect is feature specific, then the TAE magnitude should be different across conditions of different surround orientations.

3.3 Methods

Participants

Four observers, aged between 20 and 30 years, including one of the authors (Y.S.L., referred to in the following as P0) and three participants naïve with respect to the purpose of the experiment (P1–P3) participated in the study. All observers have normal or corrected-to-normal vision. Informed consent was acquired before participation for all participants. The study procedure and protocols were approved by the University of Regensburg ethics committee (application number: 19-1591-101) and the experiment was performed according to the Declaration of Helsinki on human experimentation. Participants (except for P0) received monetary compensation or class credits as a reward for their participation. All observers first performed a short practice session to become acquainted with the stimuli and the task before continuing the formal experiment.

Apparatus

Participants viewed stimuli on a Dell S2417DG 24-inch LED monitor with 2560×1440 pixel resolution and 120 Hz refresh rate in a viewing distance of 60 cm. The monitor was calibrated and gamma-corrected with a spot photometer (MINOLTA CS-100). The mean luminance was 73.8 cd/m2. The experiment was conducted in a dimly lit room.

Stimuli

The adapter was composed of two parts: a center Gabor pattern (the center patch) and a surround grating (the annulus). The stimulus orientation here was defined by a sinusoidal luminance contrast variation, with 0° corresponding to a vertical grating and CW gratings was assigned negative values whereas counterclockwise (CCW) gratings, positive values. The

orientation of the center and surround gratings varied independently of each other along one of five orientations (0°/vertical, 11.25°, 22.5°, 45° and 90°/horizontal) in separate runs, resulting in 25 possible orientation combinations. Figure 3.1A shows some examples of the adapters. The target was a Gabor with the same spatial extend of the center patch, defined by:

$$G(x, y) = B + BC\cos{(2\pi f x')} e^{(\frac{-x'^2 - (y' - u_y)^2}{2\sigma^2})} \qquad (3.1)$$

$$x' = x\cos{\theta} + y\sin{\theta},$$

$$y' = -x\sin{\theta} + y\cos{\theta},$$

where B represents the mean luminance, C the pattern contrast, f the spatial frequency, μ_y the vertical displacement of the pattern, and σ the scale parameter. θ in the second and third equations represents the pattern orientation. The center part of the adapter and the target had a 0.3° scale parameter (σ). The annular surround part of the adapter was generated by multiplying a sinusoidal grating by an annular Gabor envelope, defined by:

$$G_a = B + BC\cos{(2\pi f x')} \cdot e^{(\frac{-(r - r_E)^2}{2\sigma_r^2})}, \qquad (3.2)$$

where $r = (x'^2 + y'^2)^{0.5}$ is the radial coordinates of x' and y' after transformation from Cartesian coordinates to polar coordinates. r_E is the eccentricity which determines the size of the annulus, whereas σ_r is the radial scale parameter that determines the width of the annulus. The annular surround part used in the current study was created with 3.5° eccentricity (r_E) from the adapter center with a 0.9° scale parameter (σ_r). There was no overlap between the adapter center (where the center patch and the target locate) and the adapter surround (where the annulus is positioned) regions.

Figure 3.1

Example Stimuli and Experimental Procedure
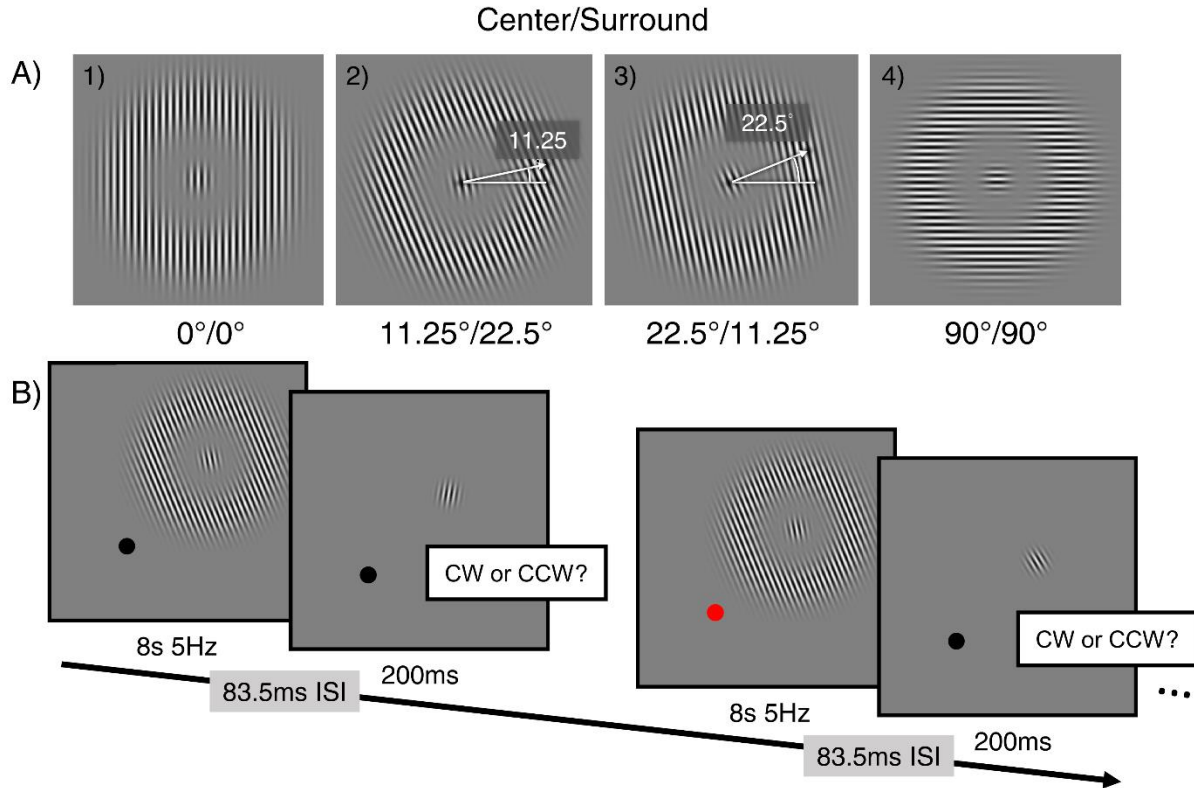
Note. (A) Example stimuli used in the current study. The adapter consists of two gratings: a central patch (having the same spatial extent as the target) and a surround annulus. (A) Four of the 25 adapters with varying center and surround orientation. The corresponding orientation of the two gratings are indicated below each panel in center/surround format. The white arrows (presented here only for the sake of illustration) in panels A2 and A3 signify the orientation of the central patch with 11.25° and 22.5° of CCW tilt, respectively. (B) An illustration of the experimental procedure. The stimuli were all presented in the upper-right visual field. The black dot represents the fixation point (not scaled to actual size). During the adaptation phase, the fixation point briefly changed its color (from black to red and back to black) at random timepoints. Participants were instructed to press a button to report the color change. See text for more details.

The adapter and the target were presented on the upper right quadrant of the visual display, centered at 10° eccentricity (7.07° in the x and y directions) from the central fixation point. The visual stimuli were all generated using Matlab (MathWorks, Inc., Natick, MA, USA) with PsychToolbox (http://psychtoolbox.org/).

Procedure

A single interval binary choice task was used to estimate how much the percept of the target orientation appeared tilted following adaptation. In every run, the adapter had 1 of the 25 orientation combinations. Each orientation combination was repeated at least three times. The sequence of the orientation combination was randomly determined. Each run contained 72 trials, including two practice trials at the very beginning. On each trial, the adapter flickered at 5Hz in counterphase for 8 seconds, followed by an 83.3 ms interstimulus interval then the target, which lasted for 200 ms (see Figure 3.1B for an illustration of the procedure). Observers were instructed to judge the target orientation (CCW or CW) by pressing the corresponding keyboard buttons. The next trial began automatically after the response. Two types of targets were presented in random sequence in the experiment: a CCW-tilted or a CW-tilted one. To determine the placement of the orientation of either target in the next trial, we used the Ψ threshold-and-slope-seeking staircase (Kontsevich & Tyler, 1999) method and created one staircase for each type of target to estimate the orientation level necessary for the observer to judge the target as oriented in the same direction as its physical orientation at 86% rate. In each staircase, if the observer judged the target as oriented the same as the physical appearance in a previous trial, the target orientation in the next trial became closer to the vertical orientation; Otherwise, the target orientation deviated more away from the vertical orientation in the next trial.

To make sure observers maintained steady fixation during the task, we added a central fixation task, in which they were instructed to press the space bar whenever the color of the fixation dot turned from black to red (see Figure 3.2B). All participants were trained to reach a high accuracy (>95%) in the fixation task during the practice session before we started the real experiment.

3.4. Results

We combined the CW and CCW trials of each orientation combination condition together and fit one psychometric function (PF) to the combined data (see Lin, Chen, and Greenlee, 2020 for a comparison between the TAE estimated by the Ψ method and the PF fitting method). We first pooled all trials of all runs of each condition for every observer, and assigned CW trials with negative orientation values, whereas the CCW trials with positive ones. We then calculated the proportion of the observer responding CCW at all orientation levels. We used the Palamedes toolbox (Prins & Kingdom, 2018) to fit a cumulative normal Gaussian PF to every adapter condition. Alpha (50% CCW response rate, essentially the point of subjective verticality) and beta (slope at 50% CCW response rate) were set as free parameters, whereas gamma (guessing rate) and lambda (finger error rate) were fixed with the value 0.01. We took the alpha values, or the point of subjective verticality, of the fitted PF of each condition as the magnitude of the TAE and determined how such value varied with different adapter orientations. In the following, the magnitude of the TAE is expressed in degrees of orientation tilted away from the physical vertical for the target to be perceived as vertical.

The data (including the Ψ estimates and the raw trial data) of individual participants are presented in Supplementary File S1 and File S2 in .xlsx (Excel) format.

Orientation-specific lateral modulation

Figure 3.2 shows the averaged data of the four participants (the individual data are included in the Supplementary File S3, Appendix B in this thesis). In panel A, the TAE is plotted against the adapter center orientation and different color curves/marker types represent different surround orientations; in contrast, in panel B, the TAE is plotted against the adapter surround orientation. The data suggest that the TAE peaked between 10° to 20° center orientation, regardless of the surround orientation and that the surround orientation modulated the overall adaptation effect. The surround modulation resulted in a dipper shape trend shown in Figure 3.2B, where the TAE first decreased then increased as the surround orientation increased from 0° to 90°. Such a trend is present in the data of all participants (see Figure B.1 in Appendix B). The lateral modulation observed in the data can be captured by sensitivity modulating parameters in a modified divisive inhibition model shown in the later section. A -way repeated measures analysis of variance showed that the interaction between center and surround orientation, $F(16, 72) = 1.36$, $p = 0.19$, was not significant, whereas the adapter center and surround main effects, $F(4, 72) = 77.52$, $p < 0.01$, $\hat{f} = 1.75$; $F(4, 72) = 8.09$, $p < 0.01$, $\hat{f} = 0.53$, were significant. The significant main effects suggest that the effect of both the center and surround orientations affect the target TAE magnitude.

Figure 3.2

The Averaged TAE
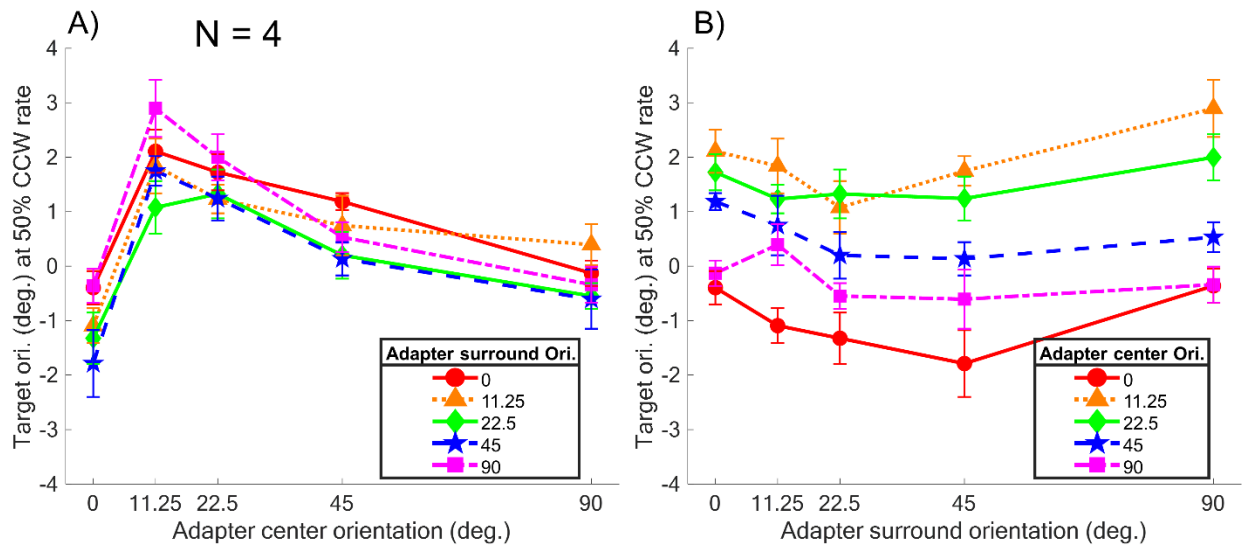
Note. The averaged TAE (corresponding to a 50% CCW response rate of the four observers) is shown. In (A), the TAE is plotted against different adapter center orientations with different color symbols and curves representing different surround orientations; in (B), the TAE is instead plotted against different adapter surround orientations, whereby the different color symbols and curves represent different center orientations. The error bars are ±1 standard error of measurement.

To further investigate the lateral modulation effect observed in the psychophysical data where the TAE highly depended on the surround orientation, in the following section, we fitted the data with a divisive inhibition model inspired by previous studies (C.-C. Chen & Tyler, 2002; Foley & Chen, 1997).

Model

We implemented a divisive inhibition model in which the response to a visual stimulus is computed by dividing the excitatory component with an inhibitory component plus a normalizing constant. Researchers have long used divisive inhibition models to explain lateral modulation effects such as lateral masking (C.-C. Chen & Tyler, 2001, 2002; Meese et al., 2007; Xing & Heeger, 2001) and tilt illusion (Clifford, 2014; Goddard et al., 2008; Schwartz et al., 2009). Prior studies have also used divisive inhibition models to fit the results of adaptation experiments (Foley & Chen, 1997; Meese & Holmes, 2002; Wilson & Humanski, 1993). In the current study, we would like to integrate these two aspects, the lateral modulation and the adaptation effect, in our model, modified from the one used in the previous study (Lin et al., 2020), in which the lateral modulation effect is captured by two multiplicative sensitivity (or gain) modulating parameters (C.-C. Chen & Tyler, 2002), whereas the adaptation effect represented by changes in the normalizing constant (Foley & Chen, 1997).

Model architecture

In the model (illustrated in Figure 3.3), we implemented population coding (Deneve et al., 1999; M A Paradiso, 1988; Pouget et al., 2000) and assumed multiple evenly distributed orientation channels with preferred orientation ranging from -90° (CW) to 90° (CCW) at 30° interval and 30° full width at half maximum. The response of the jth channel to the ith image first goes through a receptive field-like linear operator (the oriented-receptive field/linear filter in Figure 3.3), then a nonlinear operator (the divisive inhibition process in Figure 3.3).

Figure 3.3

A Schematic Diagram of the Divisive Inhibition Model
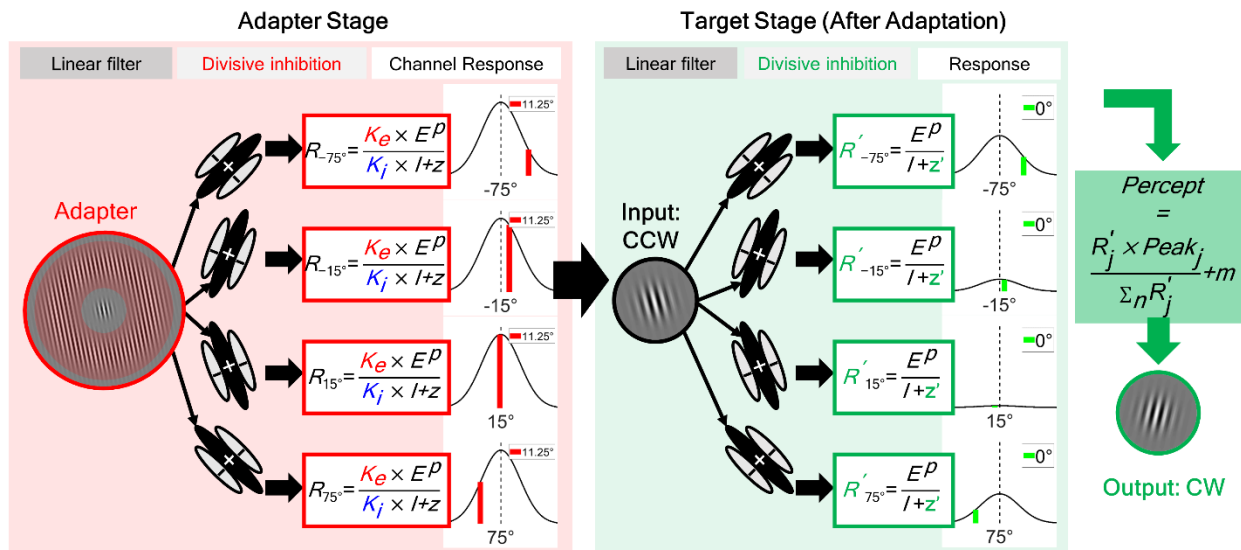
Note. In this population coding model, each channel response to the input image is calculated by a contrast gain control process. The adapter response determines the adaptation effect induced on the target. The lateral modulation effect is captured by two sensitivity modulation parameters, K_e and K_i. See the text for further details.

The excitatory component of channel j is calculated by the product of the sensitivity profile of the linear operator and the image i (C.-C. Chen et al., 2000; Foley & Chen, 1999; Phillips & Wilson, 1984). The sensitivity profile is assumed to be a Gabor function that matches the Gabor pattern used in the experiment (see the section on *Stimuli* in the Methods section). Integrating the product of the sensitivity profile and the stimulus over space, we end up with the following three components shown in Equation 3.3: C_i, the luminance contrast of ith image (which is independent of the image spatial structure, thus is taken out as a separate term), the

orientation dependent component (i.e. the orientation-tuning function) that can be represented by

a Gaussian function (M A Paradiso, 1988; Pouget et al., 1998; Westrick et al., 2016; Wilson &

Humanski, 1993), and finally the orientation independent part of product that deemed as a

constant in the current case. This last constant component is termed the sensitivity parameter, Se.

Combined, the excitation component thus is defined as,

$$E'_{ij} = Se \cdot C_i \cdot e^{-\frac{(\theta_i - \theta_j)^2}{\sigma^2}}, \tag{3.3}$$

where θ_i is the image orientation and θ_j the channel preferred orientation. σ^2 is the channel

variance determining the channel bandwidth. If a surround region is added to the center, as is the

case for the center-surround grating adapter, the excitation can be modified as the following,

$$E'_{ij} = E'_{icj} + E'_{isj} = Ke \times \left(Se_c \cdot C_{ic} \cdot e^{-\frac{(\theta_{ic} - \theta_j)^2}{\sigma^2}} + Se_s \cdot C_{is} \cdot e^{-\frac{(\theta_{is} - \theta_j)^2}{\sigma^2}} \right), \tag{3.4}$$

in which the center and surround parts of the image belong to separate components, E'_{icj} and E'_{isj}

with C_{ic} and θ_{ic} representing the features of the image center, whereas. C_{is} and θ_{is} represent

those of the image surround. Se_c and Se_s are the excitatory sensitivity parameters for the two

regions. Parameter Ke is included to capture the lateral modulation effect from the surround to

the center. The excitation term is then halfwave rectified, as in many previous cases (C.-C. Chen

& Tyler, 2001, 2002; Foley, 1994; Foley & Chen, 1997, 1999), shown in Equation 3.5, where

$max\ (a, b)$ indicates the operation of choosing the larger value among a, b.

$$E_{ij} = max\ (E'_{ij}, 0), \tag{3.5}$$

Note that, in the current experiment, because no terms in Equation 3.3 or 3.4 are negative, the

halfwave rectification transformation can be skipped without changing the excitatory component

value. However, we retain such a step to align with previous studies and to keep the model

flexible for future cases in which negative terms could be involved.

Next, before adaptation, the excitation component is raised by a power, p, and divided by the

inhibitory component, I_{ij}, as well as the normalizing constant, z, as

$$R_{ij} = \frac{E_{ij}{}^p}{I_{ij}+z},$$ (3.6)

where I_{ij} is

$$I_{ij} = Si \cdot (E_{ij})^q,$$ (3.7)

for images without a surround pattern with Si the inhibitory sensitivity parameter, and

$$I_{ij} = Ki \times \left(Si_c \cdot (E_{icj})^q + Si_s \cdot (E_{isj})^q\right),$$ (3.8)

when the surround region is added, where contributions from the center and surround are

represented again by separate components (with individual sensitivity parameters Si_c and Si_s);

the sum of the two is then multiplied by the lateral modulation parameter, Ki.

Ke and Ki are determined by two Gaussian functions of the surround orientation (θ_{is}).

$$Ke = e^{-\frac{(\theta_{is}-\theta_{excitatory})^2}{\sigma^2_{excitatory}}} \quad \text{and } Ki = e^{-\frac{(\theta_{is}-\theta_{inhibitory})^2}{\sigma^2_{inhibitory}}},$$ (3.9)

Each Gaussian function has a mean (the $\theta_{excitatory}$ or $\theta_{inhibitory}$) and standard deviation

parameter (the $\sigma_{excitatory}$ or $\sigma_{inhibitory}$) to determine the center orientation and bandwidth of the

function. These four center and bandwidths parameters control how the excitatory and inhibitory

sensitivities vary with surround orientation.

We determine the perceived orientation of the input image, i, with a population coding operation where the preferred orientation of each channel, θ_j, is weighed by the channel response, R_{ij}, then divided by the sum of all channel responses, as

$$P_i = \frac{\sum_{j=1}^{N} R_{ij} \cdot \theta_j}{\sum_{j=1}^{N} R_{ij}} + m. \tag{3.10}$$

An internal bias parameter m is included to account for the perceptual or response bias of each observer even without experimental manipulation such as adaptation.

The effect of adaptation has been shown by the shift of the dynamic range of V1 neuron contrast response function (Albrecht et al., 1984; Anderson et al., 1997; Gardner et al., 2005; Sclar et al., 1989) and, in a Naka-Rushton style model (Naka & Rushton, 1966), can be modeled by introducing a change in the semisaturation parameter (Greenlee & Heitger, 1988). In psychophysics results, such an adaptation effect can be captured by the change of parameter, z ,the normalizing constant (Foley & Chen, 1997; Lin et al., 2020). Thus, after adaptation is induced, the channel response, denoted by a prime, ', superscript, to the target becomes the following:

$$R'_{targetj} = \frac{E_{targetj}{}^p}{I_{targetj} + z'_j} = \frac{E_{targetj}{}^p}{I_{targetj} + z \cdot a_j}, \tag{3.11}$$

where z'_j is the normalizing constant after adaptation and a_j serves as the adaptation factor, defined as,

$$a_j = (1 + R_{adapterj}). \tag{3.12}$$

$R_{targetj}$ is calculated through Equation 3.3, 3.5, 3.6 and 3.7, and $R_{adapterj}$ is determined by through Equation 3.4, 3.5, 3.6, and 3.8, in which lateral modulation components are involved.

Model performance

We fitted the aforementioned model to the averaged data (Figure 3.2) With a Powell's algorithm (Press et al., 1988), which seeks the parameter values that minimize the sum of squared error, or the sum of the squared deviations between the TAE data and the model prediction. The smooth curves in Figure 3.4 represent the best model prediction. The markers in Figure 3.4 are the averaged TAE data as in Figure 3.3.

Figure 3.4

Model Fitting Results of the Averaged Data
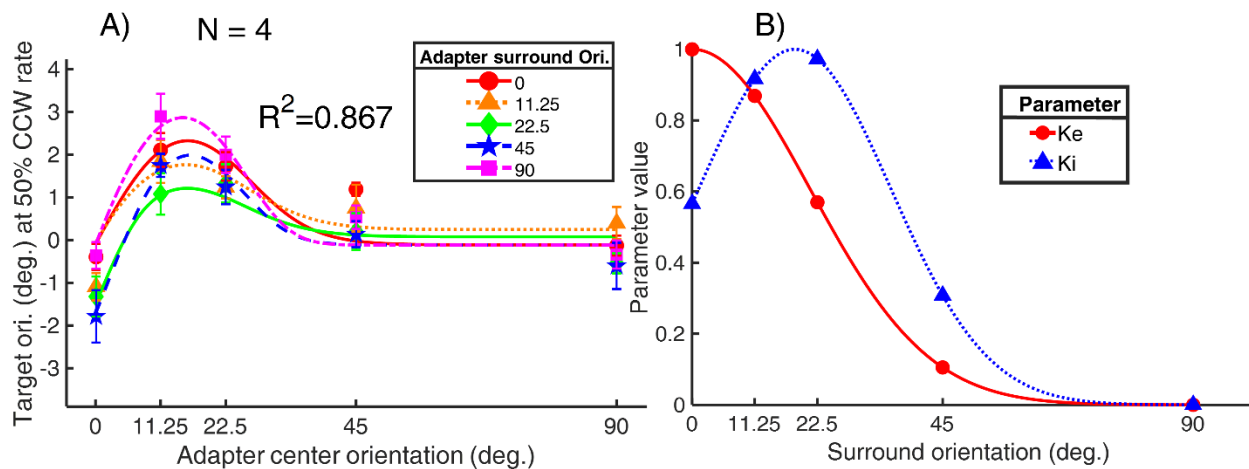
Note. In (A), the target orientation, corresponding to a 50% CCW response rate, is plotted against the adapter center orientation. Smoothed curves of different colors represent the model prediction for the different adapter surround orientations (inset), whereby the differently colored symbols show the averaged TAE data in different adapter surround orientation conditions (inset). The error bars are ±1 standard error of measurement. (B) How the parameters Ke and Ki vary with the surround orientation. Both parameters were determined by a Gaussian function.

In the model, Se (excitatory sensitivity to the target) and Se_c (excitatory sensitivity to the adapter center) are set to be the same since the target has the same spatial extent as the adapter center. Likewise, Si (inhibitory sensitivity to the target) and Si_c (inhibitory sensitivity to the adapter center) are set to be equal. Parameters other than $z, p, q, m,\ Si_s$, and the two parameters determining Ki were fixed because the goodness of fit did not change empirically whether they were free or not, resulting in a total of seven free parameters. The model can explain up to 86.7% of the variance in the averaged data, with a root mean square error ($RMSE$) of 0.43. The goodness of fit ranged from 70.5% to 89.0% in the four participants. The best fitting parameters and goodness of fit of the group-averaged data and the individual data are presented in Table 3.1. In Supplementary File S3 online (or Appendix B in the current thesis), the plots for the fitting results of the individual participant can be found in Figure B.2 in Appendix B.

Table 3.1

List of best fitting parameters and goodness of fit (R^2) of the current model on the averaged and individual TAE data.

OBSERVER	MEAN	P0	P1	P2	P3
PARAMETER					
Se/Se_c	100.00	100.00	100.00	100.00	100.00
Se_s	100.00	100.00	100.00	100.00	100.00
Si/Si_c	0.20	0.20	0.20	0.20	0.20
Si_s	**17.31**	**49.55**	**17.77**	**8.62**	**44.73**

z		**0.02**	**0.05**	**0.02**	**0.07**	**0.03**
p		**2.88**	**3.02**	**3.09**	**3.21**	**2.79**
q		**1.19**	**1.18**	**1.28**	**1.63**	**1.32**
σ		18.01	18.01	18.01	18.01	18.01
Ke	$\theta_{excitatory}$	0.00	0.00	0.00	0.00	0.00
	$\sigma_{excitatory}$	30.00	30.00	30.00	30.00	30.00
Ki	$\theta_{inhibitory}$	**18.45**	**24.02**	**12.72**	**16.23**	**22.79**
	$\sigma_{inhibitory}$	**24.46**	**24.24**	**26.91**	**25.25**	**15.63**
m		**0.28**	**0.73**	**0.07**	**1.33**	**-1.09**
R^2		0.867	0.890	0.831	0.705	0.721
RMSE		0.43	0.53	0.57	0.60	0.49
MSE		0.38	0.16	0.20	0.18	0.23
NUMBER OF FREE PARAMETERS (TOTAL PARAMETERS)		**7**(13)	**7**(13)	**7**(13)	**7**(13)	**7**(13)

Note. Free parameters and parameter values are marked in bold. Parameter σ was set as 18.01 to maintain the channel tuning FWHM as 30 degrees. The column **MEAN** represents the fitting parameters of the averaged data across the four participants.

As demonstrated in Figure 3.4B, the parameter Ke, controlling how the excitatory sensitivity is modulated when a surround is added to the adapter, decreased as the surround orientation increased from 0 to 90 degrees. In contrast, Ki, the inhibitory sensitivity modulating parameter, peaked at approximately 20° and then decreased as the surround orientation continued to increase. These results suggest that the surround interaction in the numerator terms of the normalizing process was stronger when the surround orientation was closer to 0°, whereas the surround modulation in the denominator was stronger with about 20° deviation from vertical.

3.5 Discussion

Magnussen and Kurtenbach (1980) demonstrated that adding a second oriented adapting pattern decreased the TAE on the subsequent target, suggesting a inhibitory lateral interaction between the two patterns (see also Greenlee and Magnussen (1987; 1988)). In the current study, we investigated the cross-orientation interaction in center-surround oriented gratings by manipulating the orientation of the adapter center and surround and observed its effects on the TAE. In an adaptation paradigm, we implemented a center-surround sinusoidal grating adapter that contains a center and surround regions whose orientations varied independently. We then measured how the TAE induced by the adapter on a following target changed with adapter center and surround orientation. We found that the overall TAE was determined by the orientation of the central adaptor, peaking at approximately 10° to 20°, and that the magnitude TAE is modulated by the surround orientation. In general, the TAE first decreased then increased as the surround orientation deviated away from the vertical orientation (the dipper shape in Figure 3.2B). Our results demonstrates that the surround interaction is orientation specific as has been reported in the literature (Cavanaugh et al., 2002b; C.-C. Chen & Tyler, 2002; Shushruth et al., 2012; Solomon et al., 1993).

Such orientation-specific lateral suppression that we observed has been compared to the overlay cross-orientation suppression in which a mask usually of orthogonal orientation was superimposed on the target. Petrov and colleagues (2005) measured the target detection threshold under surround masking and overlay masking configurations. They reported that the surround suppression effect was more narrowly tuned to the mask features such as orientation and spatial frequency and was more evident in the periphery than in the fovea. Similarly, Meese et al. (2009) examined the target contrast threshold under three masking configurations: cross-oriented overlay mask, orthogonal surround mask, and parallel surround mask at different eccentricity and mask contrast. Again, the surround suppression, especially from the parallel surround mask, was found to be stronger in the periphery, whereas the superimposed cross-oriented masking remained at similar strength across foveal and peripheral locations. Such findings suggest that these two forms of suppression involve different neural processes (see also Petrov and McKee, 2006; Smith et al., 2006).

Divisive inhibition in orientation-specific lateral modulation

To explain such orientation-specific lateral modulation effect, we modified the divisive inhibition model to account for our data. In the previous model implemented in the our previous study (Lin et al., 2020), the sensitivity-modulating effect was mediated by the excitatory sensitivity parameter, Se, which was most pronounced for the center, intermediately pronounced for the disk (both center and surround) and was least pronounced for the annulus (surround-only) condition in the final fitting results.

In Chen and Tyler (2002), Ke and Ki, the multiplicative sensitivity modulating parameters of the excitatory and inhibitory components, were set as free parameters. They reported that Ke and Ki both decreased as the flanker orientation increases while the ratio

104

between the two stayed approximately constant with flanker orientation. They fitted each of the two parameters with a linear combination of two Gaussian functions, one narrowly and one broadly tuned. In our model, Ke and Ki were each determined by a Gaussian function, representing how the excitatory and inhibitory terms change with the surround orientation respectively (see Fig. 4.4B and Fig. B.3 in Appendix B). Similar to the fitting results of Chen and Tyler (2002), in our case, the best fitting parameter set showed that Ke, peaking at the $0°$ surround, decreased as the surround orientation increased, whereas Ki first increased and peaked around $20°$, then decreased as the surround orientation increased. These studies demonstrated that the modified divisive inhibition model can capture not only the lateral modulation effect of the flankers on the contrast threshold of a central stimulus in the dual-masking paradigm (C.-C. Chen & Tyler, 2002) but also the lateral modulation effect of the adapter surround orientation on the percept of the adapter center in the adaptation paradigm (Lin et al., 2020 and the current study).

Comparison with the results of Lin et al. (2020)

In the previous study (Lin et al., 2020), we measured the TAE on the target after three types of adapter: a center adapter with the same spatial extent as the target, a disk adapter that occupied both the center and surround regions, and an annulus adapter that covered only the surround region. We found that the TAE was the stronger in the center adapter condition than in the disk adapter condition, suggesting that adding a surround to the adapter introduced an inhibitory effect to the adapter center. In this section, we compare the lateral modulation effects estimated from the previous and the current studies.

The reasons to make such a comparison is two-fold: 1) to see if we could replicate the previous lateral inhibition result and 2) to examine how introducing a gap between the center and surround could affect the lateral modulation effect. Because the surround region of the disk

adapter in the 2020 study always had the same orientation as the adapter center, a fair comparison condition from the current study would be when the adapter center and surround have the same orientation. Three participants (P0, P1, and P3) took part in both the 2020 study and the current one; thus, we could compare their data from the two studies.

We took the data of the center and the disk adaptation conditions from the 2020 study and compared these data with the conditions where the adapter center and surround were of the same orientation (same center and surround in Figure 3.5) in the current study. Because the data reported in Lin et al. (2020) was the psi estimates whereas the data shown in the current study were the PF-fitting results, we also fitted PFs for the center and disk conditions on the raw data of the 2020 study and took the 50% CCW reporting rate target orientation for comparison purpose. As shown in Figure 3.5, the TAE was the most pronounced in the center condition, followed by the disk condition, and the least pronounced in the center-surround condition with the same orientation. Thus, we again demonstrated that including a surround pattern during the adaptation decreased the TAE on the target. The individual data of three participants of the comparison between the two studies are shown in Figure B.4 in Appendix B.

Figure 3.5

Comparison Between the Same Center and Surround (C&S) Conditions of the Current study and the Center and Disk Conditions from the Previous Study (Lin et al., 2020).
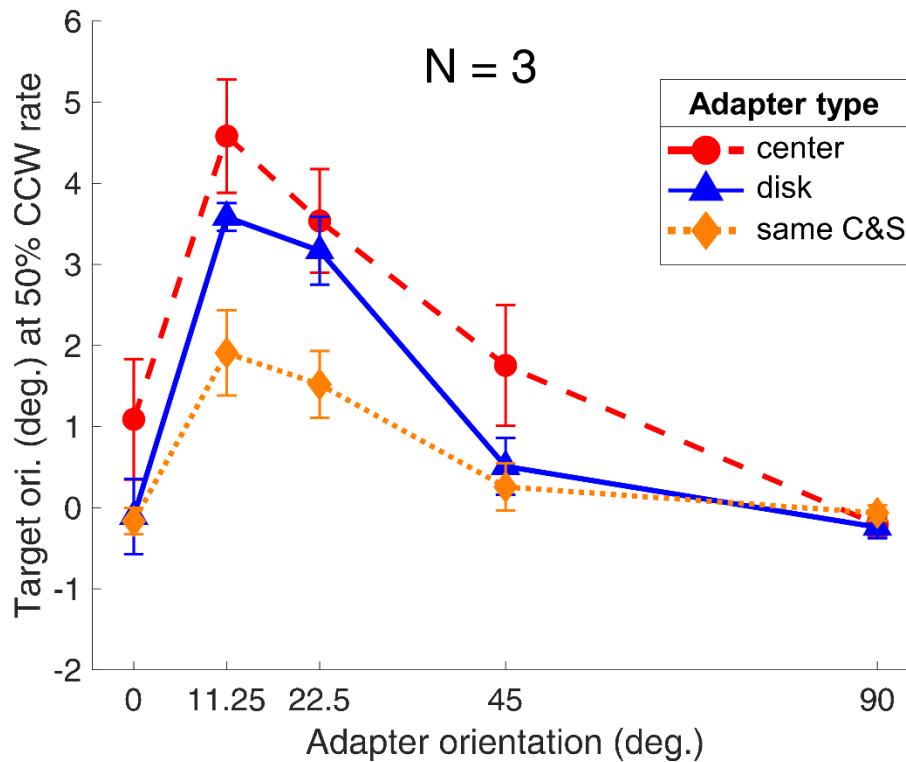
Note. The averaged TAE data of three participants (P0, P1, and P3) are plotted against the adapter orientation. The red-dashed curve with red solid circles represents the center, the blue curve with solid triangles presents the results from the disk adapter (an enlarged grating covering both the center and the surround area), and the orange-dotted curve with solid diamonds depicts the results of the center-surround adapter when both regions had the same orientation. The error bars are ±1 standard error of measurement.

Comparing the conditions where the adapter center and surround were of the same orientation (same center and surround condition in Figure 3.5) in the current study with the results from the center and the disk conditions in the previous 2020 study, we replicated the effect showing that adding a surround decreased the TAE. Interestingly, the TAE in the disk condition

was more pronounced than that exhibited in the same center and surround conditions, suggesting that adding a gap between the adapter center and surround increased the lateral inhibition effect from the surround. One possibility is that the grating filling in the gap region in the disk condition induced a near surround interaction that facilitated the adapter center and countered the surround inhibition from the more eccentric surround region (the annulus) thus resulted in a slightly stronger TAE compared with the same center-surround condition.

Introducing a gap between the center and surround regions of a stimulus could affect the amount of lateral modulation the center region received. In the tilt illusion, segmenting the center and surround gratings by adding a mean luminance ring in between, separating the two with different disparity, or changing the relative contrast decreased the perceived illusion (Durant & Clifford, 2006; Qiu et al., 2013). The perceived contrast decrease of a center grating surrounded by a grating ring also decreased as the physical distance between the ring and the center patch increased (Cannon & Fullenkamp, 1991; Yu et al., 2001). In a flanker paradigm, the target contrast detection threshold first increased (suppression) then decreased (facilitation) with the target-to-flanker distance (Polat & Sagi, 1993). Chen and Tyler (2008) manipulated the relative location of the flankers and the flankers distance to the target. The facilitative and suppressive flanker effects decreased as the flanker location deviated from the collinear axis. When the flanker-to-target distance was shortened (1.4 λ), the flankers acted like a high-contrast pedestal and it raised the target threshold regardless of the pedestal contrast. As the distance between the flankers and the target further increased, the target detection threshold further decreased. In Meese et al. (2009), the maximum contrast threshold elevation resulting from adding a annulus surround mask decreased as the gap between the annulus and the center Gabor increased. These findings indicate a complex and diverse effect of the segregation between the center and surround. In our case, future experiments manipulating the separation between the center patch

and the annulus would be required before further inference can be made on the effect of the gap on the lateral modulation.

3.6. Conclusions

Previously, Lin, Chen, and Greenlee (2020) showed that adding a surround with the same orientation to the adapter center decreased the TAE magnitude on the following target, suggesting a lateral inhibition effect. Here, we further investigated such lateral modulation effects by varying the center and surround orientations separately.

In an adaptation paradigm, participants were asked to judge the orientation of a central Gabor target (located in the upper right periphery) after viewing a flickering sinusoidal-grating adapter with a center (occupying the same spatial extend as the target) and a surround (without physical overlap with the target) gratings in eccentric vision. Because the center and surround orientations were varied independently, we could observe how the surround feature could influence the center percept quantitatively. The results showed that the TAE induced on the target was predominantly determined by the adapter center and modulated by the adapter surround. The surround modulation effect first increased then decreased as the surround orientation deviated from the vertical orientation. Such findings demonstrate an orientation-specific interaction between the center and the surround regions in the visual field. The results aligned well with the previous research focusing on the lateral modulation effect in human vision (C.-C. Chen & Tyler, 2001, 2002; Magnussen & Kurtenbach, 1980). We fitted a divisive inhibition model to the data, using the sensitivity modulating parameters in the numerator and denominator to capture the observed lateral modulation effect.

Numerous studies have focused on the cross-orientation interactions between patterns occupying the center and surround visual fields. The results of these studies have shed light on

the neural mechanisms of the long-range interactions (C.-C. Chen & Tyler, 2001, 2002; Meese et al., 2007; Solomon & Morgan, 2000; Spillmann & Werner, 1996; Xing & Heeger, 2000; Yu et al., 2001, 2002), providing insights in the fundamental neural processing of early visual cortex. Following this long line of research in lateral interactions, the current study furthers our understanding of the human visual system by showing that the magnitude of the lateral modulation is influenced by the surround orientation.

4. CHAPTER 4: STUDY 3 "NEURAL CORRELATES OF LATERAL MODULATION AND PERCEPTUAL FILLING-IN IN CENTER-SURROUND RADIAL SINUSOIDAL GRATINGS: AN FMRI STUDY"

4.1. Abstract

We investigated lateral modulation effects with functional magnetic resonance imaging. We presented radial sinusoidal gratings in random sequence: a scotoma grating with two arc-shaped blank regions (scotomata) in the periphery, one in the left and one in the right visual field, a center grating containing pattern only in the scotoma regions, and a full-field grating where the pattern occupied the whole screen. On each trial, one of the three gratings flickered in counterphase for 10 seconds, followed by a blank period. Observers were instructed to perform a fixation task and report whether filling-in was experienced during the scotoma condition. The results showed that the blood-oxygen-level-dependent (BOLD) signal was reduced in areas corresponding to the scotoma regions in the full-field compared to the center condition in V1 to V3 areas, indicating a lateral inhibition effect when the surround was added to the center pattern. The univariate analysis results showed no difference between the filling-in and no-filling-in trials. However, multivariate pattern analysis results showed that classifiers trained on activation pattern in V1 to V3 could differentiate between filling-in and no-filling-in trials, suggesting that the neural activation pattern in visual cortex correlated with the subjective percept.

Keywords: perceptual filling-in, lateral modulation, multivariate pattern analysis, functional MRI

4.2 Introduction

It is well known that a surround pattern can affect the percept of a central stimulus (Gilbert & Wiesel, 1990; Schwartz et al., 2007; Spillmann et al., 2015). In visual crowding, for example, the presence of flankers diminishes the recognition of the center target (Bouma, 1970; Herzog et al., 2015; Levi, 2008). In the lateral masking paradigm, lateral flankers first increase then decrease the detection threshold of a central target as the distance between the target and

flankers increased (Polat & Sagi, 1993). In the presence of a superimposed pedestal, colinear lateral flankers decrease the target discrimination threshold at low pedestal contrast and increase the threshold at high pedestal contrast (C.-C. Chen & Tyler, 2002). In visual illusions, such as the Ebbinghaus illusion and tilt illusion, the size or orientation percept of a central target can be modulated by its surround (Clifford, 2014; Gibson, 1937a; Gilbert & Wiesel, 1990; Wundt, 1898). Numerous studies have reported that these phenomena can result from facilitation and suppression arising from the surround and these effects depend on the stimulus eccentricity, luminance contrast, orientations and other features of such flanking stimuli (Cannon & Fullenkamp, 1991; C.-C. Chen & Tyler, 2001, 2002; Lin et al., 2020, 2022; Meese et al., 2007; Petrov & McKee, 2006; Solomon & Morgan, 2000; Xing & Heeger, 2000; Yu et al., 2002, 2001). These results imply that neurons respond to different parts of the visual field and interact with each other in a complex fashion.

Perceptual filling-in, in which the visual system compensates for missing information in a region by interpolating information of the surrounding features, is yet another demonstration of the lateral modulation effect (Devinck & Knoblauch, 2019; Pessoa & De Weerd, 2003; Ramachandran & Gregory, 1991; Spillmann, 2011). Filling-in can be observed under numerous viewing conditions. For example, with monocular viewing we do not perceive a black hole at the location of the blind spot, where there are no photoreceptors due to the optical nerves passing through. The absence of awareness of the blindspot is related to filling-in of the surround texture or color (Matsumoto & Komatsu, 2005; Ramachandran, 1992; Spillmann et al., 2006). Filling-in also happens in the retinal scotoma of patients with eye diseases such as macular degeneration (Crossland et al., 2007; Crossland & Rubin, 2007; Zur & Ullman, 2003). A further scenario where filling-in occurs is when an artificial scotoma is induced, where a blank region embedded among dynamic noise or texture background disappears after prolonged steady fixation (De

Weerd et al., 1995; Morgan et al., 2007; Ramachandran & Gregory, 1991; Spillmann & Kurtenbach, 1992). Filling-in can also be observed in certain visual illusions. In water-color illusion, color is perceived to spread to the white space in between two-toned colored wiggly stripes (Pinna et al., 2003). Similarly, in neon-color illusion, illusory color is perceived and spreads out to an illusory border (Bressan et al., 1997). Another example is the Troxler's fading effect, in which following steady fixation, a ring with blurred edges fades away from sight (Troxler, 1804). In Craik–O'Brien–Cornsweet illusion (Cornsweet, 1970), the perceived brightness level of a luminance surface is increased or decreased depending on the edge as the perceived brightness of the edge spreads out to the whole surface.

Behavioral and neuroimaging studies on perceptual filling-in have focused on the latency and properties of different types of filling-in effects as well as on the underlying mechanisms (see Komatsu (2006) and Weil and Rees (2011) for a review). However, the exact neural processes involved in the filling-in percept are still under debate. Two theories have emerged to explain the neural mechanisms of filling-in. The first, the cognitive or symbolic theory, suggests that filling-in results when the visual system ignores the scotoma regions and thus involves no active processing (Pessoa et al., 1998; von der Heydt et al., 2003). The second, the isomorphic theory, states that a spread of neural activation occurs from the border to the center of the filled-in region, pointing to an active process (De Weerd et al., 1995; Meng et al., 2005). While both theories have their merits and can explain most of the filling-in phenomena, empirical results from neurophysiological and neuroimaging studies have shown that visual areas are activated during filling-in, supporting the isomorphic theory. For instance, Murakami (1995) demonstrated that after the blind spot region of one eye was being adapted to a drifting grating, participants experienced a motion aftereffect in the corresponding region of the other eye, indicating that the filled-in motion in the blind spot activated a direction-selective neural mechanism during

114

adaptation. In a single-neuron recording experiment, Matsumoto and Komatsu (2005) detected increased neural activity in macaque V1 when filling-in occurred in the blind spot (see also Komatsu et al. (2000)). De Weerd and colleagues (1995) also discovered that neurons with receptive fields inside an artificial scotoma were activated when filling-in was perceived. More evidence of the involvement of active processing has been reported in Craik–O'Brien–Cornsweet illusion with electrophysiological recordings (Roe et al., 2005) and in neon-color spreading with functional magnetic resonance imaging (fMRI) (Sasaki & Watanabe, 2004).

In addition to results showing that the filled-in region is related to lateral excitation from the surround, other studies have shown evidence for lateral inhibition from the surround region during filling-in. Chen and colleagues (C.-C. Chen et al., 2005) presented flickering high-contrast checkerboard pinwheels to the participants in an MRI scanner and discovered that visual cortex corresponding to the unstimulated inter-wedge regions showed decreased BOLD (Blood-oxygen-level-dependent) activation. Participants reported experiencing a twinkle aftereffect in the unstimulated regions after the pinwheel stimulus disappeared, a common illusory percept observed in artificial scotoma after a surround texture is removed (Crossland & Bex, 2008; Hardage & Tyler, 1995; Morgan et al., 2007; Ramachandran et al., 1993; Tyler & Hardage, 1998). Such a "rebound" effect suggests a release from surround suppression of the unstimulated regions after the surround stimulus disappeared. Supèr and Romeo (2011) proposed a computational model in which surround inhibition creates rebound in neurons in the unstimulated regions to explain filling-in. In a later fMRI study, adapting the lateral flanker paradigm, Chen (2014) was able to partition two inhibitory components from the surround suppression in BOLD signals: an orientation-specific inhibition that happened when the central target and flankers were colinear, and a general inhibition that occurred whenever flankers were present regardless of their orientations. Weil et al. (2007) demonstrated a reduced MEG (magnetoencephalography) power

when the target was being filled in. In a subsequent fMRI study (Weil et al., 2008), the same

group showed decreased BOLD signals in V1 and V2 when filling-in was perceived. Mendola et

al. (2006) reported reduced brain activation in V1 and V2 and enhanced activation in V3 and

higher regions during filling-in. Behavioral studies also showed similar lateral inhibition effects

in filling-in. Mihaylov et al. (2007) reported elevated detection threshold of a Gabor target placed

inside an artificial scotoma surrounded by dynamic noise only when the surround texture induced

filling-in and twinkle aftereffect, suggesting that the lateral modulation involved in filling-in

contribute to the sensitivity reduction.

The fact that evidence for both lateral excitation and lateral inhibition have been shown

reveals the complexity of the underlying neural mechanism and the possibility that more than one

process is involved. More research is therefore needed to collect further empirical evidence of the

neural correlates of perceptual filling-in.

Previously, in a psychophysics study (Lin et al., 2020), we selectively adapted the center,

surround, or both the center and surround regions in the periphery with oriented-sinusoidal

gratings and estimated the tilt-aftereffect (TAE) induced in a subsequent Gabor target located in

the center region. Perceptual filling-in was observed during the surround-only adapter

presentation, where the central hole represented an artificial scotoma. Our results showed that the

TAE magnitude was strongest in the center-only condition, intermediate in the center plus

surround condition, and it was weakest in the surround-only condition. The reduction of TAE in

the center-surround compared to the center-only condition indicated an inhibitory lateral

modulation effect when a surround was added to the adapter center. We also discovered that such

lateral inhibition was orientation-specific (Lin et al., 2022). In terms of the surround-only

condition, we found a positive correlation between the subjective filling-in percept and the TAE

magnitude. Additionally, when we separately estimated the TAE on trials with and without filling-in, the adaptation effect was stronger in the former, suggesting that filling-in was associated with a more pronounced lateral modulation effect. Our behavioral results revealed clear evidence of lateral modulation effect involved in perceptual filling-in.

To further investigate the underlying neural mechanism of the lateral interaction between the center and the surround regions, in the current study, we presented three types of radial sinusoidal gratings occupying either the center, the surround, or both the center and surround of the visual fields (Figure 4.1). We then measured how the brain activation varied as estimated by fMRI. We chose the fMRI technique because of its high spatial resolution. Combined with retinotopic mapping techniques, we could define voxel clusters that correspond to the first three visual areas, V1, V2 and V3 in ventral and dorsal parts of the occipital cortex. Furthermore, using individual localizer runs, we could define the voxel clusters that correspond to the regions-of-interest (i.e., the cortical projection zone of the "center" stimuli) within early visual cortex. The effect of lateral modulation could be identified by comparing the BOLD signals for the center and the full-field gratings in the early visual cortical areas. If there was lateral excitation from the surround to the center, then the BOLD signal for the center grating should be lower than that for the full-field grating. On the other hand, if lateral inhibition predominates, then the BOLD signals for the center grating only should be greater than that for the full-field grating. Perceptual filling-in could be observed in the artificial scotomata in the surround-only gratings. Based on the previous studies, we expected to observe a change in the BOLD activation in the early visual cortex when filling-in occurred in the "scotoma" condition. We performed both univariate and multivariate pattern analyses on the data to test our hypotheses.

4.3 Results

We presented three radial sinusoidal gratings in an event-related fMRI experiment: a Full-Field grating (Figure 4.1a), a Scotoma grating with two blank crescents representing artificial scotomata on the left and right visual fields that could induce perceptual filling-in (Figure 4.1b), as well as a Center grating which was the reverse of the Scotoma grating (Figure 4.1c). During the stimulus presentation on each trial, one of the three gratings flickered at 5Hz in counterphase for 10 seconds, followed by a 14-second blank period (see Methods for more details). The brain regions in the visual cortex corresponding to the retinotopic locations of the scotomata and center patches were identified in an independent localizer session where flickering (5 Hz) high-contrast checkerboard pattern was used (Figure 4.1d). In the following sections, we analyzed the BOLD signals in these target ROIs (regions of interest). All results shown are based on brain activation within the target ROIs.

Figure 4.1

Stimuli Used in the Current Study
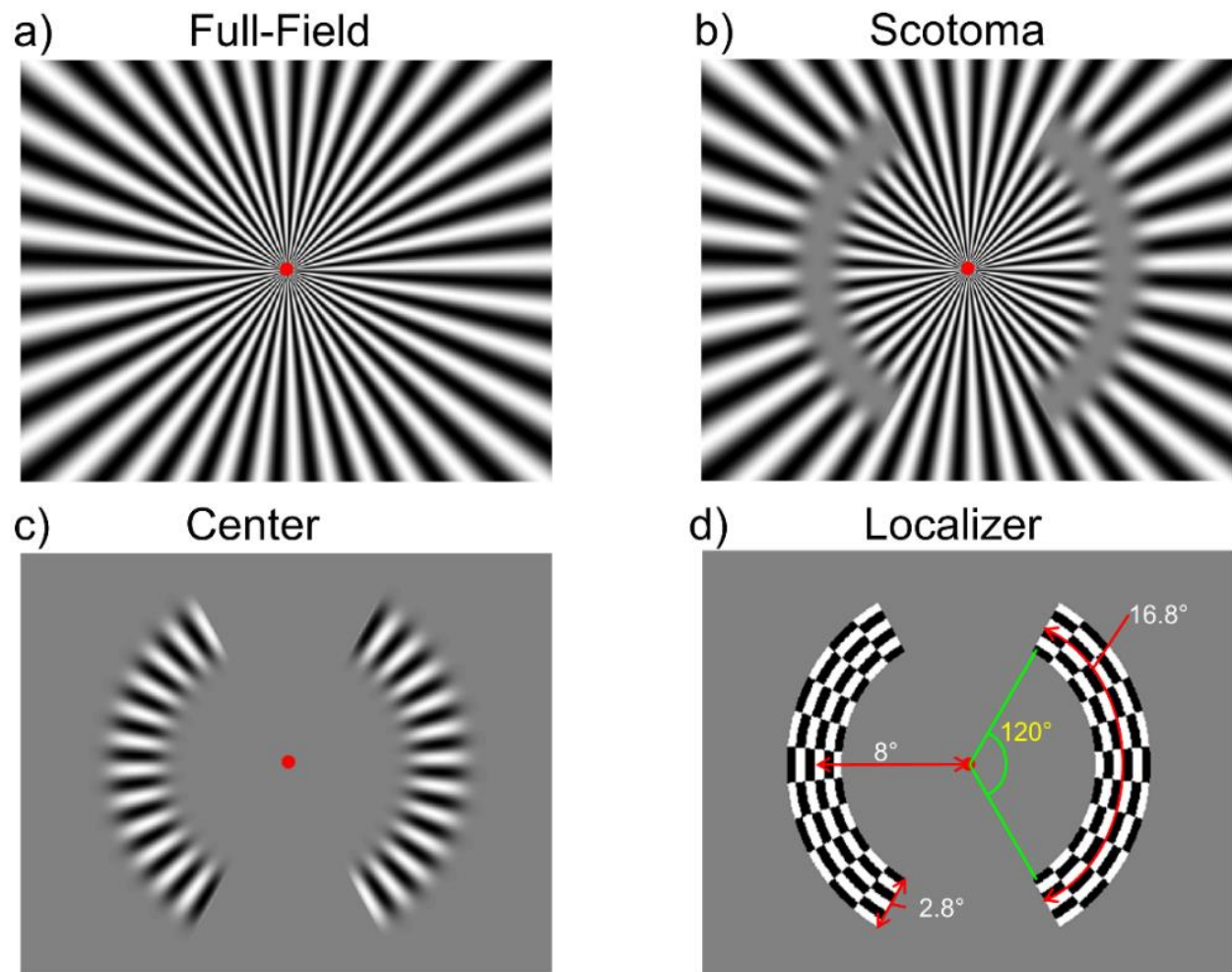
Note. a) The full-field stimulus with radial sinusoidal grating covering both the center and surround areas. b) The scotoma stimulus in which two mean-luminance blank zones ("scotomata") located on the left and right visual fields in the 8° eccentricity periphery. c) The center stimulus is the inverse of the scotoma stimulus where only the central regions corresponding to the "scotoma" contain sinusoidal grating pattern. d) The high-contrast flickering (5 Hz) checkerboard pattern located in the scotoma regions used in the localizer scanning sessions. The red arrows and white numbers indicate the eccentricity (8°) and size (16.8°) in visual angle, whereas the green lines and curve and yellow number indicate the rotation angle of one of the crescents. The crescent width was set to be 2.8°. These symbols and numbers were not presented together with the stimulus during the experiment.

In the following sections, we first discuss the univariate analysis results, in which we compare the mean BOLD signals between the Center, Scotoma (with and without filling-in) and Full-Field conditions. Afterwards, we present the results of the multivariate pattern analysis (MVPA) conducted on the results of the scotoma trials to see if the brain activation patterns correlated with the subjective percept. Overall, participants reported seeing the scotomata being filled-in on 40% to 63.8% (mean 52.9%) of trials in the scotoma condition, indicating that the scotoma grating could induce perceptual filling-in.

Univariate analysis

The BOLD amplitude (β estimated by the general linear model, GLM (Johnson & Wichern, 2007)) of each condition is shown in Figure 4.2A. We focus on the results of two condition contrasts (Figure 2B). First, to examine the effect of adding a surround to the center grating patches on the BOLD activation, we compared the activation levels of the target six ROIs (corresponding to the projection zones of the "center" or "scotoma" regions) between the Center and Full-Field conditions (see Figure 4.1). As reported earlier (Lin et al., 2020), we expected to find a reduced BOLD signal in the ROI regions in the Full-Field condition compared to the Center condition. Second, we examined whether the amplitude of the BOLD response was different between trials with filling-in report and those without. The group mean t-values of both contrasts are plotted in Figure 4.2B for the left (l) and right (r) ROIs in retinotopically defined V1, V2 and V3 regions of the occipital lobe.

Figure 4.2

Averaged normalized β in each condition and group mean of t-Values of the two univariate contrasts.
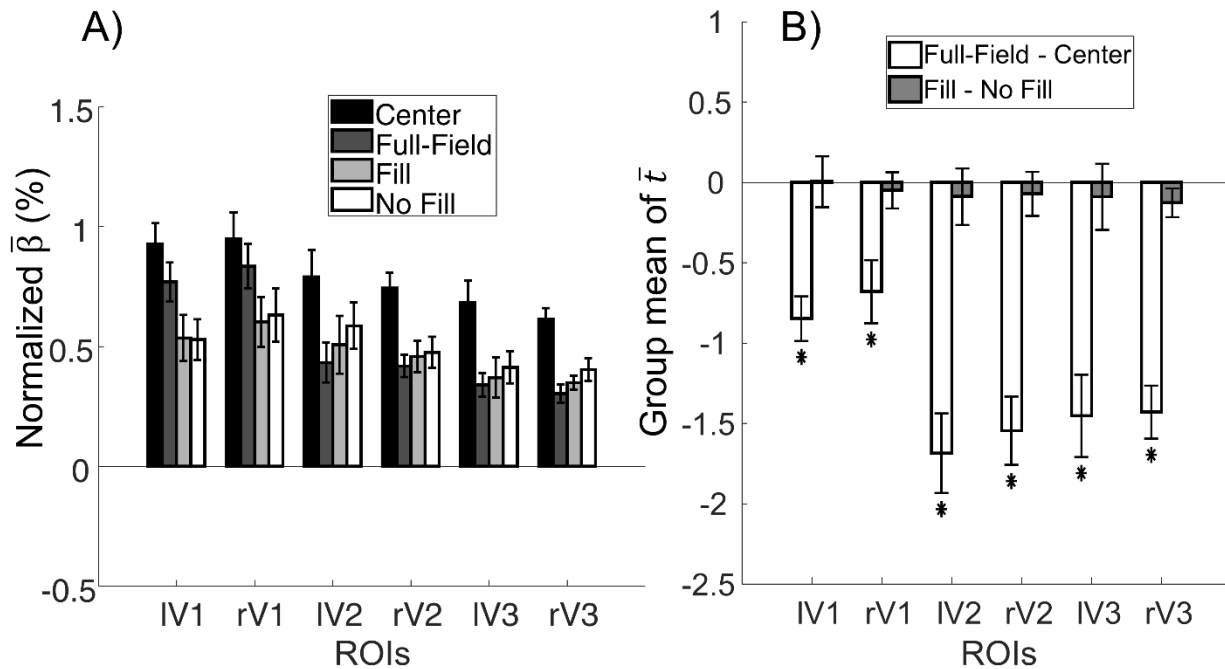
Note. For visualization purpose, we normalized β for each voxel by dividing it by the baseline activation. We averaged the normalized β across voxels in each ROI at the individual-level then computed the group-level mean normalized $\bar{\beta}$ for each ROI across observers. Panel A demonstrates the normalized β of each ROI. Panel B shows the t-values of the two contrasts in each ROI. Error bar represents +/- 1 standard error. *df* = 11. * p < α = 0.0042 (after Bonferroni correction). Results for the left (l) and right (r) visual areas V1, V2 and V3 in dorsal and ventral parts of the occipital lobe, as defined by retinotopic mapping, see Methods, are depicted.

We performed one-tail t-tests on the group mean t-values compare to zero for each contrast for all ROIs. In the case of Full Field - Center contrast, the mean t-values were significantly below zero for all ROIs (lV1: $t(11)$ = -6.13, $p < 0.001$, Cohen's d = 1.77; rV1: $t(11)$ = -3.47, p = 0.003, Cohen's d = 1.00; lV2: $t(11)$ = -6.80, $p < 0.001$, Cohen's d = 1.96; rV2: $t(11)$ = -7.26, $p < 0.001$, Cohen's d = 2.10; lV3: $t(11)$ = -5.67, Cohen's d =1.64, $p < 0.001$; rV3: $t(11)$ =

-8.63, $p < 0.001$, Cohen's $d = 2.49$), implying that the activation in the full-field condition was weaker than in the center condition, suggesting an inhibitory lateral modulation effect. In the "scotoma" condition, the Fill - No-Fill univariate contrast did not reveal any significant t-test results (lV1: $t(11) = 0.03$, $p = 0.49$; rV1: $t(11) = -0.43$, $p = 0.34$; lV2: $t(11) = -0.50$, $p = 0.31$; rV2: $t(11) = -0.52$, $p = 0.31$; lV3: $t(11) = -0.43$, $p = 0.34$; rV3: $t(11) = -1.4$, $p = 0.09$), suggesting that the overall activation level did not depend on the subjective percept of the scotoma gratings.

To examine whether there was a difference in the time course Fill and No Fill conditions, we extracted the BOLD signal across the 12 TRs (5 TRs/10s with stimulus on, 7 TRs/14s with stimulus off) in the filling-in and no filling-in trials of each ROI for each observer and plotted them in the Figure 4.3. It can be seen that the time courses of the two conditions were quite similar for all ROIs.

Figure 4.3

Time course of filling-in and no filling-in conditions.
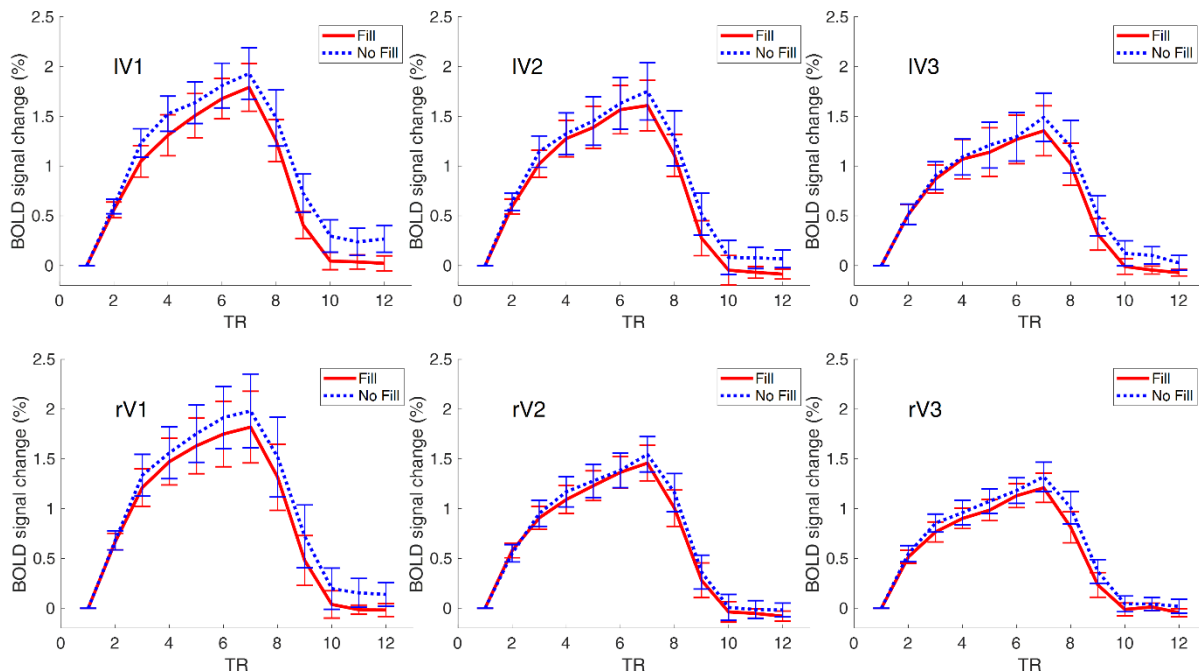
Note. We plotted the percentage of BOLD signal change relative to the first TR across the 12 time points in each ROI. We first calculated the signal change of BOLD response relative to the first TR relative to the stimulus onset for each trial in each condition and averaged them to get the individual time course of percentage BOLD signal change. At the group-level, we averaged these time courses of all subjects to get the group mean time course. The error bars represent the +/- standard error across participants. Results for left (l) and right (r) visual areas V1, V2 and V3 are shown in the upper and lower panels, respectively.

In addition, we plotted the mean time to peak of the Fill and No Fill conditions in Figure 4.4. We calculated the difference of averaged time to peak between the Fill and No Fill conditions and performed two-tailed paired t-tests for each ROI. None of the p-values were lower than the α value 0.0042 after Bonferroni correction (lV1: $t(11) = -0.43$, $p = 0.67$; rV1: $t(11) = -1.54$, $p = 0.15$; lV2: $t(11) = -1.16$, $p = 0.27$; rV2: $t(11) = -2.35$, $p = 0.04$; lV3: $t(11) = -1.91$, $p = 0.08$; rV3: $t(11) = -0.80$, $p = 0.44$), suggesting that there was no difference in time to peak between the filling-in and no filling-in trials.

Figure 4.4

*Averaged time to peak for Fill and No Fill conditions.*
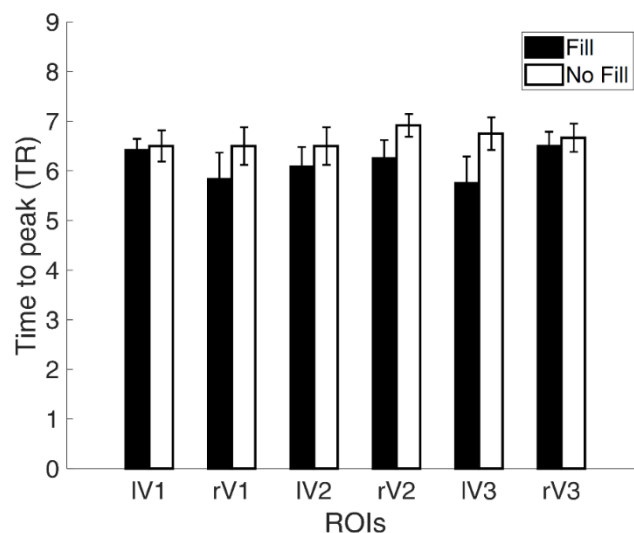
Note. We extracted the time to peak (the TR with the peak activation after stimulus onset) for each trial in each ROI then calculated the averaged time to peak for each observer in the Fill and No Fill conditions. The figure shows the average time to peak in TR across observers in each ROI. The error bars represent the +/- standard error across participants.

Multivariate analysis

It is possible that differences in filling-in percept is better reflected by the activation patterns across all voxels within projection zone of the "scotoma" region. To test this hypothesis, we performed a multivariate pattern analysis by training an SVM linear classifier to differentiate between the Fill and No-Fill trials of each participant. We then averaged the cross-validation accuracy of all twelve participants and tested this group mean classification accuracy against a null distribution generated by permutation. Figure 4.5 shows the group mean of the cross-validation averaged accuracy. The classification accuracy was considered to be significant if the averaged accuracy corresponded to *p*-value below α value of 0.017 (after Bonferroni correction) in the null permutation distribution.

Our results showed that for all targeted ROIs, the model can be successfully trained to differentiate between filling-in and no-filling-in trials (all *p*-values were below 0.001), indicating that the BOLD activation pattern in the two conditions carry enough information for the SVM models to predict the presence or absence of filling-in at above 60% accuracy.

Figure 4.5

The Group Mean of Cross-Validation Accuracy of MVPA
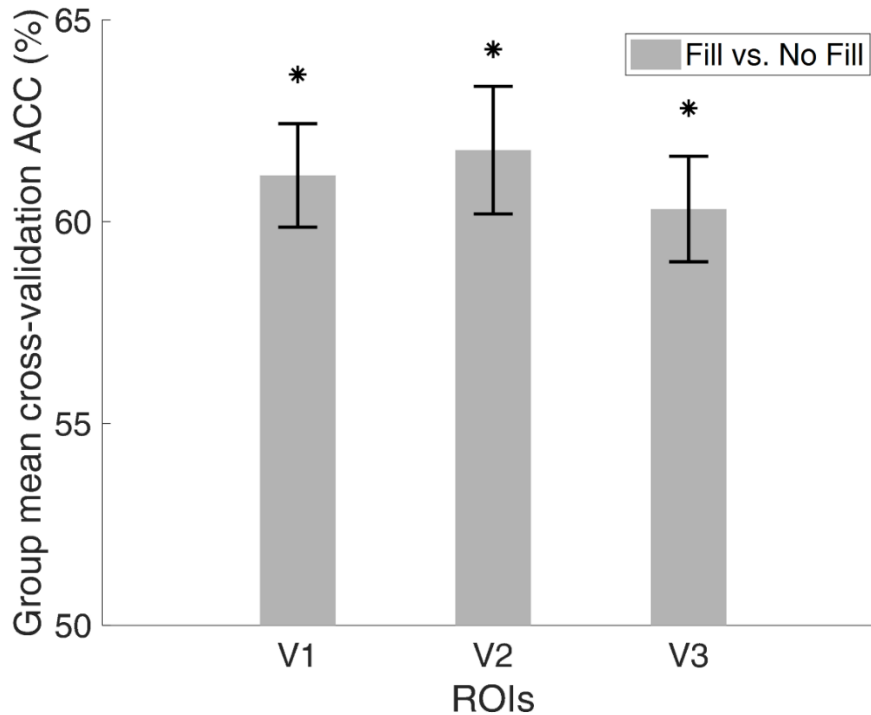
Note. The figure presents the group mean of the cross-validation accuracy. Error bar represents +/- 1 standard error. * $p < \alpha = 0.017$ (after Bonferroni correction). Results for the visual areas V1, V2 and V3 are depicted (see Methods for details of ROI definition).

Fixation stability test

To make sure that the differences of BOLD signal levels or activation patterns found between conditions did not originate from variation of how well the participants fixated during the stimulus presentation, we recorded the eye movement of the observers. Two observers, P1 and P2, performed the same experiment outside of the scanner after the main experiment while their eye movements were recorded by an eye tracker. The eye positions of the other four participants, P3 to P6, were recorded during the fMRI main experiment (see Methods for more

details). P3 to P6 were not available for the out-of-scanner eye tracking control experiment. To preprocess the raw eye tracking data recorded during stimulus presentation, we removed eye positions that indicate missing data, blinks or gaze positions beyond the stimulus screen to remove artifacts. We also ruled out eye positions that indicate eye movement between two stimulus frames that exceeded eye velocities of 30° per second to exclude large saccades (Crossland & Rubin, 2002). We calculated the bivariate contour ellipse area (BCEA) values to evaluate the level of fixation stability (Castet & Crossland, 2012; Crossland & Rubin, 2002; Niehorster et al., 2020; Schönbach et al., 2017) in our different stimulus conditions. The BCEA is defined by,

$$BCEA = 2k\pi\sigma_H\sigma_V(1 - \rho^2)^{0.5}, \tag{4.1}$$

in which k is a constant determining the probability area as in the next equation:

$$P = 1 - e^{-k}, \tag{4.2}$$

with e the base of the natural logarithm and P the probability area. σ_H and σ_V are the standard deviations of the horizontal and vertical eye positions recorded, whereas ρ is the Pearson's correlation coefficient between the eye positions in the two directions. We used $k = 1$, where the BCEA encompasses about 63.2% of the fixations, to estimate the BCEA value.

We estimated the BCEA value for each participant in each stimulus condition. We compared the BCEA values between the center and full-field conditions, the Center - Full-field contrast, as well as the contrast in the filling-in and no-filling-in trials. We performed two one-way repeated measurement ANOVA on the two contrasts and found no significant difference between the BCEA values in different conditions (Center - Full-Field: $F(1, 5) = 1.6$, $p = 0.26$; Fill - No Fill: $F(1, 5) = 0.39$, $p = 0.56$). Due to the small sample size ($n = 6$), besides F-tests, we used

random sampling with replacement, i.e. bootstrapping method, to generate a null distribution out

of 10,000 iterations. We calculated the *p*-values of the two mean differences of the two contrasts

(i.e., center vs. full-field and filling-in vs. no filling-in) in their corresponding distributions and

compared them to α value of 0.025 (two-tail). The tests showed that both p-values were not

significant (Center - Full-Field: mean = 1.84, $p = 0.40$; Fill - No-Fill: mean = -0.49, $p = 0.48$).

Both parametric and non-parametric statistics results indicate that there were no significant

differences in the fixation stability in the different stimulus conditions. After establishing that no

difference was found in the fixation variability, we further examined if the positions of the BCEA

ellipses' center differed between conditions in the two contrasts. We found that for both

contrasts, in all six participants, the BCEA ellipse center of one condition fell within the contour

of the other condition, suggesting that the fixational stability was more or less constant across

conditions. The fixation density map and the BCEA ellipses of two representative participants are

presented in Figure 4.6. The details of how we constructed the density map and the summary of

the BCEA sizes and positions of different stimulus conditions of all six participants can be found

in the Appendix C. Our fixation stability test results indicated that the difference in BOLD

activation we observed in the Center and Full-Field conditions as well as between the Fill and

No-Fill trials in the "scotoma" condition was unlikely to be explained by variability in fixation

stability.

Figure 4.6

Fixation data of participant P1 and P2 recorded in the out-of-scanner control experiment
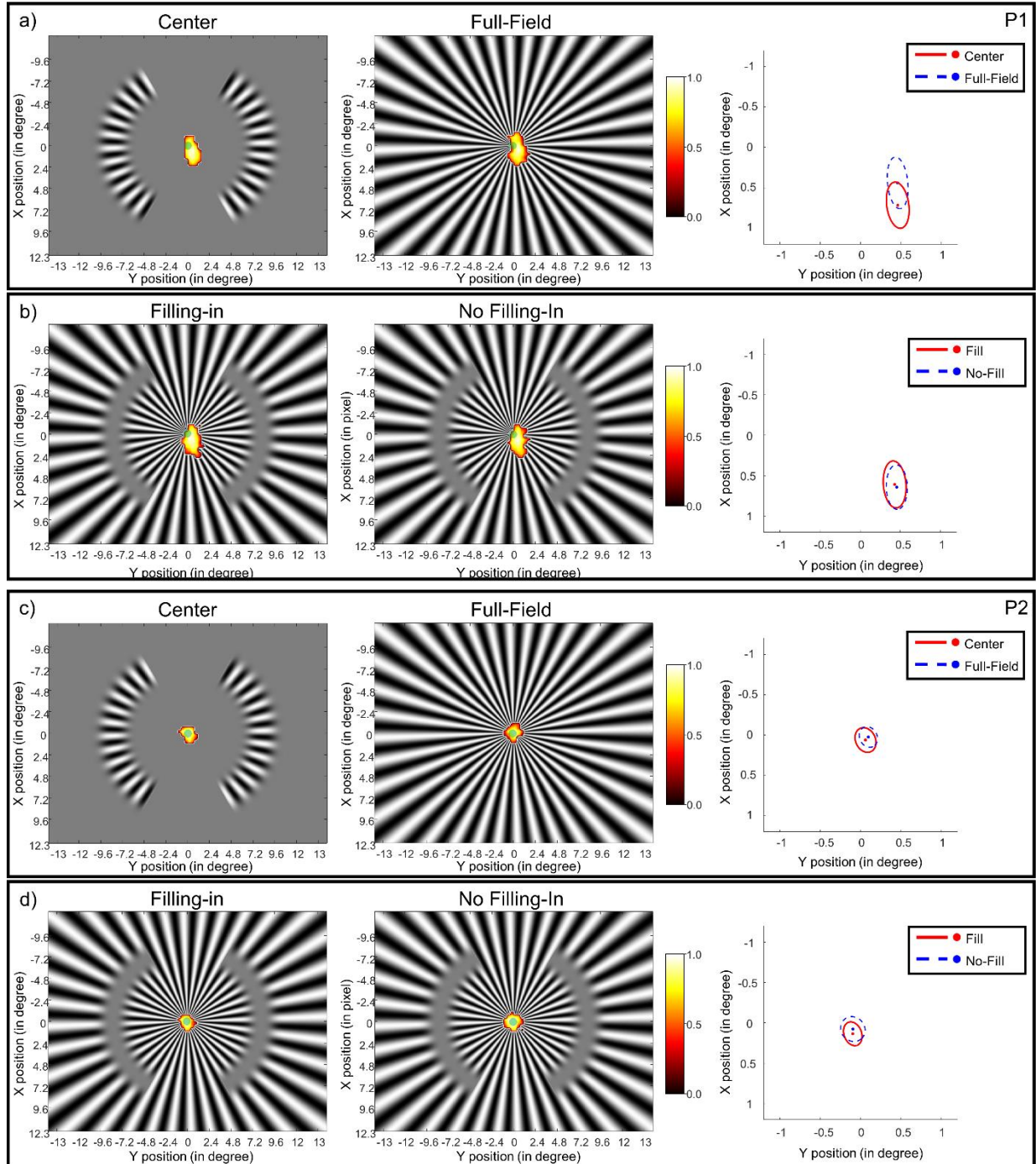
Note. Panel a) and b) demonstrates the data of P1, whereas panel c) and d) the data of P2. Panel a) and c) show the

data of Center and Full-Field conditions. The left and middle plots in panel a) and c) represent the density maps of

the Center and Full-Field gratings. The density value is shown according to the color bar on the right side, with white corresponding to 1.0 and black 0.0. The green dots in the middle of the gratings represent the fixation point. The right plots in a) and c) shows the BCEA ellipses of the Center, with the red solid-line oval and the red dot, and the Full-Field condition, with the blue dashed-line oval and the blue dot. Panel b) and d) show the data of Fill and No-Fill conditions, with the left plots presenting the density map of the Fill and the middle the No-Fill condition. The right plots in b) and d) shows the BCEA ellipses of the Fill, with the red solid-line oval and the red dot, and the No-Fill condition, with the blue dashed-line oval and the blue dot.

4.4 Discussion

To better understand the cortical response associated with the lateral modulation effects such as lateral inhibition and filling-in phenomenon, we presented to participants radial sinusoidal gratings during fMRI. Three types of gratings were used (Figure 4.1): a Center grating with two radial sinusoidal grating patches centering at 8° eccentricity, one in each visual hemifield, a Scotoma grating that was the reverse of the Center grating with two blank "scotoma" regions embedded in the radial gratings, and a Full-Field grating with a radial grating extending over the central and near peripheral visual field.

Comparing between the Center and Full-Field grating allowed us to observe the lateral modulation effect when the surround pattern was added to the center. In a univariate analysis on the BOLD responses in the voxel clusters corresponding to the "center" or scotoma regions of the display we found evidence for lateral inhibition in V1 to V3 regions (Figure 4.2). This lateral inhibition effect supports our previous psychophysical experiments (Lin et al., 2020, 2022), where we discovered that adding a surround to the adapter center decreased the adaptation effect, suggesting the existence of surround suppression. Similar lateral inhibition has been reported in other neuroimaging studies (C.-C. Chen, 2014; C.-C. Chen et al., 2005).

In the "scotoma" conditions, participants were requested to report whether they experienced "filling-in", i.e., the percept of a continuous radial sinusoidal grating, allowing us to compare the BOLD activation between the trials when filling-in was perceived and when it was not. Contrary to previous studies (Mendola et al., 2006; Weil et al., 2008), we did not find a significant BOLD amplitude difference between trials with and without filling-in. Unlike the homogeneous disk used in Mendola et al. (2006) or the random flickering noise in Weil et al. (2008), we used blank crescents positioned left and right of central fixation. Therefore, the filling-in percept perceived by our participants corresponds more to a "fading" of the blank scotoma region instead of a complete disappearance of homogenously illuminated region. Moreover, some participants reported experiencing partial filling-in in the scotoma regions or that different parts of the scotoma appeared to be filled-in at different time points. Our forced-choice task could not allow for the detection of such nuisances in the filling-in percepts. It is also possible that we had higher level of noise in the current experiment that the filling-in effect was not discernable from the noise. We also did not observe a difference in the time course or the time to peak in the Fill and No Fill conditions (Figure 4.3 and 4.4). In the multivariate analysis, however, the linear SVM classifier trained on the filling-in and no-filling-in trials did successfully predict the subjective percept in the test trials in V1, V2, as well as V3 at above 60% accuracy level (Figure 4.5). Such results suggest that even though the mean BOLD signals did not differ between the two conditions, differences in brain activation patterns were present in early visual cortex.

To rule out the alternative explanation that our findings related to variation in fixation stability across our stimulus conditions, we recorded the eye positions of six out of the twelve participants during the different stimulus conditions. An analysis of fixation stability across conditions indicated that it did not differ for the center and full-field conditions or for the filling-

in and no-filling-in trials in the "scotoma" condition, indicating that the effects we found in BOLD activations were unlikely to arise from differences in fixation stability.

One limitation of the current paradigm is that we did not monitor the attention state of the participants on the trial-by-trial base. Since a scotoma trial was classified as a filling-in or a no filling-in trial depending on the response of the participants, it could be misclassified if the participants failed to respond due to a momentary lapse of attention rather than a lack of filling-in percept. The lack of attention would then lead to a lower filling-in report rate than expected. Having said that, any effect of attention does not seem to be substantial in our experiment. We found that the filling-in rate remained around 50%, close to what we expected estimated from the pre-tests, for all experimental runs, suggesting that there was not much fluctuation of the filling-in reporting rate across runs. This could serve as indirect evidence that the loss of attention did not contribute systematically to the percepts reported on the no filling-in trials. In addition, in the Center and Full-Field conditions, participants were not asked to make a filling-in judgment. Consequently, the allocation of attention in these two conditions might be different than that evident in the scotoma condition.

To conclude, we used a simple paradigm to study the lateral modulation effect in vision. We found evidence of lateral inhibition in V1 to V3 regions when a surround pattern was added to the center grating. We also discovered that the brain activation pattern was different when filling-in was perceived from when it was not perceived. During the main experiment, all our stimuli had a constant contrast level. It is well known that the magnitude and direction of the lateral modulation effect can vary with the contrast and orientation of the center/surround stimuli (C.-C. Chen, 2014; C.-C. Chen & Tyler, 2001, 2002; Lin et al., 2022; Meese et al., 2009; Petrov & McKee, 2006; Solomon & Morgan, 2000). Future studies might incorporate such variations to

determine their effect on the resultant BOLD response in early visual cortex. Other related

phenomena like contour erasure (Anstis, 2013; Anstis & Greenlee, 2014) or water color illusion

(Pinna et al., 2001, 2003; Pinna & Grossberg, 2005) could exhibit neural correlates similar to

those reported for filling-in.

4.5 Methods

Participants

Twelve participants including one author, YSL, coded with P1, and eleven naïve

observers unaware of the experiment purpose, aged between 20 to 31, took part in the fMRI

experiment. All of them had normal or corrected-to-normal vision. Every participant completed

three sessions: the ROI localizer session, the pre-test session, and the main experiment session.

P1 and P2 participated in an additional eye tracking control experiment outside of the scanner.

Informed consent was received from all observers before MRI scanning and monetary

compensation was provided after each session as rewards for the naïve participants. The

experiment was approved by the IRB of the National Taiwan University Hospital and was

performed according to the Declaration of Helsinki on human experimentation.

Apparatus and Image acquisition

During the MRI scans, all stimuli and experiment procedure were presented on a pair of

MR-compatible head-mounted goggles (Resonance Technology, USA), delivered by a Windows

7 PC in the MR control room. Each of the two goggle displays (one for each eye) had a resolution

was 800×600 with one pixel size set to $0.035°$ visual angle and a refresh rate of 60 Hz. The

visual acuity of the observer could be corrected with the convex lenses inserted in front of the

goggle displays. Two MR-compatible response boxes were placed below the left and right hands

of the participants to record their behavioral responses with respect to the presence or absence of filling-in.

The T2* weighted images were collected with the Siemens Prisma 3T scanner in National Taiwan University with a 64 channel surface head coil. The anatomical images (T1-weighted, MPRAGE sequence, TR = 2000 ms, TE = 2.3 ms, FA (flip angle) = 8°, image matrix = 256 × 256 × 192, FOV = 240 × 240, voxel size = 0.93 × 0.93 × 0.93 mm) were acquired at the beginning of each scan to construct the anatomy brain model of each participant. The functional images (T2*-weighted) were collected in 32 transverse planes aligned with the AC-PC (anterior commissure-posterior commissure) direction. An echo-planar imaging sequence (Stehling et al., 1991) was used to acquire 32 transverse planes parallel to the AC-PC (anterior commissure-posterior commissure) for the functional data (TR = 2000 ms for the pretest and the main experiment, TR = 3000 ms for the retinotopic and scotoma localizer scans, TE = 25 ms, FA = 90°, image matrix = 96 × 96 × 32, FOV = 192 × 192, voxel size = 2 × 2 × 2 mm). An extra low-resolution T1 inplane (TR = 595 ms, TE = 6 ms, FA = 70°, image matrix = 192 × 192 × 32, FOV = 192 × 192, voxel size = 1 × 1 × 2 mm) acquired in planes identical to the functional images was collected to facilitate alignment between the functional and anatomical images.

Eye tracking apparatus

To record the participants' eye positions during stimulus presentation, we used two eye trackers in the current study. The first is the MR-safe ViewPoint EyeTracker system by Arrington Research®, Inc (www.ArringtonResearch.com) with 60 Hz data acquisition rate controlled by a Windows 7 PC which recorded eye positions during the stimulus presentation in the scanner. The second is the EyeLink 1000 (SR Research Ltd., Canada) system used in an out-of-the scanner control experiment controlled by a Windows 10 PC. The data acquisition rate was 1000 Hz. The

stimuli for the out-of-scanner control measures were presented on a 17-inch EIZO FlexScan

S1910 monitor calibrated with a PR-655 SpectraScan® photometer, with a refresh rate of 60 Hz

and a resolution of 1280×1024 with one pixel size of $0.023°$ visual angle. The fixation stability

test conducted outside of the scanner was carried out in a dimly lit room.

Stimuli

To maximize brain response induced by the visual stimuli, instead of using small

sinusoidal patterns presented in one visual quadrant like was done in our previous psychophysics

experiments (Lin et al., 2020, 2022), we generated radial sinusoidal gratings (patterns expanding

from the fixation center to the display border) that occupied larger regions of the visual field.

Three such radial sinusoidal gratings were used in the experiments: a Full-field grating (Figure

4.1a), a Scotoma grating (Figure 4.1b), and a Center grating (Figure 4.1c). The Full-Field radial

grating were defined by the following equation,

$$G = B + BC\cos(2\pi f\theta),\qquad(4.3)$$

where θ is the angular coordinate in the polar coordinate system, B the mean luminance, C the

stimulus contrast, and f the spatial frequency. In the current study, f was set to 0.1 cycle-per-

degree. The Center grating was created by multiplying the grating in equation (4.3) with the

following window:

$$W = e^{-(\frac{(r-r_E)^2}{2\sigma_r^2})^P},\qquad(4.4)$$

in which r is the radial coordinate of the polar coordinate system, r_E determines the eccentricity

of the center of the window and σ_r, the radial scaling parameter, decides the width of the

window. In the current study, the r_E was set to $8°$ and σ_r $1°$. We masked out the grating pattern

positioned between $-30°$ and $+30°$ rotation angle from the vertical meridian to separate the center

grating into two crescent patches that span across 120° rotation angle (16.8° length in visual

angle), one on each side of the visual field. The scotoma grating was the reversed pattern of the

center grating, where two scotomata were positioned at the patches' locations.

The, the power of the Gaussian mask, P value in equation (4.4), determines the sharpness

the edges of the patches in the center grating and the scotomata in the scotoma grating. In a pilot

study, we tested scotoma stimuli of different P values on two observers (P1 and P2) and found

that when P was equal to 3, perceptual filling-in was perceived about 50% of the time for -6 dB

(50%) surround luminance contrast level. Thus, we chose such P value for the stimuli used in the

formal experiments. The localizer pattern (Figure 4.1d) was created by applying the same

window in equation (4.4) but with a power value of 1000 to create a sharp edge in the radial

direction. The width of the scotoma/center patches were 2.8°, wide enough to cover the receptive

fields of early visual areas that were about 0.5° in V1, 1.9° in V2, and 3.4° in V3 at 8°

eccentricity according to the estimates from single-neuron recording studies in primate visual

cortex (meta-analysis shown in Figure 9 in Smith, Singh, Williams and Greenlee (2001), based

on the data of (Burkhalter & Van Essen, 1986; Felleman & Van Essen, 1987; Gaska et al., 1987;

Gattass et al., 1981, 1988; Zeki, 1978)).

Procedure

Luminance contrast calibration task in the scanner

During a calibration session of the MRI-safe goggles, the left side of the screen was filled

with a homogeneous square whereas the right side a high spatial frequency flickering square

wave grating of maximal contrast. The observers were to adjust the luminance level of the

homogeneous square to match the perceived luminance of the grating. We then fitted a power

function between the subjective luminance percept and the display values to determine the

gamma value used for calibrating the visual display during the experiment, i.e. gamma correction. The deduced gamma value was then used to compute the linear look-up table for the goggles for the following experiment sessions. Such calibration task was conducted at the beginning of each scanning session.

ROI localization

The regions of interest (ROIs) in the visual cortices of each observer were identified before the experiment sessions with the following method.

1. Retinotopic mapping: To identify the first-tier visual areas (V1, V2 and V3), we combined a rotating wedge and an expanding ring made of high-contrast checkerboards patterns that moved across the visual field (Engel et al., 1997; Wandell & Winawer, 2011). The patterns flickering in counterphase at 4 Hz. The rotating wedge spanned across 45° and rotated 22.5° in clockwise direction every TR (3000 ms), thus mapping the whole visual field in every 48 seconds, whereas the expanding ring of a width of 1.77° moved from the foveal area (0.25°) to the periphery (10.6°) with a step of 0.86° every TR, taking up 36 seconds to finish the whole cycle. One retinotopic mapping run took 288 seconds (96 TRs) to complete, resulting in 6 repetition cycles for the rotating wedge and 8 cycles for the expanding ring. Each run was repeated for at least four times for each participant.

2. Scotoma localizer: To target the brain regions corresponding to the scotomata of our stimuli, we conducted an independent localizer scan in which two high-contrast checkerboard crescent patterns flickering at 5 Hz located at the scotoma regions (Figure 4.1D) were presented in an on-and-off manner with on and off period taking 6 TRs (TR = 3000 ms) each and repeating six times resulting in a total of 72 TRs per scan. The scotoma scan was repeated for at least two times for each participant.

To make sure the observer maintained steady fixation during each scan, we added a center fixation task during the stimulus presentation in the localizer runs. Participants were to count the times the fixation dot changed color during the scan and reported the number at the end of each scan. Only runs with high accuracy (over 95% correct) fixation task performance on the central counting task were retained and analyzed. The same performance criterion was applied in the following pre-test and main experiment scans to ensure steady fixation of participants.

Pre-test

The purpose of the pre-test session was to adjust the luminance contrast level for each observer until they could perceive filling-in about 50% of the time for the Scotoma condition (Fig. 1b). Thus, only the scotoma stimulus was used in the pre-test scans. Each run contained 10 trials; on each trial, the surround grating flickered at 5 Hz for 10 seconds and then followed by a 14-second blank period. The participants were instructed to press a button on a response box held by their left-hand whenever they perceive a filling-in during the scotoma trials. The scotoma trials with filling-in button pressed were categorized as trials with perceived filling-in, whereas the trials without filling-in button pressed were categorized as no filling-in trials. In addition, they were to press another button on response box at their right hand whenever the fixation color changed from green to red during the whole experiment. If the participants reported perceiving filling-in more than six times out of the ten trials, the inducer contrast would increase in the next run. Otherwise, if, they should perceive filling-in less than four times out of ten, the inducer contrast would decrease on the next run. Each observer participated in at least four runs. We then used the most suitable luminance contrast for all three types of radial gratings for each participant in the main experiment. As a result, all stimuli in the main experiment were of the same luminance contrast. The pretest was complete in between 20 to 30 minutes.

Main experiment

In the main experiment, all three radial sinusoidal gratings were used. There were 20 trials in each run, containing five center grating trials, five full-field grating trials, and ten scotoma grating trials in random sequence. One each trial, one of the three stimulus gratings flickered at 5 Hz for 10 seconds (5 TRs) then replaced by a 14-second (7 TRs) blank period. A fixation task, in which the participants were to press a button on their right hand when the fixation changed color, was performed during the whole experiment to control the attention of the participants. All participants had an accuracy for this task greater than 95%. In addition, in scotoma trials, participants were to press a button on their left hand when filling-in was perceived during the scotoma grating presentation. Participants were instructed to keep their eyes open during the stimulus presentation and blink only after the stimulus disappeared during each trial throughout the experiment. Each participant completed eight runs in the main experiment, resulting in forty center and full-field trials, and eighty scotoma trials that contained trials with filling-in percept and those without. The main experiment took around seventy minutes to complete.

Fixation stability test

To test whether there were differences in eye movements and fixation stability during different conditions, we collected eye-tracking data in four participants (P3 to P6) during MRI scanning. Calibration of the eye tracker was performed at the beginning of the fMRI main experiment. During the calibration process, the participants were instructed to fixate a white calibration dot target positioned on a mean luminance background that appeared in one of the sixteen positions in a random sequence. The calibration dot changed to the next position once it recorded stable eye fixation. The fMRI main experiment was performed after good calibration was achieved. In the remaining two participants (P1 and P2), we conducted an additional control

experiment with the same stimulus conditions outside of the scanner. The experiment procedure was the same as the main experiment except that a calibration and validation sessions were performed before each run. We performed a nine-dot calibration procedure, where participants were to fixate on the white calibration dot target in a mean luminance background that appeared in one of the nine calibration positions in random order. The target moved to the next position only when it recorded stable fixation. After the calibration was accepted, a validation procedure where participants were to fixate at the target dot sequentially presented in the same nine positions was performed again. The eye tracker system then computed the deviations between the target positions and the computed fixation positions according to the calibration estimates. The calibration/validation cycle was accepted only when none of the deviations of the nine positions exceeded 0.5 degree. The control experiment was performed after good calibration/validation results were achieved. Eye positions were recorded during the 10-second ON period on each trial during the experiment.

All stimuli generation and experiment procedure controls were done with MATLAB (MathWorks, Inc., Natick, MA) with PsychToolbox Version 3, (http://psychtoolbox.org/).

Data analysis

For the anatomical images, we reconstructed cortical surface models for all participants with Freesurfer (Dale et al., 1999; Fischl, 2012; Fischl et al., 1999), which involved automated reconstruction of each MPRAGE anatomical scan that separated the brain into gray- and white-matter surfaces. As for the functional imaging scans, after DICOM conversion done by the MRIcron (https://www.nitrc.org/projects/mricron), preprocessing steps that include motion correction referenced to the first image and slice time correction were done with SPM8 (http://www.fil.ion.ucl.ac.uk/spm/software/spm8/), a MATLAB-based toolbox. No spatial

normalization or spatial smoothing was performed for the individual brain images for univariate

and multivariate analyses. The analyzed images were then fed to the mrVista toolbox

(https://web.stanford.edu/group/vista/cgi-bin/wiki/index.php/MrVista) where co-registration and

data visualization were performed. The General Linear Model (GLM) and further statistical

analyses were done by customized MATLAB codes according to the standard GLM methods

(Johnson & Wichern, 2007). To test the target contrasts between conditions, we calculated the t-

values based on the mean and variance of each contrast (difference in β values between the two

conditions) for each voxel. We averaged the t-values across all voxels for each ROI as one

datapoint for each observer. We then performed a t-test on these averaged t-values at the group-

level for each ROI (Figure 4.2B).

We used the mrVista toolox to delineate early visual areas for each participant based on

the images of the retinotopic mapping localizer sessions. We used the phase-reversals according

to the rotating wedge data to define the boundaries between visual areas. For the first-tier visual

area, we defined five visual areas: V1, dorsal V2, ventral V2, dorsal V3, and ventral V3 for each

hemisphere. Then we restricted the area responding more to the scotoma localizer than the gray

background within each retinotopically defined ROI. A voxel was considered activated if the t-

statistics of the regression coefficient exceeded 5.09 ($|r| > 0.52$). The criterion corresponded to a

one-tail Bonferroni corrected α-level at 0.05 for each voxel considering the total number of gray

matter voxels. Figure 4.7 demonstrates such restricted ROIs in the left hemisphere of one

participant. To make sure that the voxels in these ROIs received minimal contribution from the

surround region outside of the scotoma localizer center, we further restricted the ROI by leaving

only the voxels that had greater activation to the Center grating (Figure 4.1c) than to the Scotoma

grating (Figure 4.1b) used in the main experiment. We achieved this by computing the activation

difference between the Center grating and Scotoma grating and removing the voxels with

activation in the Scotoma condition greater than that in the Center condition. We combined the

ventral and dorsal subregions of V2 and V3 together as one V2 and V3 areas for data analysis,

resulting in three ROIs per hemisphere and six in total for each participant for univariate analysis

(Figure 4.2-4.4). For the multivariate analysis, to ensure we had enough voxels left in each ROI

as features for SVM model training, we further combined corresponding ROIs in both

hemispheres together and resulted in three ROIs, V1, V2, and V3 regions. Therefore, the MVPA

results were discussed in only three ROIs (Figure 4.5).

Figure 4.7

Demonstration of ROIs of the Left Hemisphere of one Participant
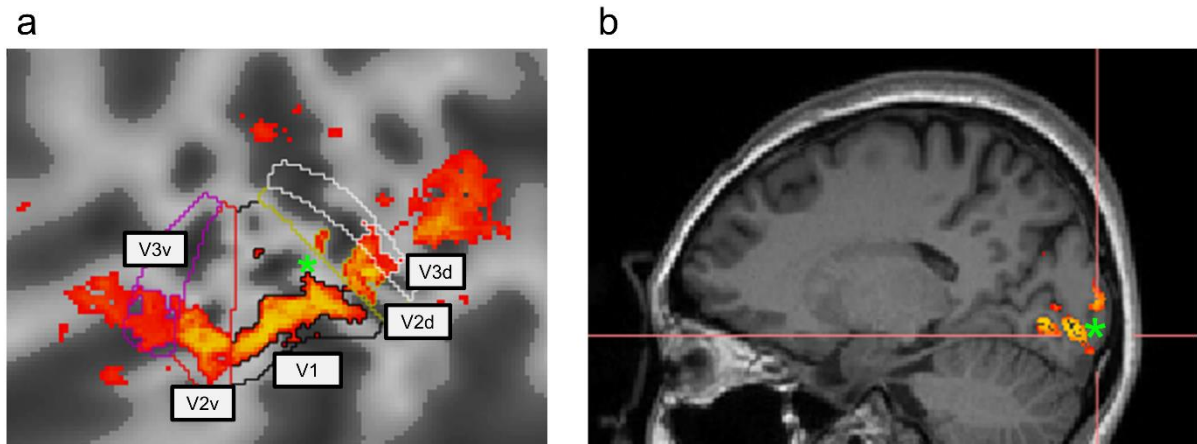
Note. This figure shows the examples of defined ROIs of the left hemisphere used for data extraction and analysis in

the current study. Panel a represents the ROIs in an inflated and flattened view. The color outlines indicate the

contours of each early visual area delineated from the retinotopic mapping data. The orange patches demonstrate the

regions activated by the "scotoma" localizer. Panel b shows the same activation pattern in the sagittal view of the

anatomical brain. The green asterisks correspond to the same position in the brain on the two different views.

To examine if there was a difference in the activation pattern, we used LIBSVM toolbox (Chang & Lin, 2011) to perform a multivariate pattern analysis (MVPA) on the trial-by-trial data (Kriegeskorte et al., 2006). We first transformed the unsmoothed preprocessed data of all voxels in each ROI into z-scores by normalizing the data across the time points in each run. We then rescaled the z-scores to range 0 to 1 and averaged the BOLD activation from 3rd to 7th TRs relative to stimulus onset for model training and testing. The choice of such activation period was to target the peak BOLD response. For each participant, we used leave-one-out method to train a linear SVM classifier on the data of filling-in and no-filling-in trials of seven runs, which included 70 trials, then tested the model on the remaining run, which contained 10 trials. We performed such training and testing procedure eight times until all runs were being tested once and then we averaged the classification accuracies across the eight cross-validations. To examine the classification result, we performed a permutation test (Etzel & Braver, 2013; Hanke et al., 2009; Nichols & Holmes, 2002). We randomly relabeled the test and train data in each ROI of each participant with respect to "filling-in" and "no filling-in" trials for every cross-validation and average the prediction accuracy across the eight repetitions. We then computed the group mean value of the averaged cross-validation accuracy across all participants. Such process with random assignment was repeated 5000 times, leading to a distribution of group mean accuracy for each ROI.

5. CHAPTER 5: CONCLUDING REMARKS

Lateral modulation effect describes how the context, in which a stimulus is presented, can affect its percept. Such lateral modulation effect can be observed in many visual phenomena and its neural correlates have been reported in several areas of the visual system. Despite many decades of research, some research issues remain to be answered. It is unclear how selectively adapting different regions in the visual field could affect the orientation percept of a subsequently viewed target, especially when the adapter center is modulated by a surround pattern. Also, the underlying neural mechanism(s) of perceptual filling-in is still under debate. To address these research questions, we set up three main goals in this thesis. First, we aim to establish psychophysics and neuroimaging paradigms that can reveal new evidence for an orientation-specific lateral modulation effect. Second, we explain the lateral modulation effects observed in the paradigms with a computational model that incorporated divisive inhibition. Last, we investigate the neural mechanism of perceptual filling-in.

In the following sections, we discuss the results with respect to these three research goals. We summarize the major findings in the three studies (Chapter 2 to 4) and examine how well our empirical data and computational modeling obtain these main goals. Afterwards, we focus on the limitations of the present research and possible future directions, followed by a conclusion.

5.1 General Discussion: Key Research Goals

We divide this section into three parts, each corresponding to one key research goal. After a brief recap of the results and conclusion of the three main studies, we reflect on how well our empirical findings achieve these goals and answer the key research questions.

Goal 1: Establish Paradigms to Investigate Orientation-Specific Lateral Modulation Effects

To investigate how lateral modulation varied with center and surround orientation, we designed an adaptation paradigm that allows us to investigate the orientation percept of a target following selective adaptation to the center, the surround, and combined stimulus regions. Doing so provides us with a chance to not only estimate the impact of lateral modulation effect in different center-surround patterns, but also the effect of the filled-in percept on the target. We discovered that 1) the TAE depended on the adapter orientation and peaked at around 10 to 20 degree and 2) the aftereffect magnitude was the strongest with the center adaptation, followed by the full field adaptation, and the least with the surround-only adaption. The difference in TAE magnitude between the center and the full-field adapter conditions showed that adding a surround to the adapter decreased the adaptation effect, suggesting an inhibitory lateral modulation effect. To further investigate the property of such lateral inhibition, we manipulated the stimulus center and surround orientations independently and found that the TAE first decreased then increased as the surround orientation deviated from the center orientation, showing that the lateral inhibition was indeed orientation specific.

In the surround-only adapter condition, perceptual filling-in was perceived in the central blank region that did not physically overlap with the target. The fact that such a filled-in percept could induce an aftereffect suggests that the adapter surround induced modulation effect on the blank region. With further examination, we found that participants with higher filling-in rating also experienced stronger TAE magnitude. In addition, when we separately estimated the TAE magnitude for trials with filling-in and trials without, trials with filling-in revealed stronger TAE. Both results again hinted that the lateral modulation effect from the surround to the central blank region was the source of both perceptual filling-in and the TAE.

Based on these empirical findings, our behavioral paradigm successfully provided new evidence in the orientation tuning of lateral modulation in center-surround orientation grating. The psychophysics studies have shown how the aftereffect changes as a function of the center and surround features, and demonstrated the link between lateral modulation effect and perceptual filling-in.

Next, we investigated the neural correlates of the lateral modulation effects observed in the psychophysics studies with fMRI. We presented radial sinusoidal gratings that subtended different parts of the visual field, allowing us to compare the BOLD signal when the center, the surround, and both the center and surround regions were being stimulated. In the univariate analysis, we discovered that when the surround was added to the central pattern, the BOLD signal of early visual areas decreased, indicating a lateral inhibition effect, supporting the finding of inhibitory lateral modulation in the psychophysical experiments. In the multivariate pattern analysis, we found that trained linear SVM classifiers could predict whether filling-in was reported in the scotoma grating trials, revealing that the brain activation patterns of the filling-in and no filling-in trials were different, matching our psychophysical findings that the lateral modulation effect was different when filling-in was perceived compared to when it was not. Combined, our psychophysical results and fMRI findings provide coherent new evidence that contribute to our understanding of the lateral modulation effect.

Goal 2: Explain Lateral Modulation Effect with a Divisive Inhibition Model.

To further examine the empirical results observed in the psychophysics studies, we aimed to develop a computational model that could capture the behavioral results with meaningful parameters. Analyzing these model parameters should enhance our understanding of the underlying mechanisms of the visual system.

The divisive inhibition model has been proposed to explain multiple different lateral

modulation effects including the tilt-illusion (Clifford, 2014; Goddard et al., 2008; Schwartz et

al., 2009), lateral masking (C.-C. Chen & Tyler, 2001; Meese et al., 2007; Xing & Heeger, 2001),

and visual crowding (Solomon et al., 2004). We developed a variant of such a divisive inhibition

to capture three main aspects in the psychophysical data: 1) orientation population coding, 2) the

adaptation effect, and 3) the lateral modulation from the surround to the center. For the first

aspect, we assumed the existence of multiple orientation detecting channels that prefer different

orientations. We further assume that the final stimulus percept is determined by the weighted sum

of all these channel responses. The channel response to an oriented grating is computed by an

excitatory component raised by a power then divided by an inhibitory component plus a

normalizing constant, z, shown in Equation 2.4 (Foley & Chen, 1997). Our model manifested the

adaptation effect by changing the z parameter: the stronger the adaptation, the larger the post-

adaptation z, resulting in weaker channel response. The magnitude of the adaptation effect

depends on how strongly the channel responds to the adapter. As for the lateral modulation effect,

the model contained two multiplicative sensitivity modulating parameters, Ke and Ki (Equations

3.4, 3.8 and 3.9), representing the excitatory component in the numerator and the inhibitory

component in the denominator, respectively. These two parameters are functions of surround

orientation which reflect the magnitude of the excitatory and inhibitory lateral modulation from

the surround pattern.

Our model can explain most data variance in the psychophysical experiments. When the

surround has the same orientation as the center in the center-surround condition, we used a

reduced model in which the variation of the excitatory sensitivity, Se (Equation 2.2), alone could

capture the surround modulation between different adapter types. We found that the value of Se

was the highest in the center-only condition, intermediate in the center-surround condition, and the lowest in the surround-only condition where filling-in was perceived. Such a trend in Se variation matches that of the TAE data. The Se reduction in the center-surround condition reflects the lateral inhibition effect when the surround pattern was added to the center. When the center and surround have different orientations, we used the full model in which both Ke and Ki varied to model the orientation-specific lateral modulation effect. We discovered that parameters Ke decreased with the surround orientation increased and Ki first increased then decreased as the surround orientation increased. These two lateral modulation parameters capture the fact that the TAE first decreased then increased as the adapter surround orientation increased, revealing that the adaptation induced on the target was the interplay between the excitatory and inhibitory lateral modulation effects as the surround orientation deviated from the adapter center orientation. Such parameter changes demonstrate the orientation tuning of lateral excitation and inhibition effects in our center-surround orientation grating adaptation.

These model fitting results again suggest that the divisive inhibition model implemented in this thesis, when the sensitivity modulation is considered, is flexible enough to explain both the adaptation and the lateral modulation aspects in the data. We therefore fulfilled the second goal of investigating the lateral modulation effects quantitatively via a computational model.

Goal 3: Understand the Underlying Neural Mechanism of Perceptual Filling-in

As mentioned in the introduction (Chapter 1), two main theories can be found in the literature that seeks to explain the neural mechanisms underlying filling-in. One is the symbolic or cognitive theory, stating that filling-in involves a passive process in which higher visual areas ignore the missing input in the scotoma and represent the blank spot with surround pattern

properties. The other is the isomorphic, suggesting an active process that reconstructs the missing information by interpolation of the surround pattern.

Based on the cognitive theory, no activation is needed in the artificial scotoma region for filling-in to occur. Therefore, the filled-in area should not induce any aftereffect. Contrary to such prediction, our psychophysics results showed that, without physical stimulation on the central region corresponding to the target, the filled-in percept in our surround-only adapter could induce weaker albeit significant TAE on the target orientation percept. And such TAE has the same surround orientation specific pattern as in the center-only and center-surround adapters. Such evidence suggests that an active process initiated in the surround and spreading to the center blank region contributes to the lateral modulation effect during the filling-in percept. Therefore, our behavioral data supports the second theory: an active process is involved during filling-in. Our fMRI results showed that the brain activation pattern in the early visual cortex was different when filling-in was perceived compared to when it was not. Again, according to the cognitive theory, no activation difference should be present in the early visual areas between filling-in and no filling-in percepts, as higher cognitive areas are responsible for representing the missing information. As a result, our neuroimaging data align with the second theory as well as with our previous findings.

After ascertaining that the filling-in percept we observed involved an active process, the question about the nature of such process arises. In theory, both lateral excitation and lateral inhibition can cause perceptual filling-in. Empirical evidence in previous psychophysical and neurophysiological studies have support both possibilities. Examining our model fitting results, the filling-in condition is associated with a higher excitatory sensitivity parameter compared to

the no filling-in condition. Such finding suggests that lateral excitation was more likely to be involved.

5.2 Significance of this Research

The underlying mechanism of lateral modulation remains one of the most intriguing mysteries yet to be solved in visual neuroscience. We described key research questions in lateral modulation and addressed them with three major studies. Our empirical findings and data interpretation have shed light on how neurons respond to different visual field regions interact with each other. The thesis has achieved three aforementioned goals of providing new evidence of lateral modulation with well-designed paradigms, utilizing a computational model to explain the observed lateral modulation effects, and reconciling the long-debated controversy of perceptual filling-in. These achievements have led to numerous conference presentations and publications in leading international journals.

The current doctoral thesis integrated multiple methodologies including psychophysics, computational modeling, and neuroimaging with advanced analyses including machine learning, showing the power of bridging interdisciplinary techniques to produce substantial results contributing to the field of visual neuroscience. The paradigms and model developed in the thesis can inspire multiple future research projects that further expand the horizon of understanding the fundamental processing of visual system demonstrated with lateral modulation effects. The project has also served as part of the bilateral collaboration between the groups of Prof. Mark Greenlee in Germany and Prof. Chien-Chung Chen in Taiwan. The fruitful collaborating results demonstrated in the thesis have spawned further research ideas based on the milestones of our work to date.

5.3 Research Limitations

Limitation of the binary-choice task

In our psychophysics experiments, the participants made a binary-choice on the target orientation to indicate whether they perceive the target as oriented clockwise or counterclockwise. Doing so, we can estimate how much orientation bias was induced by the previously presented adapter. However, in a binary-choice task, such an orientation bias could contain two components: the perceptual bias caused by the adaptation effect and the decision-making bias that represents the tendency of the participants reporting one direction more than the other. Therefore, to separate such a decision-making bias from the perception bias, we needed to include an extra internal bias parameter, m (Equation 2.6), to represent the internal bias of the participants. To avoid this issue, an objective estimate of the perceived orientation without involvement of the decision-making bias needs to be developed. As such an objective estimate has not been available yet, the best strategy to capture the decision-making bias is to incorporate the internal bias in our model.

Limitations of Investigating Perceptual Filling-in

Unlike the filling-in in the retinal scotoma or blind spot, where the eccentricity and size are limited by physiological factors, artificial scotoma filling-in has many merits: the relatively definite and measurable onset time, easily inducible across observers, and controllable size and location across the visual field (De Weerd et al., 1998). Unfortunately, studying filling-in in artificial scotoma is not without limitations. The major difficulty is that we rely on the subjective report to determine whether filling-in was perceived in a trial or not, making it hard to verify objectively whether filling-in occurs. In addition, the timing when participants report seeing filling-in is influenced by the reaction- and decision-making time, which might deviate from the

timepoint when filling-in happens, making it difficult to pinpoint the exact timing when filling-in

occurs. Finally, in our fMRI study, some participants reported perceiving partial filling-in within

the two scotoma patches and different parts of the scotoma being filled-in at different time points,

but our yes-no forced choice filling-in response was unable to detect such perceptual variations.

Thus, unless an objective measurement of the perceptual filling-in in artificial scotoma can be

developed, we always need to consider to what extent the subjective report might influence our

results. However, judging from the findings in our psychophysical experiment, in which we

discovered that filling-in trials corresponded to stronger TAE, and that in our fMRI experiment,

the brain activation pattern was different between filling-in and no filling-in trials, we could still

conclude that even with the potential nuisances of subjective filling-in report, our paradigms are

valid and sensitive enough to study the underlying mechanisms of perceptual filling-in.

Limitations of functional MRI

Although MRI has become one of the most popular neuroimaging techniques due to its

many merits, one must be cautious when interpreting fMRI data (Logothetis, 2008). First, the

BOLD signal, although highly correlated to the neuron action potentials, reflects the metabolic

correlates of neuronal activity. More specifically, how the blood oxygenation level changes due

to active neurons during the experimental manipulation. Therefore, it is a rather indirect

measurement of the actual neural activity. Second, due to the scale of its spatial resolution, one

voxel in a fMRI experiment typically covers millions of neurons and tens of billions of synapses.

Even for submillimeter voxel, each voxel would still contain up to a million neurons (see Cheng

and colleagues (2001) where they used higher field MRI and clever design to map out the ocular

dominance columns in human visual cortex). In addition, fMRI has an intermediate level

temporal resolution ranging from a few hundred milliseconds to a couple of seconds. Such a

resolution is not enough to capture the activity of a single neuron, which has the scale of ten milliseconds (Huettel et al., 2014). In other words, what is recorded in an fMRI experiment are not the neural activities of individual neurons but the overall activation level of neuron populations when stimulated with given stimulus. Therefore, we should not interpret the fMRI results as we do when inferring from single neuron recording studies and must be careful when comparing the results between the two techniques. For example, in the filling-in literature, single cell recording studies have shown cells in early visual cortex corresponding to the blind spot or artificial scotoma were activated when filling-in occurred (De Weerd et al., 1995; Komatsu et al., 2000; Matsumoto & Komatsu, 2005), suggesting an excitatory effect. On the other hand, fMRI studies have shown reduction in BOLD signal in early visual cortex when an artificial scotoma or a luminance patch was filled-in (Mendola et al., 2006; Weil et al., 2008), suggesting an inhibitory effect. Such seemingly contradicting results might not only reflect the difference in stimuli and paradigm used, but the fact that the former measured responses of individual neurons while the latter estimate the response of neuron populations. Therefore, the lateral modulation effects manifested by these studies could indicate neural interaction at different levels.

However, even when its limitations in spatial and temporal resolutions are considered, fMRI still serves as an ideal non-intrusive neuroimaging tool for vision research as it reveals the overall, albeit indirect, activation of a population of neurons. When combined with behavioral evidence such as the psychophysical results, fMRI can become a valuable and powerful technique. One strategy, implemented in the current thesis, is to first establish a solid visual phenomenon in behavioral studies then present the stimuli, adjustment is usually needed to elicit most brain activation, in an MRI scanner to explore how the visual cortex is activated during stimulus presentation. Another strategy is to use fMRI data to form data-driven hypotheses that could lead to future experiments. For example, in our psychophysical studies, we discovered

evidence of lateral inhibition when the surround was added to the center, which led us to the hypothesis that the BOLD signal should be reduced in the full-field condition compared to the center condition in our fMRI study. Indeed, we found a decrease in BOLD activation in V1 to V3 areas when the surround was presented with the center pattern, supporting that an inhibitory lateral modulation effect was involved according to the neuron population activation recorded in fMRI. Similarly, we observed stronger TAE in filling-in trials within the psychophysical experiment, leading us to infer that the brain activation should be different between the filling-in and no-filling-in percepts. In the fMRI study, we did not find a difference in the overall BOLD activation level, suggesting that at the neuron population level, not enough activation difference was observed to support the evidence of lateral excitation or lateral inhibition involvement. However, we did find evidence of brain activation pattern being different between the two percepts, indicating that there could be a difference in neural responses of the individual neurons which affects the overall population response that is reflected by the brain activation pattern. To further isolate the responses of the individual neurons during filling-in requires single-cell recording techniques such as implemented in Matsumoto and Komatsu (2005).

5.3 Future Directions

In the adaptation paradigm used in the current thesis, we focused on the impact of adapter orientation on the following target and kept the stimulus luminance contrast constant across different conditions. Similarly, in the fMRI study, the luminance contrast was kept constant across different stimulus conditions. Therefore, one of the future directions worth exploring is the manipulation of the luminance contrast of the stimuli and observe how the target threshold in the behavioral paradigm and the BOLD signal in fMRI paradigm changes as a result. Doing so offers the opportunity to estimate how the lateral modulation effect varies as a function of the stimulus

contrast, allowing us to compare the data with previous studies focusing on luminance contrast as the main independent variable. As luminance contrast is one input in our divisive inhibition model, we could easily adjust our model to capture the data variance when luminance contrast is manipulated. By presenting a stimulus with multiple contrast levels in the fMRI experiment, we could observe how the brain activation varies as the contrast changes and examine whether our contrast-gain-control-model could predict how the BOLD signal varies as a function of luminance contrast. In addition, only one orientation was used in our fMRI experiment. In future studies, we could present gratings with different orientations and implement the forward model proposed by Brouwer and Heeger (2009, 2011) to estimate the orientation tuning of orientation channels and further examine the neural correlates of the lateral modulation effects.

Besides artificial scotoma, perceptual filling-in can be manifested under different viewing conditions such as the blind spot and various visual illusions, suggesting that multiple neural processes might be involve during different filling-in percepts. Another future direction that can be derived from the current project is the investigation of different types of filling-in effects to compare the resulting lateral interaction between the filled-in area and the surround region. One possibility is to study the filled-in surface created by illusory contour. Chen and colleagues (2018) presented Kanizsa-style square with various configurations that led to different levels of illusory contour and surface percept (see Kellman and Shipley (1991) for an earlier application of the paradigm). From high to low surface and contour information, the authors included a Kanizsa square where four Pac-man shape inducers had the opening facing inwards which created an illusory square surface, a shape pattern where two adjacent Pac-main inducers faced outwards and created only half a surface, a contour pattern where three inducers faced outwards and induced only an illusory contour, and the baseline condition where all four inducers faced outwards, leaving no illusory contour and surface percept. The observers were to determine

154

whether a target dot was located inside or outside of the illusory surface. The results showed that

the location detection performance improved as the level of contour and surface information

increased, suggesting that the illusory filled-in surface and contour facilitate target detection. In a

later fMRI study (S. Chen et al., 2021), the authors presented the Kanizsa square and baseline

conditions and measured the luminance discrimination and target localization performance of the

participants. Compared to the baseline condition, performance improvement in Kanizsa condition

only happened in the dot localization task, suggesting that the illusory surface facilitation

occurred only when the stimulus configuration was task relevant. In addition, the fMRI data

presented evidence of feedback connection from the lateral occipital cortex (LOC) to V1 and V2

areas, indicating that LOC plays an important role in object and surface configuration by

integrating low-level information from and sending feedback information to V1/V2 regions. By

manipulating the inducer configuration, these studies could control the level of illusory surface

perceived by the observers without relying on the subjective report. Similar instant filling-in

effects are present in watercolor and neon color illusions (Pinna et al., 2001, 2003; Pinna &

Grossberg, 2005). In future research, we could potentially implement these types of filling-in

illusions as adapters in our adaptation paradigm and estimate the adaptation effect on a following

target to infer the study mechanisms. Another filling-in phenomenon that is worth exploring is

the contour erasure effect. Anstis (2013) reported that after briefly adapting the contour of a low

luminance object for three seconds, the object was filled-in immediately and disappeared into the

background (see also Anstis and Greenlee (2014)). Inducing contour erasure and estimating how

such an effect changes the percept of a following target also allows us to explore the role of edge

and border in filling-in percept. To this day, no quantitative measurements have been done on the

contour erasure effect. In future studies, we could estimate how adapting to the contour could

affect the target detection and discrimination threshold in a 2AFC paradigm. Furthermore,

previous contour erasure effects focused only on homogeneous targets embedded among a mean luminance background. We could use oriented gratings as target and surround pattern to examine the orientation tuning of the lateral modulation mechanism during the contour erasure effect in the future. Such a paradigm could reveal an interesting interaction between border deletion filling-in (contour erasure) and pattern filling-in (artificial scotoma).

Yet another future direction is to apply our experiment paradigms in researching lateral modulation mechanism in patients with visual impairment. According to the WHO report on global visual impairment (Pascolini & Mariotti, 2012), 285 million people were estimated to be suffering from various eye diseases leading to low vision or blindness, suggesting that visual impairment has become a major global health issue. As the population in many developed countries are aging rapidly, more and more people could be expected to suffer from age-related visual disorders such as macular degeneration. Thus, investigating the neural mechanisms behind visual impairments to potentially help enhance the vision of eye disease patients is a crucial task for vision scientists nowadays. Some studies have shown promising visual improvement after perceptual learning sessions in patients with central vision loss (Chung, 2011; Plank et al., 2014) or with amblyopia (Chung et al., 2012). These findings suggest that after vision loss, the brain has a certain level of plasticity which allows improvement in vision given efficient training (Sabel et al., 2011; Wandell & Smirnakis, 2009). Better understanding of the lateral modulation effect between the surround areas and the vision loss location could help develop more suitable eye disease detection tool and promote potential training techniques for rehabilitation as well as image enhancement methods that could benefit patients with visual impairment (Zur & Ullman, 2003). We expect our findings in the current thesis can serve as the foundation of applying similar paradigms to investigate the lateral modulation effect in impaired vision and eventually lead to improving the quality of life in patients with visual difficulties.

5.4 Conclusions

In this project, we investigated the lateral modulation effects by psychophysics, computational modeling, as well as neuroimaging techniques. For psychophysics experiments, we differentially adapted different parts of the visual field and estimated the resulting TAE magnitude to infer the lateral modulation effect between the center and surround regions during the adaptation phase in psychophysics experiments. We found that adding a surround pattern to the adapter center reduced the adaptation effect, suggesting a lateral inhibition effect. In the surround-only condition, where perceptual filling-in could be observed, even without physical overlap between the adapter and the target, TAE was induced, indicating that the lateral interaction coming from the surround that contributed to the filled-in percept could affect the orientation percept of the following target. Additionally, stronger TAE was observed in trials with subjectively reported filling-in than those without. We then varied the orientation of the adapter center and surround independently to estimate how the lateral inhibition effect could change with the surround feature. The results showed that the lateral modulation effect first increased then decreased as the surround orientation deviated from the center orientation, revealing an orientation-specific lateral modulation effect. We proposed a variant of the divisive inhibition model to capture both the adaption effect and the lateral modulation effect observed in the empirical data. To examine the lateral modulation effects observed in the psychophysics studies, in a fMRI experiment, we presented grating stimuli that stimulated different subparts of the visual field. We found evidence of lateral inhibition in V1 to V3 areas when the surround pattern was added to the center pattern. In addition, the brain activation pattern was different when filling-in was perceived than when it was not. The behavioral and neuroimaging paradigms in the current thesis offer new evidence of lateral modulation in human vision. The implementation of the divisive inhibition model offers new insight in the underlying

normalization process during the lateral modulation. We expect to explore other types of filling-in phenomena with the established paradigms and computation model in the future. The findings in this thesis have the potential to be applied in clinical research with visually impaired patients to develop better detection tools and training programs for visually impaired patients. In sum, this thesis has achieved fruitful results that can contribute to the field of lateral modulation in human vision and inspire future research and application.

REFERENCE

Albrecht, D. G., Farrar, S. B., & Hamilton, D. B. (1984). Spatial contrast adaptation characteristics of neurones recorded in the cat's visual cortex. *The Journal of Physiology*, *347*(1), 713–739. https://doi.org/10.1113/jphysiol.1984.sp015092

Albrecht, D. G., & Geisler, W. S. (1991). Motion selectivity and the contrast-response function of simple cells in the visual cortex. *Visual Neuroscience*, *7*(6), 531–546. https://doi.org/10.1017/S0952523800010336

Anderson, J., Barlow, H. B., Gregory, R. L., Carandini, M., Barlow, H. B., O'keefe, L. P., Poirson, A. B., & Movshon, J. A. (1997). Adaptation to contingencies in macaque primary visual cortex. *Philosophical Transactions of the Royal Society of London. Series B: Biological Sciences*, *352*(1358), 1149–1154. https://doi.org/10.1098/rstb.1997.0098

Andriessen, J. J., & Bouma, H. (1976). Eccentric vision: Adverse interactions between line segments. *Vision Research*, *16*(1), 71–78. https://doi.org/https://doi.org/10.1016/0042-6989(76)90078-X

Angelucci, A., Bijanzadeh, M., Nurminen, L., Federer, F., Merlin, S., & Bressloff, P. C. (2017). Circuits and Mechanisms for Surround Modulation in Visual Cortex. *Annual Review of Neuroscience*, *40*(1), 425–451. https://doi.org/10.1146/annurev-neuro-072116-031418

Angelucci, A., & Bressloff, P. C. (2006). Contribution of feedforward, lateral and feedback connections to the classical receptive field center and extra-classical receptive field surround of primate V1 neurons. In S. Martinez-Conde, S. L. Macknik, L. M. Martinez, J.-M. Alonso, & P. U. B. T.-P. in B. R. Tse (Eds.), *Visual Perception Part 1: Fundamentals of Vision: Low and Mid-Level Processes in Perception* (Vol. 154, pp. 93–120). Elsevier. https://doi.org/10.1016/S0079-6123(06)54005-1

Anstis, S. (2013). Contour adaptation. *Journal of Vision*, *13*(2), 25. http://dx.doi.org/10.1167/13.2.25

Anstis, S., & Greenlee, M. W. (2014). Contour Erasure and Filling-in: New Observations. *I-Perception*, *5*(2), 79–86. https://doi.org/10.1068/i0624rep

Anstis, S., Verstraten, F. A. J., & Mather, G. (1998). The motion aftereffect. *Trends in Cognitive Sciences*, *2*(3), 111–117. https://doi.org/https://doi.org/10.1016/S1364-6613(98)01142-5

Barlow, H. B. (1953). Summation and inhibition in the frog's retina. *The Journal of Physiology*, *119*(1), 69–88. https://doi.org/10.1113/jphysiol.1953.sp004829

Barlow, H. B. (1972). Dark and Light Adaptation: Psychophysics. In D. Jameson & L. M. Hurvich (Eds.), *Visual Psychophysics* (pp. 1–28). Springer-Verlag. https://doi.org/10.1007/978-3-642-88658-4_1

Barlow, H. B., & Földiák, P. (1989). Adaptation and decorrelation in the cortex. In R. Durbin & C. Miall (Eds.), *The computing neuron* (pp. 54–72). Addison-Wesley Longman Publishing Co., Inc.

Baylor, D. A., Fuortes, M. G., & O'Bryan, P. M. (1971). Receptive fields of cones in the retina of

the turtle. *The Journal of Physiology*, *214*(2), 265–294. https://doi.org/10.1113/jphysiol.1971.sp009432

Blakemore, C., Carpenter, R. H. S., & Georgeson, M. A. (1970). Lateral inhibition between orientation detectors in the human visual system. *Nature*, *228*(5266), 37.

Blakemore, C., & Tobin, E. A. (1972). Lateral inhibition between orientation detectors in the cat's visual cortex. *Experimental Brain Research*, *15*(4), 439–440. https://doi.org/10.1007/BF00234129

Bonin, V., Mante, V., & Carandini, M. (2005). The Suppressive Field of Neurons in Lateral Geniculate Nucleus. *The Journal of Neuroscience*, *25*(47), 10844 LP – 10856. https://doi.org/10.1523/JNEUROSCI.3562-05.2005

Bouma, H. (1970). Interaction Effects in Parafoveal Letter Recognition. *Nature*, *226*(5241), 177–178. https://doi.org/10.1038/226177a0

Boynton, R. M., & Whitten, D. N. (1970). Visual Adaptation in Monkey Cones: Recordings of Late Receptor Potentials. *Science*, *170*(3965), 1423–1426. https://doi.org/10.1126/science.170.3965.1423

Bressan, P., Mingolla, E., Spillmann, L., & Watanabe, T. (1997). Neon color spreading: a review. *Perception*, *26*(11), 1353–1366.

Bringuier, V., Chavane, F., Glaeser, L., & Frégnac, Y. (1999). Horizontal Propagation of Visual Activity in the Synaptic Integration Field of Area 17 Neurons. *Science*, *283*(5402), 695–699.

Brouwer, G. J., & Heeger, D. J. (2009). Decoding and Reconstructing Color from Responses in Human Visual Cortex. *The Journal of Neuroscience*, *29*(44), 13992 LP – 14003. https://doi.org/10.1523/JNEUROSCI.3577-09.2009

Brouwer, G. J., & Heeger, D. J. (2011). Cross-orientation suppression in human visual cortex. *Journal of Neurophysiology*, *106*(5), 2108–2119. https://doi.org/10.1152/jn.00540.2011

Burkhalter, A., & Van Essen, D. C. (1986). Processing of color, form and disparity information in visual areas VP and V2 of ventral extrastriate cortex in the macaque monkey. *The Journal of Neuroscience*, *6*(8), 2327 LP – 2351. https://doi.org/10.1523/JNEUROSCI.06-08-02327.1986

Campbell, F. W., & Maffei, L. (1971). The tilt after-effect: A fresh look. *Vision Research*, *11*(8), 833–840. https://doi.org/10.1016/0042-6989(71)90005-8

Cannon, M. W., & Fullenkamp, S. C. (1991). Spatial interactions in apparent contrast: Inhibitory effects among grating patterns of different spatial frequencies, spatial positions and orientations. *Vision Research*, *31*(11), 1985–1998. https://doi.org/https://doi.org/10.1016/0042-6989(91)90193-9

Carandini, M., & Heeger, D. J. (2012). Normalization as a canonical neural computation. *Nature Reviews Neuroscience*, *13*, 51. https://doi.org/10.1038/nrn3136

Carpenter, R. H. S. (1988). *Movements of the eyes* (2nd rev.). Pion Limited.

Carpenter, R. H. S., & Blakemore, C. (1973). Interactions between orientations in human vision.

Experimental Brain Research, *18*(3), 287–303.

Castet, E., & Crossland, M. (2012). Quantifying eye stability during a fixation task: a review of definitions and methods. *Seeing and Perceiving*, *25*(5), 449–469. https://doi.org/10.1163/187847611X620955

Cavanaugh, J. R., Bair, W., & Movshon, J. A. (2002a). Nature and Interaction of Signals From the Receptive Field Center and Surround in Macaque V1 Neurons. *Journal of Neurophysiology*, *88*(5), 2530–2546. https://doi.org/10.1152/jn.00692.2001

Cavanaugh, J. R., Bair, W., & Movshon, J. A. (2002b). Selectivity and Spatial Distribution of Signals From the Receptive Field Surround in Macaque V1 Neurons. *Journal of Neurophysiology*, *88*(5), 2547–2556. https://doi.org/10.1152/jn.00693.2001

Chang, C.-C., & Lin, C.-J. (2011). LIBSVM: A library for support vector machines. *ACM Transactions on Intelligent Systems and Technology (TIST)*, *2*(3), 1–27.

Chen, C.-C. (2014). Partitioning two components of BOLD activation suppression in flanker effects. *Frontiers in Neuroscience*, *8*, 149. https://doi.org/10.3389/fnins.2014.00149

Chen, C.-C., Foley, J. M., & Brainard, D. H. (2000). Detection of chromoluminance patterns on chromoluminance pedestals II: model. *Vision Research*, *40*(7), 789–803. https://doi.org/10.1016/S0042-6989(99)00228-X

Chen, C.-C., Kasamatsu, T., Polat, U., & Norcia, A. M. (2001). Contrast response characteristics of long-range lateral interactions in cat striate cortex. *NeuroReport*, *12*(4), 655–661. https://doi.org/10.1097/00001756-200103260-00008

Chen, C.-C., & Tyler, C. W. (2001). Lateral sensitivity modulation explains the flanker effect in contrast discrimination. *Proceedings of the Royal Society of London B: Biological Sciences*, *268*(1466), 509–516. https://doi.org/10.1098/rspb.2000.1387

Chen, C.-C., & Tyler, C. W. (2002). Lateral modulation of contrast discrimination: Flanker orientation effects. *Journal of Vision*, *2*(6), 520–530. https://doi.org/10.1167/2.6.8

Chen, C.-C., & Tyler, C. W. (2008). Excitatory and inhibitory interaction fields of flankers revealed by contrast-masking functions. *Journal of Vision*, *8*(4), 1–14. http://dx.doi.org/10.1167/8.4.10

Chen, C.-C., Tyler, C. W., Liu, C.-L., & Wang, Y.-H. (2005). Lateral modulation of BOLD activation in unstimulated regions of the human visual cortex. *Neuroimage*, *24*(3), 802–809. https://doi.org/10.1016/j.neuroimage.2004.09.021

Chen, C.-C., Yeh, Y.-H. C., & Tyler, C. W. (2019). Length summation in noise. *Journal of Vision*, *19*(9), 11. https://doi.org/10.1167/19.9.11

Chen, S., Glasauer, S., Müller, H. J., & Conci, M. (2018). Surface filling-in and contour interpolation contribute independently to Kanizsa figure formation. In *Journal of Experimental Psychology: Human Perception and Performance* (Vol. 44, Issue 9, pp. 1399–1413). American Psychological Association. https://doi.org/10.1037/xhp0000540

Chen, S., Weidner, R., Zeng, H., Fink, G. R., Müller, H. J., & Conci, M. (2021). Feedback from lateral occipital cortex to V1/V2 triggers object completion: Evidence from functional

magnetic resonance imaging and dynamic causal modeling. *Human Brain Mapping*, *n/a*(n/a). https://doi.org/https://doi.org/10.1002/hbm.25637

Cheng, K., Waggoner, R. A., & Tanaka, K. (2001). Human Ocular Dominance Columns as Revealed by High-Field Functional Magnetic Resonance Imaging. *Neuron*, *32*(2), 359–374. https://doi.org/https://doi.org/10.1016/S0896-6273(01)00477-9

Chubb, C., Sperling, G., & Solomon, J. A. (1989). Texture interactions determine perceived contrast. *Proceedings of the National Academy of Sciences*, *86*(23), 9631–9635. https://doi.org/10.1073/pnas.86.23.9631

Chung, S. T. L. (2011). Improving Reading Speed for People with Central Vision Loss through Perceptual Learning. *Investigative Ophthalmology & Visual Science*, *52*(2), 1164–1170. https://doi.org/10.1167/iovs.10-6034

Chung, S. T. L., Li, R. W., & Levi, D. M. (2012). Learning to identify near-acuity letters, either with or without flankers, results in improved letter size and spacing limits in adults with amblyopia. *Plos One*, *7*(4), e35829.

Clifford, C. W. ., Wyatt, A. M., Arnold, D. H., Smith, S. T., & Wenderoth, P. (2001). Orthogonal adaptation improves orientation discrimination. *Vision Research*, *41*(2), 151–159. https://doi.org/10.1016/S0042-6989(00)00248-0

Clifford, C. W. G. (2014). The tilt illusion: Phenomenology and functional implications. *Vision Research*, *104*, 3–11. https://doi.org/10.1016/j.visres.2014.06.009

Cohen, M. A., & Grossberg, S. (1984). Neural dynamics of brightness perception: Features, boundaries, diffusion, and resonance. *Perception & Psychophysics*, *36*(5), 428–456. https://doi.org/10.3758/bf03207497

Cornsweet, T. (1970). *Visual perception*. Academic press. https://books.google.de/books?hl=en&lr=&id=ubaGAAAAQBAJ&oi=fnd&pg=PP1&ots=TDBpxw3Jl5&sig=V-ACg_vlFuUiAMsOY8_LBO-g7cw&redir_esc=y#v=onepage&q&f=false

Crossland, M. D., & Bex, P. J. (2008). The twinkle aftereffect is pre-cortical and is independent of filling-in. *Journal of Vision*, *8*(11), 13. https://doi.org/10.1167/8.11.13

Crossland, M. D., Dakin, S. C., & Bex, P. J. (2007). Illusory Stimuli Can Be Used to Identify Retinal Blind Spots. *PLOS ONE*, *2*(10), e1060. https://doi.org/10.1371/journal.pone.0001060

Crossland, M. D., & Rubin, and G. S. (2002). The Use of an Infrared Eyetracker to Measure Fixation Stability. *Optometry and Vision Science*, *79*(11). https://journals.lww.com/optvissci/Fulltext/2002/11000/The_Use_of_an_Infrared_Eyetracker_to_Measure.11.aspx

Crossland, M. D., & Rubin, G. (2007). The Amsler chart: absence of evidence is not evidence of absence. *British Journal of Ophthalmology*, *91*(3), 391–393. https://doi.org/10.1136/bjo.2006.095315

Dale, A. M., Fischl, B., & Sereno, M. I. (1999). Cortical Surface-Based Analysis: I. Segmentation and Surface Reconstruction. *NeuroImage*, *9*(2), 179–194.

https://doi.org/https://doi.org/10.1006/nimg.1998.0395

De Weerd, P., Desimone, R., & Ungerleider, L. G. (1998). Perceptual filling-in: a parametric study. *Vision Research*, *38*(18), 2721–2734. https://doi.org/https://doi.org/10.1016/S0042-6989(97)00432-X

De Weerd, P., Gattass, R., Desimone, R., & Ungerleider, L. G. (1995). Responses of cells in monkey visual cortex during perceptual filling-in of an artificial scotoma. *Nature*, *377*(6551), 731–734. https://doi.org/10.1038/377731a0

De Weerd, P., & Pessoa, L. (2003). Introduction: Filling-in: More than meets the eye. In L. Pessoa & P. De Weerd (Eds.), *Filling-in: From perceptual completion to cortical reorganization* (pp. 1–10). Oxford University Press.

DeAngelis, G. C., Freeman, R. D., & Ohzawa, I. (1994). Length and width tuning of neurons in the cat's primary visual cortex. *Journal of Neurophysiology*, *71*(1), 347–374. https://doi.org/10.1152/jn.1994.71.1.347

Deneve, S., Latham, P. E., & Pouget, A. (1999). Reading population codes: a neural implementation of ideal observers. *Nature Neuroscience*, *2*(8), 740–745. https://doi.org/10.1038/11205

Devinck, F., & Knoblauch, K. (2019). Central mechanisms of perceptual filling-in. *Current Opinion in Behavioral Sciences*, *30*, 135–140. https://doi.org/https://doi.org/10.1016/j.cobeha.2019.08.003

Durant, S., & Clifford, C. W. G. (2006). Dynamics of the influence of segmentation cues on orientation perception. *Vision Research*, *46*(18), 2934–2940. https://doi.org/https://doi.org/10.1016/j.visres.2006.02.027

Ebbinghaus, H. (1902). Grundzüge der Psychologie volumes I and II. *Leipzig: Verlag von Viet & Co*.

Engel, S. A., Glover, G. H., & Wandell, B. A. (1997). Retinotopic organization in human visual cortex and the spatial precision of functional MRI. *Cerebral Cortex*, *7*(2), 181–192. https://doi.org/10.1093/cercor/7.2.181

Etzel, J. A., & Braver, T. S. (2013). MVPA Permutation Schemes: Permutation Testing in the Land of Cross-Validation. *2013 International Workshop on Pattern Recognition in Neuroimaging*, 140–143. https://doi.org/10.1109/PRNI.2013.44

Falkenberg, H. K., & Bex, P. J. (2007). Contextual modulation of the motion aftereffect. In *Journal of Experimental Psychology: Human Perception and Performance* (Vol. 33, Issue 2, pp. 257–270). American Psychological Association. https://doi.org/10.1037/0096-1523.33.2.257

Felleman, D. J., & Van Essen, D. C. (1987). Receptive field properties of neurons in area V3 of macaque monkey extrastriate cortex. *Journal of Neurophysiology*, *57*(4), 889–920. https://doi.org/10.1152/jn.1987.57.4.889

Fiorani Júnior, M., Rosa, M. G., Gattass, R., & Rocha-Miranda, C. E. (1992). Dynamic surrounds of receptive fields in primate striate cortex: a physiological basis for perceptual completion? *Proceedings of the National Academy of Sciences*, *89*(18), 8547 LP – 8551.

https://doi.org/10.1073/pnas.89.18.8547

Fischl, B. (2012). FreeSurfer. *NeuroImage*, *62*(2), 774–781. https://doi.org/https://doi.org/10.1016/j.neuroimage.2012.01.021

Fischl, B., Sereno, M. I., & Dale, A. M. (1999). Cortical Surface-Based Analysis: II: Inflation, Flattening, and a Surface-Based Coordinate System. *NeuroImage*, *9*(2), 195–207. https://doi.org/https://doi.org/10.1006/nimg.1998.0396

Foley, J. M. (1994). Human luminance pattern-vision mechanisms: masking experiments require a new model. *Journal of the Optical Society of America A*, *11*(6), 1710–1719. https://doi.org/10.1364/JOSAA.11.001710

Foley, J. M., & Chen, C.-C. (1997). Analysis of the effect of pattern adaptation on pattern pedestal effects: A two-process model. *Vision Research*, *37*(19), 2779–2788. https://doi.org/10.1016/s0042-6989(97)00081-3

Foley, J. M., & Chen, C.-C. (1999). Pattern detection in the presence of maskers that differ in spatial phase and temporal offset: threshold measurements and a model. *Vision Research*, *39*(23), 3855–3872. https://doi.org/10.1016/S0042-6989(99)00104-2

Gardner, J. L., Sun, P., Waggoner, R. A., Ueno, K., Tanaka, K., & Cheng, K. (2005). Contrast Adaptation and Representation in Human Early Visual Cortex. *Neuron*, *47*(4), 607–620. https://doi.org/10.1016/j.neuron.2005.07.016

Gaska, J. P., Jacobson, L. D., & Pollen, D. A. (1987). Reponse suppression by extending sine-wave gratings within the receptive fields of neurons in visual cortical area V3A of the macaque monkey. *Vision Research*, *27*(10), 1687–1692. https://doi.org/https://doi.org/10.1016/0042-6989(87)90098-8

Gattass, R., Gross, C. G., & Sandell, J. H. (1981). Visual topography of V2 in the macaque. *Journal of Comparative Neurology*, *201*(4), 519–539. https://doi.org/https://doi.org/10.1002/cne.902010405

Gattass, R., Sousa, A. P., & Gross, C. G. (1988). Visuotopic organization and extent of V3 and V4 of the macaque. *The Journal of Neuroscience*, *8*(6), 1831 LP – 1845. https://doi.org/10.1523/JNEUROSCI.08-06-01831.1988

Georgeson, M. A. (1992). Human vision combines oriented filters to compute edges. *Proceedings of the Royal Society of London. Series B: Biological Sciences*, *249*(1326), 235–245. https://doi.org/10.1098/rspb.1992.0110

Georgeson, M. A., & Meese, T. S. (1996). Perceived structure of plaids implies variable combination of oriented filters in edge finding. *Proc.SPIE*, *2657*, 175–189. https://doi.org/10.1117/12.238714

Gerrits, H. J. M., & Vendrik, A. J. H. (1970). Simultaneous contrast, filling-in process and information processing in man's visual system. *Experimental Brain Research*, *11*(4), 411–430. https://doi.org/10.1007/BF00237914

Gibson, J. J. (1937a). Adaptation, after-effect, and contrast in the perception of tilted lines. II. Simultaneous contrast and the areal restriction of the after-effect. *Journal of Experimental Psychology*, *20*(6), 553–569. https://doi.org/10.1037/h0057585

Gibson, J. J. (1937b). Adaptation with negative after-effect. *Psychological Review*, *44*(3), 222–244. https://doi.org/10.1037/h0061358

Gibson, J. J., & Radner, M. (1937). Adaptation, after-effect and contrast in the perception of tilted lines. I. Quantitative studies. *Journal of Experimental Psychology*, *20*(5), 453–467. https://doi.org/10.1037/h0059826

Gilbert, C. D., & Wiesel, T. N. (1990). The influence of contextual stimuli on the orientation selectivity of cells in primary visual cortex of the cat. *Vision Research*, *30*(11), 1689–1701. https://doi.org/10.1016/0042-6989(90)90153-C

Goddard, E., Clifford, C. W. G., & Solomon, S. G. (2008). Centre-surround effects on perceived orientation in complex images. *Vision Research*, *48*(12), 1374–1382. https://doi.org/https://doi.org/10.1016/j.visres.2008.02.023

Greenlee, M. W., & Heitger, F. (1988). The functional role of contrast adaptation. *Vision Research*, *28*(7), 791–797. https://doi.org/https://doi.org/10.1016/0042-6989(88)90026-0

Greenlee, M. W., & Magnussen, S. (1987). Higher-harmonic adaptation and the detection of squarewave gratings. *Vision Research*, *27*(2), 249–255. https://doi.org/https://doi.org/10.1016/0042-6989(87)90187-8

Greenlee, M. W., & Magnussen, S. (1988). Interactions among spatial frequency and orientation channels adapted concurrently. *Vision Research*, *28*(12), 1303–1310. https://doi.org/https://doi.org/10.1016/0042-6989(88)90061-2

Grossberg, S., & Mingolla, E. (1985). Neural dynamics of form perception: Boundary completion, illusory figures, and neon color spreading. *Psychological Review*, *92*(2), 173–211. https://doi.org/10.1037/0033-295X.92.2.173

Hanke, M., Halchenko, Y. O., Sederberg, P. B., Hanson, S. J., Haxby, J. V, & Pollmann, S. (2009). PyMVPA: a Python Toolbox for Multivariate Pattern Analysis of fMRI Data. *Neuroinformatics*, *7*(1), 37–53. https://doi.org/10.1007/s12021-008-9041-y

Hardage, L., & Tyler, C. W. (1995). Induced twinkle aftereffect as a probe of dynamic visual processing mechanisms. *Vision Research*, *35*(6), 757–766. https://doi.org/http://dx.doi.org/10.1016/0042-6989(94)00167-K

Harvey, B. M., & Dumoulin, S. O. (2011). The Relationship between Cortical Magnification Factor and Population Receptive Field Size in Human Visual Cortex: Constancies in Cortical Architecture. *The Journal of Neuroscience*, *31*(38), 13604 LP – 13612. https://doi.org/10.1523/JNEUROSCI.2572-11.2011

Heeger, D. J. (1991). Nonlinear model of neural responses in cat visual cortex. *Computational Models of Visual Processing*, 119–133.

Heeger, D. J. (1992). Normalization of cell responses in cat striate cortex. *Visual Neuroscience*, *9*(2), 181–197. https://doi.org/DOI: 10.1017/S0952523800009640

Herzog, M. H., Sayim, B., Chicherov, V., & Manassi, M. (2015). Crowding, grouping, and object recognition: A matter of appearance. *Journal of Vision*, *15*(6), 5. http://dx.doi.org/10.1167/15.6.5

Hubel, D. H., & Wiesel, T. N. (1959). Receptive fields of single neurones in the cat's striate cortex. *The Journal of Physiology*, *148*(3), 574–591. https://doi.org/10.1113/jphysiol.1959.sp006308

Hubel, D. H., & Wiesel, T. N. (1962). Receptive fields, binocular interaction and functional architecture in the cat's visual cortex. *The Journal of Physiology*, *160*(1), 106–154. https://doi.org/10.1113/jphysiol.1962.sp006837

Hubel, D. H., & Wiesel, T. N. (1968). Receptive fields and functional architecture of monkey striate cortex. *The Journal of Physiology*, *195*(1), 215–243. https://doi.org/https://doi.org/10.1113/jphysiol.1968.sp008455

Huettel, S. A., Song, A. W., & McCarthy, G. (2014). BOLD fMRI: Origins and Properties. In *Functional Magnetic Resonance Imaging* (3rd ed., pp. 211–264). Sinauer Associates.

Ichida, J. M., Schwabe, L., Bressloff, P. C., & Angelucci, A. (2007). Response Facilitation From the "Suppressive" Receptive Field Surround of Macaque V1 Neurons. *Journal of Neurophysiology*, *98*(4), 2168–2181. https://doi.org/10.1152/jn.00298.2007

Jin, D. Z., Dragoi, V., Sur, M., & Seung, H. S. (2005). Tilt Aftereffect and Adaptation-Induced Changes in Orientation Tuning in Visual Cortex. *Journal of Neurophysiology*, *94*(6), 4038–4050. https://doi.org/10.1152/jn.00571.2004

Johnson, R. A., & Wichern, D. W. (2007). Multivariate Linear Regression Models. In *Applied Multivariate Statistical Analysis* (6th ed., pp. 360–419). Pearson Education, Inc.

Kanizsa, G. (1979). *Organization in vision: Essays on Gestalt perception*. Praeger.

Kanizsa, G. (1987). Quasi-Perceptual Margins in Homogeneously Stimulated Fields. In S. Petry & G. E. Meyer (Eds.), *The Perception of Illusory Contours* (pp. 40–49). Springer New York. https://doi.org/10.1007/978-1-4612-4760-9_4

Kapadia, M. K., Westheimer, G., & Gilbert, C. D. (1999). Dynamics of spatial summation in primary visual cortex of alert monkeys. *Proceedings of the National Academy of Sciences*, *96*(21), 12073–12078. http://www.pnas.org/content/96/21/12073.abstract

Kellman, P. J., & Shipley, T. F. (1991). A theory of visual interpolation in object perception. *Cognitive Psychology*, *23*(2), 141–221. https://doi.org/https://doi.org/10.1016/0010-0285(91)90009-D

Kinoshita, M., & Komatsu, H. (2001). Neural Representation of the Luminance and Brightness of a Uniform Surface in the Macaque Primary Visual Cortex. *Journal of Neurophysiology*, *86*(5), 2559–2570. https://doi.org/10.1152/jn.2001.86.5.2559

Komatsu, H. (2006). The neural mechanisms of perceptual filling-in. *Nat Rev Neurosci*, *7*(3), 220–231. https://doi.org/10.1038/nrn1869

Komatsu, H., Kinoshita, M., & Murakami, I. (2000). Neural Responses in the Retinotopic Representation of the Blind Spot in the Macaque V1 to Stimuli for Perceptual Filling-In. *The Journal of Neuroscience*, *20*(24), 9310 LP – 9319. https://doi.org/10.1523/JNEUROSCI.20-24-09310.2000

Komatsu, H., Kinoshita, M., & Murakami, I. (2002). Neural responses in the primary visual

cortex of the monkey during perceptual filling-in at the blind spot. *Neuroscience Research*, *44*(3), 231–236. https://doi.org/10.1016/S0168-0102(02)00149-9

Kontsevich, L. L., & Tyler, C. W. (1999). Bayesian adaptive estimation of psychometric slope and threshold. *Vision Research*, *39*(16), 2729–2737. https://doi.org/10.1016/S0042-6989(98)00285-5

Kriegeskorte, N., Goebel, R., & Bandettini, P. (2006). Information-based functional brain mapping. *Proceedings of the National Academy of Sciences of the United States of America*, *103*(10), 3863 LP – 3868. https://doi.org/10.1073/pnas.0600244103

Kurtenbach, W., & Magnussen, S. (1981). Inhibition, disinhibition, and summation among orientation detectors in human vision. *Experimental Brain Research*, *43*(2), 193–198. https://doi.org/10.1007/BF00237763

Levi, D. M. (2008). Crowding—An essential bottleneck for object recognition: A mini-review. *Vision Research*, *48*(5), 635–654. https://doi.org/https://doi.org/10.1016/j.visres.2007.12.009

Levitt, J. B., & Lund, J. S. (2002). The spatial extent over which neurons in macaque striate cortex pool visual signals. *Visual Neuroscience*, *19*(4), 439–452. https://doi.org/DOI: 10.1017/S0952523802194065

Li, C.-Y., & Li, W. (1994). Extensive integration field beyond the classical receptive field of cat's striate cortical neurons—Classification and tuning properties. *Vision Research*, *34*(18), 2337–2355. https://doi.org/https://doi.org/10.1016/0042-6989(94)90280-1

Lin, Y.-S., Chen, C.-C., & Greenlee, M. W. (2020). Lateral modulation of orientation perception in center-surround sinusoidal stimuli: Divisive inhibition in perceptual filling-in. *Journal of Vision*, *20*(9:5), 1–18. https://doi.org/10.1167/jov.20.9.5

Lin, Y.-S., Chen, C.-C., & Greenlee, M. W. (2022). The role of lateral modulation in orientation-specific adaptation effect. *Journal of Vision*, *22*(2:13), 1–16. https://doi.org/10.1167/jov.22.2.13

Logothetis, N. K. (2008). What we can do and what we cannot do with fMRI. *Nature*, *453*, 869. http://dx.doi.org/10.1038/nature06976

Maffei, L., & Fiorentini, A. (1976). The unresponsive regions of visual cortical receptive fields. *Vision Research*, *16*(10), 1131-IN5. https://doi.org/10.1016/0042-6989(76)90253-4

Magnussen, S., & Kurtenbach, W. (1980). Adapting to two orientations: disinhibition in a visual aftereffect. *Science*, *207*(4433), 908–909. https://doi.org/10.1126/science.7355271

Malania, M., Pawellek, M., Plank, T., & Greenlee, M. W. (2020). Training-Induced Changes in Radial–Tangential Anisotropy of Visual Crowding. *Translational Vision Science & Technology*, *9*(9), 25. https://doi.org/10.1167/tvst.9.9.25

Mather, G., & Harris, J. P. (1998). Theoretical models of the motion aftereffect. In G. Mather, F. Verstraten, & S. Anstis (Eds.), *The motion aftereffect: A modern perspective* (pp. 157–185). MIT Press.

Matsumoto, M., & Komatsu, H. (2005). Neural Responses in the Macaque V1 to Bar Stimuli With Various Lengths Presented on the Blind Spot. *Journal of Neurophysiology*, *93*(5),

2374–2387. https://doi.org/10.1152/jn.00811.2004

McManus, J. N. J., Ullman, S., & Gilbert, C. D. (2008). A Computational Model of Perceptual Fill-in Following Retinal Degeneration. *Journal of Neurophysiology*, *99*(5), 2086–2100. https://doi.org/10.1152/jn.00871.2007

Meese, T. S., Challinor, K. L., Summers, R. J., & Baker, D. H. (2009). Suppression pathways saturate with contrast for parallel surrounds but not for superimposed cross-oriented masks. *Vision Research*, *49*(24), 2927–2935. https://doi.org/https://doi.org/10.1016/j.visres.2009.09.006

Meese, T. S., & Georgeson, M. A. (1996a). The tilt aftereffect in plaids and gratings: channel codes, local signs and "patchwise" transforms. *Vision Research*, *36*(10), 1421–1437. https://doi.org/https://doi.org/10.1016/0042-6989(95)00212-X

Meese, T. S., & Georgeson, M. A. (1996b). Spatial Filter Combination in Human Pattern Vision: Channel Interactions Revealed by Adaptation. *Perception*, *25*(3), 255–277. https://doi.org/10.1068/p250255

Meese, T. S., & Holmes, D. J. (2002). Adaptation and gain pool summation: alternative models and masking data. *Vision Research*, *42*(9), 1113–1125. https://doi.org/10.1016/S0042-6989(01)00291-7

Meese, T. S., & Holmes, D. J. (2007). Spatial and temporal dependencies of cross-orientation suppression in human vision. *Proceedings of the Royal Society B: Biological Sciences*, *274*(1606), 127–136. https://doi.org/10.1098/rspb.2006.3697

Meese, T. S., Summers, R. J., Holmes, D. J., & Wallis, S. A. (2007). Contextual modulation involves suppression and facilitation from the center and the surround. *Journal of Vision*, *7*(4:7), 1–27. https://doi.org/10.1167/7.4.7

Mély, D. A., Linsley, D., & Serre, T. (2018). Complementary surrounds explain diverse contextual phenomena across visual modalities. *Psychological Review*, *125*(5), 769–784. https://doi.org/10.1037/rev0000109

Mendola, J. D., Conner, I. P., Sharma, S., Bahekar, A., & Lemieux, S. (2006). fMRI Measures of Perceptual Filling-in in the Human Visual Cortex. *Journal of Cognitive Neuroscience*, *18*(3), 363–375. https://doi.org/10.1162/jocn.2006.18.3.363

Meng, M., Remus, D. A., & Tong, F. (2005). Filling-in of visual phantoms in the human brain. *Nat Neurosci*, *8*(9), 1248–1254. https://doi.org/http://www.nature.com/neuro/journal/v8/n9/suppinfo/nn1518_S1.html

Mihaylov, P., Manahilov, V., Simpson, W. A., & Strang, N. C. (2007). Induced internal noise in perceptual artificial scotomas created by surrounding dynamic noise. *Vision Research*, *47*(11), 1479–1489. https://doi.org/http://dx.doi.org/10.1016/j.visres.2007.01.028

Morgan, M. J., & Dresp, B. (1995). Contrast detection facilitation by spatially separated targets and inducers. *Vision Research*, *35*(8), 1019–1024. https://doi.org/https://doi.org/10.1016/0042-6989(94)00216-9

Morgan, M. J., McEwan, W., & Solomon, J. (2007). The lingering effects of an artificial blind spot. *PloS One*, *2*(2), e256. https://doi.org/10.1371/journal.pone.0000256

Müller, J. R., Metha, A. B., Krauskopf, J., & Lennie, P. (2003). Local Signals From Beyond the Receptive Fields of Striate Cortical Neurons. *Journal of Neurophysiology*, *90*(2), 822–831. https://doi.org/10.1152/jn.00005.2003

Murakami, I. (1995). Motion aftereffect after monocular adaptation to filled-in motion at the blind spot. *Vision Research*, *35*(8), 1041–1045. https://doi.org/https://doi.org/10.1016/0042-6989(94)00201-V

Naka, K. I., & Rushton, W. A. H. (1966). S-potentials from luminosity units in the retina of fish (Cyprinidae). *The Journal of Physiology*, *185*(3), 587–599. https://doi.org/10.1113/jphysiol.1966.sp008003

Nelson, J. I., & Frost, B. J. (1978). Orientation-selective inhibition from beyond the classic visual receptive field. *Brain Research*, *139*(2), 359–365. https://doi.org/10.1016/0006-8993(78)90937-X

Nelson, J. I., & Frost, B. J. (1985). Intracortical facilitation among co-oriented, co-axially aligned simple cells in cat striate cortex. *Experimental Brain Research*, *61*(1), 54–61. https://doi.org/10.1007/BF00235620

Neumann, H., Pessoa, L., & Hansen, T. (2001). Visual filling-in for computing perceptual surface properties. *Biological Cybernetics*, *85*(5), 355–369. https://doi.org/10.1007/s004220100258

Nichols, T. E., & Holmes, A. P. (2002). Nonparametric permutation tests for functional neuroimaging: A primer with examples. *Human Brain Mapping*, *15*(1), 1–25. https://doi.org/https://doi.org/10.1002/hbm.1058

Niehorster, D. C., Zemblys, R., Beelders, T., & Holmqvist, K. (2020). Characterizing gaze position signals and synthesizing noise during fixations in eye-tracking data. *Behavior Research Methods*, *52*(6), 2515–2534. https://doi.org/10.3758/s13428-020-01400-9

Ohzawa, I., Sclar, G., & Freeman, R. D. (1985). Contrast gain control in the cat's visual system. *Journal of Neurophysiology*, *54*(3), 651–667. https://doi.org/10.1152/jn.1985.54.3.651

Ozeki, H., Sadakane, O., Akasaki, T., Naito, T., Shimegi, S., & Sato, H. (2004). Relationship between Excitation and Inhibition Underlying Size Tuning and Contextual Response Modulation in the Cat Primary Visual Cortex. *The Journal of Neuroscience*, *24*(6), 1428 LP – 1438. https://doi.org/10.1523/JNEUROSCI.3852-03.2004

Paradiso, M A. (1988). A theory for the use of visual orientation information which exploits the columnar structure of striate cortex. *Biological Cybernetics*, *58*(1), 35–49. https://doi.org/10.1007/BF00363954

Paradiso, Michael A, & Nakayama, K. (1991). Brightness perception and filling-in. *Vision Research*, *31*(7–8), 1221–1236. https://doi.org/http://dx.doi.org/10.1016/0042-6989(91)90047-9

Pascolini, D., & Mariotti, S. P. (2012). Global estimates of visual impairment: 2010. *British Journal of Ophthalmology*, *96*(5), 614–618.

Pessoa, L., & De Weerd, P. (2003). *Filling-in: From perceptual completion to cortical reorganization*. Oxford University Press.

Pessoa, L., Thompson, E., & Noë, A. (1998). Finding out about filling-in: A guide to perceptual completion for visual science and the philosophy of perception. *Behavioral and Brain Sciences*, *21*(6), 723–748. https://doi.org/10.1017/s0140525x98001757

Peters, J. C., Jans, B., van de Ven, V., De Weerd, P., & Goebel, R. (2010). Dynamic brightness induction in V1: Analyzing simulated and empirically acquired fMRI data in a "common brain space" framework. *NeuroImage*, *52*(3), 973–984. https://doi.org/http://dx.doi.org/10.1016/j.neuroimage.2010.03.070

Petrov, Y., Carandini, M., & McKee, S. (2005). Two Distinct Mechanisms of Suppression in Human Vision. *The Journal of Neuroscience*, *25*(38), 8704–8707. http://www.jneurosci.org/content/25/38/8704.abstract

Petrov, Y., & McKee, S. P. (2006). The effect of spatial configuration on surround suppression of contrast sensitivity. *Journal of Vision*, *6*(3:4), 224–238. http://dx.doi.org/10.1167/6.3.4

Phillips, G. C., & Wilson, H. R. (1984). Orientation bandwidths of spatial mechanisms measured by masking. *Journal of the Optical Society of America A*, *1*(2), 226–232. https://doi.org/10.1364/JOSAA.1.000226

Pinna, B., Brelstaff, G., & Spillmann, L. (2001). Surface color from boundaries: a new 'watercolor' illusion. *Vision Research*, *41*(20), 2669–2676. https://doi.org/https://doi.org/10.1016/S0042-6989(01)00105-5

Pinna, B., & Grossberg, S. (2005). The watercolor illusion and neon color spreading: a unified analysis of new cases and neural mechanisms. *Journal of the Optical Society of America A*, *22*(10), 2207–2221. https://doi.org/10.1364/JOSAA.22.002207

Pinna, B., Werner, J. S., & Spillmann, L. (2003). The watercolor effect: a new principle of grouping and figure–ground organization. *Vision Research*, *43*(1), 43–52. https://doi.org/https://doi.org/10.1016/S0042-6989(02)00132-3

Plank, T., Rosengarth, K., Schmalhofer, C., Goldhacker, M., Brandl-Rühle, S., & Greenlee, M. W. (2014). Perceptual learning in patients with macular degeneration. In *Frontiers in Psychology* (Vol. 5, p. 1189). http://journal.frontiersin.org/article/10.3389/fpsyg.2014.01189

Polat, U., Mizobe, K., Pettet, M. W., Kasamatsu, T., & Norcia, A. M. (1998). Collinear stimuli regulate visual responses depending on cell's contrast threshold. *Nature*, *391*(6667), 580–584. http://dx.doi.org/10.1038/35372

Polat, U., & Sagi, D. (1993). Lateral interactions between spatial channels: Suppression and facilitation revealed by lateral masking experiments. *Vision Research*, *33*(7), 993–999. https://doi.org/10.1016/0042-6989(93)90081-7

Polat, U., & Sagi, D. (1994). The architecture of perceptual spatial interactions. *Vision Research*, *34*(1), 73–78. https://doi.org/10.1016/0042-6989(94)90258-5

Pouget, A., Dayan, P., & Zemel, R. (2000). Information processing with population codes. *Nature Reviews Neuroscience*, *1*, 125. https://doi.org/10.1038/35039062

Pouget, A., Zhang, K., Deneve, S., & Latham, P. E. (1998). Statistically Efficient Estimation Using Population Coding. *Neural Computation*, *10*(2), 373–401. https://doi.org/10.1162/089976698300017809

Press, W. H., Teukolsky, S. A., Vetterling, W. T., & Flannery, B. P. (1988). *Numerical recipes in C*. Cambridge university press.

Prins, N., & Kingdom, F. A. A. (2018). Applying the Model-Comparison Approach to Test Specific Research Hypotheses in Psychophysical Research Using the Palamedes Toolbox. *Frontiers in Psychology*, *9*, 1250. https://www.frontiersin.org/article/10.3389/fpsyg.2018.01250

Qiu, C., Kersten, D., & Olman, C. A. (2013). Segmentation decreases the magnitude of the tilt illusion. *Journal of Vision*, *13*(13), 19. https://doi.org/10.1167/13.13.19

Ramachandran, V. S. (1992). Blind spots. *Scientific American*, *266*(5), 86–91. https://doi.org/10.1038/scientificamerican0592-86

Ramachandran, V. S., & Gregory, R. L. (1991). Perceptual filling in of artificially induced scotomas in human vision. *Nature*, *350*(6320), 699–702. https://doi.org/10.1038/350699a0

Ramachandran, V. S., Gregory, R. L., & Aiken, W. (1993). Perceptual fading of visual texture borders. *Vision Research*, *33*(5), 717–721. https://doi.org/https://doi.org/10.1016/0042-6989(93)90191-X

Roberts, B., Harris, M. G., & Yates, T. A. (2005). The Roles of Inducer Size and Distance in the Ebbinghaus Illusion (Titchener Circles). *Perception*, *34*(7), 847–856. https://doi.org/10.1068/p5273

Roe, A. W., Lu, H. D., & Hung, C. P. (2005). Cortical processing of a brightness illusion. *Proceedings of the National Academy of Sciences of the United States of America*, *102*(10), 3869–3874. https://doi.org/10.1073/pnas.0500097102

Ross, J., & Speed, H. D. (1991). Contrast adaptation and contrast masking in human vision. *Proceedings of the Royal Society of London. Series B: Biological Sciences*, *246*(1315), 61–70. https://doi.org/10.1098/rspb.1991.0125

Sabel, B. A., Henrich-Noack, P., Fedorov, A., & Gall, C. (2011). Chapter 13 - Vision restoration after brain and retina damage: The "residual vision activation theory." In A. Green, C. E. Chapman, J. F. Kalaska, & F. B. T.-P. in B. R. Lepore (Eds.), *Enhancing performance for action and perception* (Vol. 192, pp. 199–262). Elsevier. https://doi.org/https://doi.org/10.1016/B978-0-444-53355-5.00013-0

Sakaguchi, Y. (2001). Target/surround asymmetry in perceptual filling-in. *Vision Research*, *41*(16), 2065–2077. https://doi.org/https://doi.org/10.1016/S0042-6989(01)00095-5

Sakaguchi, Y. (2006). Contrast dependency in perceptual filling-in. *Vision Research*, *46*(20), 3304–3312. https://doi.org/https://doi.org/10.1016/j.visres.2006.05.015

Sasaki, Y., & Watanabe, T. (2004). The primary visual cortex fills in color. *Proceedings of the National Academy of Sciences*, *101*(52), 18251–18256. https://doi.org/10.1073/pnas.0406293102

Satoh, S., & Usui, S. (2008). Computational theory and applications of a filling-in process at the blind spot. *Neural Networks*, *21*(9), 1261–1271. https://doi.org/http://dx.doi.org/10.1016/j.neunet.2008.05.001

Sceniak, M. P., Ringach, D. L., Hawken, M. J., & Shapley, R. (1999). Contrast's effect on spatial summation by macaque V1 neurons. *Nature Neuroscience*, *2*, 733–739. https://doi.org/10.1038/11197

Schönbach, E. M., Ibrahim, M. A., Strauss, R. W., Birch, D. G., Cideciyan, A. V, Hahn, G. A., Ho, A., Kong, X., Nasser, F., & Sunness, J. S. (2017). Fixation location and stability using the MP-1 microperimeter in Stargardt disease: ProgStar Report No. 3. *Ophthalmology Retina*, *1*(1), 68–76. https://doi.org/10.1016/j.oret.2016.08.009

Schwabe, L., Ichida, J. M., Shushruth, S., Mangapathy, P., & Angelucci, A. (2010). Contrast-dependence of surround suppression in Macaque V1: Experimental testing of a recurrent network model. *NeuroImage*, *52*(3), 777–792. https://doi.org/https://doi.org/10.1016/j.neuroimage.2010.01.032

Schwabe, L., Obermayer, K., Angelucci, A., & Bressloff, P. C. (2006). The Role of Feedback in Shaping the Extra-Classical Receptive Field of Cortical Neurons: A Recurrent Network Model. *The Journal of Neuroscience*, *26*(36), 9117–9129. http://www.jneurosci.org/content/26/36/9117.abstract

Schwartz, O., Hsu, A., & Dayan, P. (2007). Space and time in visual context. *Nature Reviews Neuroscience*, *8*(7), 522–535. https://doi.org/10.1038/nrn2155

Schwartz, O., Sejnowski, T. J., & Dayan, P. (2009). Perceptual organization in the tilt illusion. *Journal of Vision*, *9*(4:19), 1–20. http://dx.doi.org/10.1167/9.4.19

Sclar, G., Lennie, P., & DePriest, D. D. (1989). Contrast adaptation in striate cortex of macaque. *Vision Research*, *29*(7), 747–755. https://doi.org/10.1016/0042-6989(89)90087-4

Sengpiel, F., Baddeley, R. J., Freeman, T. C. B., Harrad, R., & Blakemore, C. (1998). Different mechanisms underlie three inhibitory phenomena in cat area 17. *Vision Research*, *38*(14), 2067–2080. https://doi.org/https://doi.org/10.1016/S0042-6989(97)00413-6

Sengpiel, F., Sen, A., & Blakemore, C. (1997). Characteristics of surround inhibition in cat area 17. *Experimental Brain Research*, *116*(2), 216–228. https://doi.org/10.1007/PL00005751

Shushruth, S., Ichida, J. M., Levitt, J. B., & Angelucci, A. (2009). Comparison of Spatial Summation Properties of Neurons in Macaque V1 and V2. *Journal of Neurophysiology*, *102*(4), 2069–2083. https://doi.org/10.1152/jn.00512.2009

Shushruth, S., Mangapathy, P., Ichida, J. M., Bressloff, P. C., Schwabe, L., & Angelucci, A. (2012). Strong Recurrent Networks Compute the Orientation Tuning of Surround Modulation in the Primate Primary Visual Cortex. *The Journal of Neuroscience*, *32*(1), 308–321. https://doi.org/10.1523/JNEUROSCI.3789-11.2012

Sillito, A. M., Grieve, K. L., Jones, H. E., Cudeiro, J., & Davls, J. (1995). Visual cortical mechanisms detecting focal orientation discontinuities. *Nature*, *378*, 492. https://doi.org/10.1038/378492a0

Smith, A. T., Singh, K. D., Williams, A. L., & Greenlee, M. W. (2001). Estimating Receptive Field Size from fMRI Data in Human Striate and Extrastriate Visual Cortex. *Cerebral Cortex*, *11*(12), 1182–1190. https://doi.org/10.1093/cercor/11.12.1182

Smith, M. A., Bair, W., & Movshon, J. A. (2006). Dynamics of Suppression in Macaque Primary

Visual Cortex. *The Journal of Neuroscience*, *26*(18), 4826–4834. https://doi.org/10.1523/JNEUROSCI.5542-06.2006

Snowden, R. J., & Hammett, S. T. (1998). The effects of surround contrast on contrast thresholds, perceived contrast and contrast discrimination. *Vision Research*, *38*(13), 1935–1945. https://doi.org/https://doi.org/10.1016/S0042-6989(97)00379-9

Solomon, J. A., Felisberti, F. M., & Morgan, M. J. (2004). Crowding and the tilt illusion: Toward a unified account. *Journal of Vision*, *4*(6:9), 500–508. https://doi.org/10.1167/4.6.9

Solomon, J. A., & Morgan, M. J. (2000). Facilitation from collinear flanks is cancelled by non-collinear flanks. *Vision Research*, *40*(3), 279–286. https://doi.org/10.1016/S0275-5408(99)00059-9

Solomon, J. A., & Morgan, M. J. (2006). Stochastic re-calibration: contextual effects on perceived tilt. *Proceedings of the Royal Society B: Biological Sciences*, *273*(1601), 2681–2686. https://doi.org/10.1098/rspb.2006.3634

Solomon, J. A., Sperling, G., & Chubb, C. (1993). The lateral inhibition of perceived contrast is indifferent to on-center/off-center segregation, but specific to orientation. *Vision Research*, *33*(18), 2671–2683. https://doi.org/https://doi.org/10.1016/0042-6989(93)90227-N

Solomon, J. A., Watson, A. B., & Morgan, M. J. (1999). Transducer model produces facilitation from opposite-sign flanks. *Vision Research*, *39*(5), 987–992. https://doi.org/10.1016/S0042-6989(98)00143-6

Spillmann, L. (2011). Fading, Perceptual Filling-in, and Motion-Induced Blindness: Phenomenology, Psychophysics, and Neurophysiology. *Chinese Journal of Psychology*, *53*(4), 393–397. internal-pdf://228.60.152.24/10139656-201112-201202220012-201202220012-29-3.pdf

Spillmann, L., Dresp-Langley, B., & Tseng, C. (2015). Beyond the classical receptive field: The effect of contextual stimuli. *Journal of Vision*, *15*(9), 7. https://doi.org/10.1167/15.9.7

Spillmann, L., & Kurtenbach, A. (1992). Dynamic noise backgrounds facilitate target fading. *Vision Research*, *32*(10), 1941–1946. https://doi.org/https://doi.org/10.1016/0042-6989(92)90053-L

Spillmann, L., Otte, T., Hamburger, K., & Magnussen, S. (2006). Perceptual filling-in from the edge of the blind spot. *Vision Research*, *46*(25), 4252–4257. https://doi.org/http://dx.doi.org/10.1016/j.visres.2006.08.033

Spillmann, L., & Werner, J. S. (1996). Long-range interactions in visual perception. *Trends in Neurosciences*, *19*(10), 428–434. https://doi.org/https://doi.org/10.1016/0166-2236(96)10038-2

Supèr, H., & Romeo, A. (2011). Rebound Spiking as a Neural Mechanism for Surface Filling-in. *Journal of Cognitive Neuroscience*, *23*(2), 491–501. https://doi.org/10.1162/jocn.2010.21512

Tong, F., & Engel, S. A. (2001). Interocular rivalry revealed in the human cortical blind-spot representation. *Nature*, *411*, 195. https://doi.org/10.1016/S1053-8119(01)92293-1

Troxler, D. (1804). Über das Verschwinden gegebener Gegenstände innerhalb unseres Gesichtskreises. In K. Himly & J. Schmidt (Eds.), *Ophthalmologische bibliothek* (Vol. 2, Issue 2, pp. 1–119). Fromann.

Tyler, C. W., & Hardage, L. (1998). Long-Range Twinkle Induction: An Achromatic Rebound Effect in the Magnocellular Processing System? *Perception*, *27*(2), 203–214. https://doi.org/10.1068/p270203

van de Ven, V., Jans, B., Goebel, R., & De Weerd, P. (2011). Early Human Visual Cortex Encodes Surface Brightness Induced by Dynamic Context. *Journal of Cognitive Neuroscience*, *24*(2), 367–377. https://doi.org/10.1162/jocn_a_00126

von der Heydt, R., Friedman, H. S., & Zhou, H. (2003). Searching for the neural mechanisms of color filling-in. In L. Pessoa & P. De Weerd (Eds.), *Filling-in: From perceptual completion to cortical reorganization* (pp. 106–127). Oxford University Press. https://doi.org/10.1093/acprof:oso/9780195140132.003.0006

Wandell, B. A., Dumoulin, S. O., & Brewer, A. A. (2007). Visual Field Maps in Human Cortex. *Neuron*, *56*(2), 366–383. https://doi.org/https://doi.org/10.1016/j.neuron.2007.10.012

Wandell, B. A., & Smirnakis, S. M. (2009). Plasticity and stability of visual field maps in adult primary visual cortex. *Nature Reviews Neuroscience*, *10*(12), 873–884. https://doi.org/10.1038/nrn2741

Wandell, B. A., & Winawer, J. (2011). Imaging retinotopic maps in the human brain. *Vision Research*, *51*(7), 718–737. https://doi.org/https://doi.org/10.1016/j.visres.2010.08.004

Watson, A. B., & Solomon, J. A. (1997). Model of visual contrast gain control and pattern masking. *Journal of the Optical Society of America A*, *14*(9), 2379–2391. https://doi.org/10.1364/JOSAA.14.002379

Weil, R. S., Kilner, J. M., Haynes, J. D., & Rees, G. (2007). Neural correlates of perceptual filling-in of an artificial scotoma in humans. *Proceedings of the National Academy of Sciences*, *104*(12), 5211–5216. https://doi.org/10.1073/pnas.0609294104

Weil, R. S., & Rees, G. (2011). A new taxonomy for perceptual filling-in. *Brain Research Reviews*, *67*(1–2), 40–55. https://doi.org/http://dx.doi.org/10.1016/j.brainresrev.2010.10.004

Weil, R. S., Watkins, S., & Rees, G. (2008). Neural correlates of perceptual completion of an artificial scotoma in human visual cortex measured using functional MRI. *NeuroImage*, *42*(4), 1519–1528. https://doi.org/10.1016/j.neuroimage.2008.06.007

Westrick, Z. M., Heeger, D. J., & Landy, M. S. (2016). Pattern Adaptation and Normalization Reweighting. *Journal of Neuroscience*, *36*(38), 9805–9816. https://doi.org/10.1523/jneurosci.1067-16.2016

Williams, A. L., Singh, K. D., & Smith, A. T. (2003). Surround Modulation Measured With Functional MRI in the Human Visual Cortex. *Journal of Neurophysiology*, *89*(1), 525–533. https://doi.org/10.1152/jn.00048.2002

Wilson, H. R., & Humanski, R. (1993). Spatial frequency adaptation and contrast gain control. *Vision Research*, *33*(8), 1133–1149. https://doi.org/https://doi.org/10.1016/0042-6989(93)90248-U

Wundt, W. (1898). Die geometrisch-optischen Täuschungen. In *Abhandlungen der Sächsischen Akademie der Wissenschaften zu Leipzig* (pp. 55–178). http://digital.slub-dresden.de/werkansicht/dlf/8096/102/

Xing, J., & Heeger, D. J. (2000). Center-surround interactions in foveal and peripheral vision. *Vision Research*, *40*(22), 3065–3072. https://doi.org/https://doi.org/10.1016/S0042-6989(00)00152-8

Xing, J., & Heeger, D. J. (2001). Measurement and modeling of center-surround suppression and enhancement. *Vision Research*, *41*(5), 571–583. https://doi.org/https://doi.org/10.1016/S0042-6989(00)00270-4

Yu, C., Klein, S. A., & Levi, D. M. (2001). Surround modulation of perceived contrast and the role of brightness induction. *Journal of Vision*, *1*(1:3), 18–31. https://doi.org/10.1167/1.1.3

Yu, C., Klein, S. A., & Levi, D. M. (2002). Facilitation of contrast detection by cross-oriented surround stimuli and its psychophysical mechanisms. *Journal of Vision*, *2*(3:4), 243–256. https://doi.org/10.1167/2.3.4

Zeki, S. M. (1978). Uniformity and diversity of structure and function in rhesus monkey prestriate visual cortex. *The Journal of Physiology*, *277*(1), 273–290. https://doi.org/https://doi.org/10.1113/jphysiol.1978.sp012272

Zenger, B., & Sagi, D. O. V. (1996). Isolating Excitatory and Inhibitory Nonlinear Spatial Interactions Involved in Contrast Detection. *Vision Research*, *36*(16), 2497–2513. https://doi.org/10.1016/0042-6989(95)00303-7

Zur, D., & Ullman, S. (2003). Filling-in of retinal scotomas. *Vision Research*, *43*(9), 971–982. https://doi.org/10.1016/S0042-6989(03)00038-5

APPENDIX

## A. Study 1 Supplementary materials

Figure A.1

The Individual Data of the Estimated CCW Orientation Shifts in Experiment 1
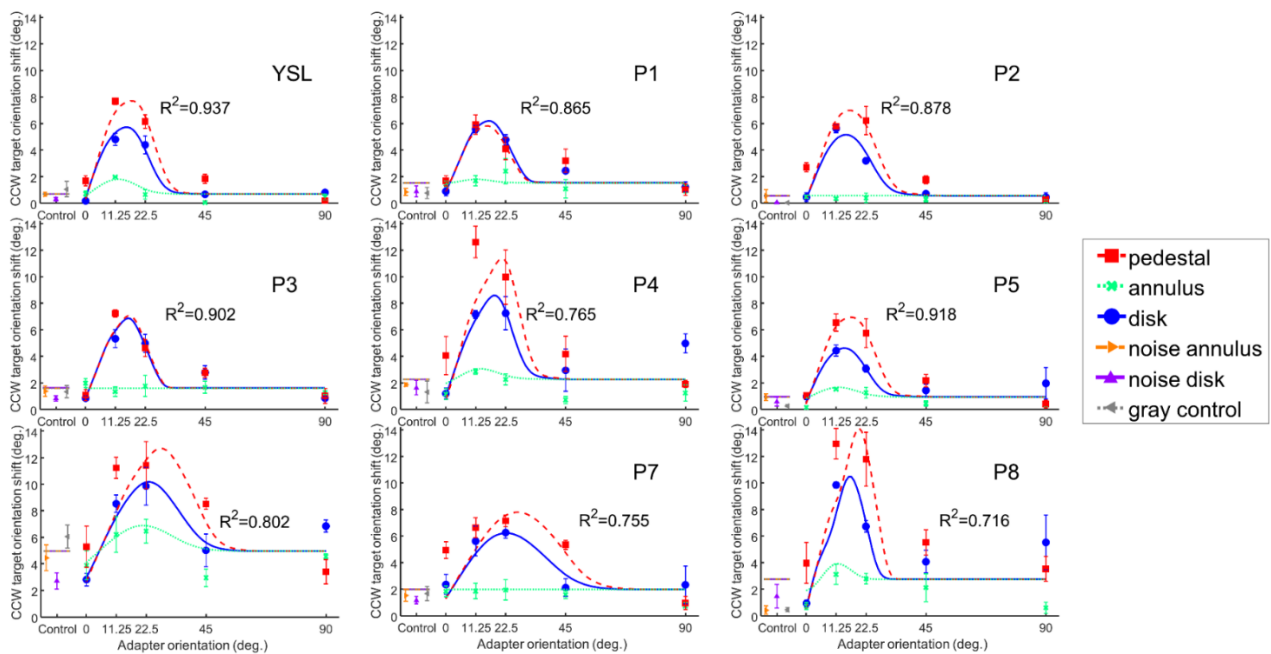
Note. The symbols represent the behavioral data (red square: pedestal adapter; green cross: annulus adapter; blue circle: disk adapter, orange right-pointing triangle: noise annulus adapter; purple up-pointing triangle: noise disk adapter; gray left-pointing triangle: gray control/no adapter condition), while smooth curves and the horizontal lines the best fits of our computational model. The error bars are ±1 standard error of mean. See caption in Figure 2.2 in the main manuscript for further details.

Figure A.2

The Individual Data of the Estimated CCW Orientation Shifts in Experiment 2.
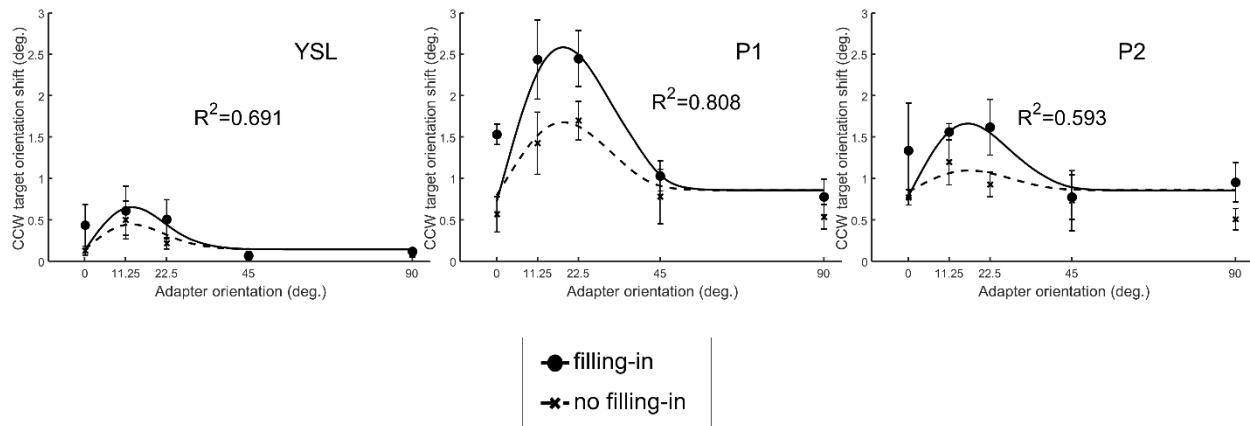
Note. The symbols represent the empirical data (disk: with filling-in; cross: without filling-in), while smooth curves (solid curve: with filling-in; dotted curve: without filling-in) the best fits of our computational model. The error bars are ±1 standard error of mean. See caption in Figure 2.3 in the main manuscript for further details.

Comparison between the PSI method and Psychometric function (PF) fitting results
Psychometric function (PF) fitting Procedure

We fitted a cumulative normal psychometric function (PF) to the raw data (the CCW trials) of each participant and examined the relationship between the estimates of this PF fitting results and the ones from the PSI method (the data in Figure 2.2a). To increase the number of trials per orientation level, we pooled trials from all runs of the same adapter condition together, and binned the data into 0.5° orientation steps from 0° to 15°. We calculated the proportion of responding CCW at each orientation step. We fitted a cumulative normal PF to the CCW proportion using the Matlab-based Palamedes toolbox (http://www.palamedestoolbox.org/) PF fitting function using a maximum likelihood criterion (PAL_PFML_Fit.m). Four parameters were

returned for each PF fit, namely, alpha (threshold), beta (slope parameter), gamma (guessing rate or lapses), and lambda (finger-error rate). Gamma and lambda were fixed at values of 0.5 and 0 respectively, while alpha and beta were set as free parameters. Thus, the alpha value represents the threshold level at 75% CCW response. We used the Palamedes toolbox bootstrapping goodness-of-fit function (PAL_PFML_GoodnessOfFit.m) to determine goodness-of-fit of each fitted PF. We used 1000 simulations for each fitting result. We ruled out the fitting results that failed to return valid alpha and beta value (e.g. due to noisy data), returning alpha value lower than -3° (negative value means CW-oriented), or having poor goodness-of-fit (with less than 5% of the simulations having larger deviance/transformed likelihood ratio than that from the data).

Comparing parameters between the PSI estimates and PF fitting results

We calculate the Pearson correlation coefficient of the PSI estimated parameters and the PF fitting parameters of each participant. Figure A.3 below demonstrates the relationship between the threshold estimates from the PSI method and the PF fitting to the raw data. The alpha/threshold value returned by the PF fitting represents the orientation corresponding to a 75% CCW reporting rate while the PSI estimate was estimated at 86% CCW response. To make a fairer comparison, we take the orientation level producing an 86% rate on the fitted cumulative normal function as the PF fitting estimate. If the estimates of the two methods agree well, there should be a significant positive correlation between the parameters, and the data points should lie close to the diagonal line.

Figure A.3

The Correlation Between the Threshold Estimates from the PSI Method and the Cumulative Normal PF Fitting Results
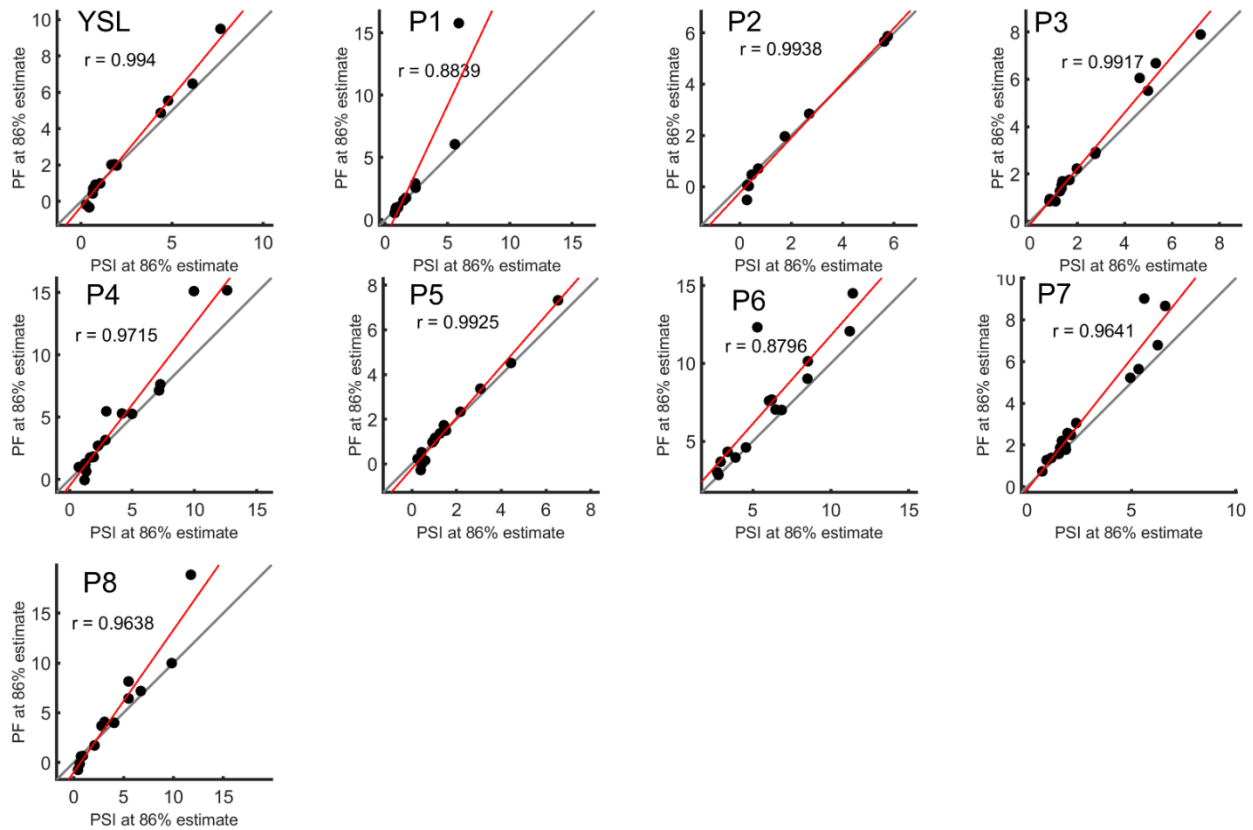
Note. The PSI estimate is plotted on the x-axis, while PF fitting on the y-axis. The solid red line represents the least-squares fitted regression line.

As can be seen in Figure A.3, the threshold estimates from the two methods correspond reasonably well with each other, whereby the PF fitting estimate is higher than PSI estimate for data points of higher threshold value of some observers (i.e., the data points lie on the left side of the diagonal line). The correlation coefficient values and the *p*-values are shown in Table A.1.

Table A.1

Correlation Between Threshold Estimates From PSI and PF Method.

|	LYS	P1	P2	P3	P4	P5	P6	P7	P8
PSI / PF threshold	.99	.88	.99	.99	.97	.99	.88	.96	.96
p-value	<0.001*	<0.001*	<0.001*	<0.001*	<0.001*	<0.001*	<0.001*	<0.001*	<0.001*
N	15	11	9	16	17	15	15	16	13

Note. Each column represents values of one participant. The first row shows the correlation coefficient, while the second row the *p*-value between the threshold estimates of the two methods. The last row shows the number of data points. The * symbol indicates significant *p*-values (p < 0.025).

Relationship between the PF fitting threshold and slope

To examine the possible confound between the bias and unreliability (slope) in the data of each observer, we calculated the Pearson correlation coefficient between the 86% CCW responding rate and the slope value estimated from the PF fitting process. Figure A.4 below shows such correlation, while Table A.2 contains the correlation coefficient, the p-values as well as the number of data points for each participant (*N* differs due to the ruling out process mentioned in the PF fitting method). The data of two out of nine observers show a significant negative correlation between the slope and threshold values (*rs*(14) = -.51 and *rs*(14) = -.50, p = .021 and 0.024), while the data of the rest of the participants show no systematic relationship between the two estimates.

Figure A.4

The Correlation Between the Threshold and Slope Estimates PF Fitting Results
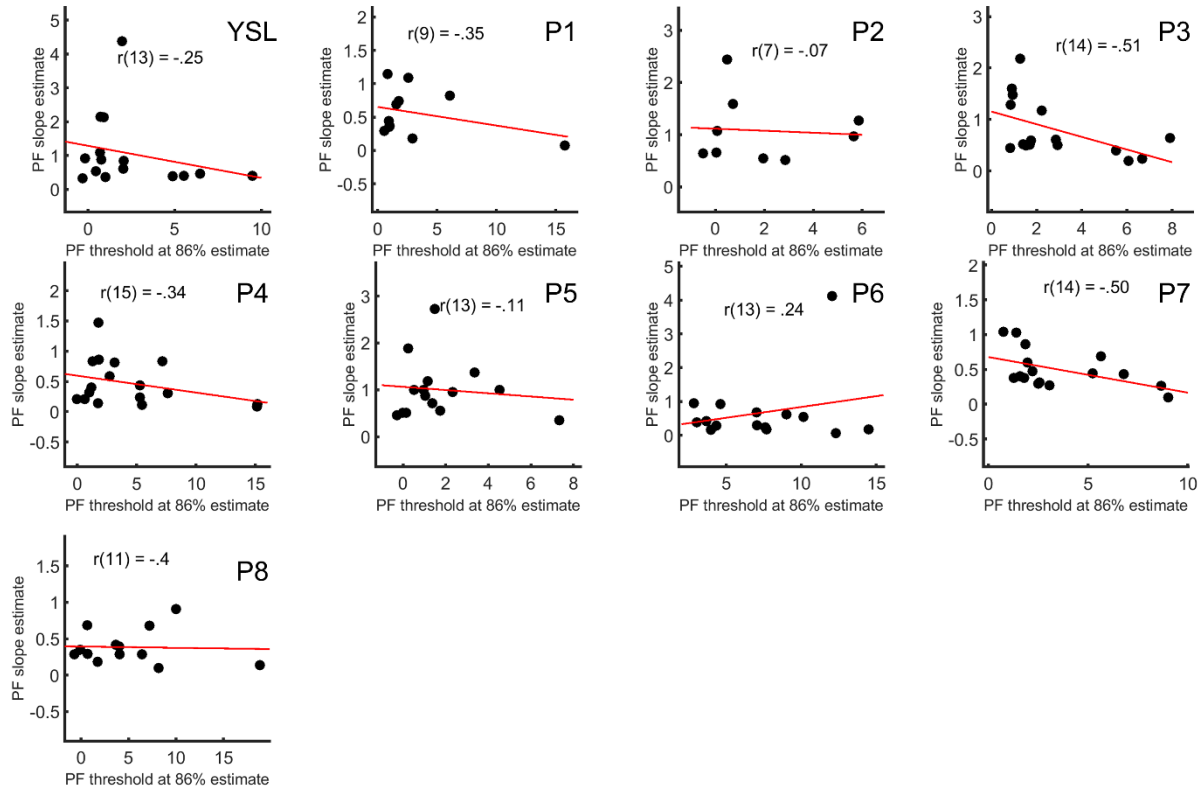
Note. The threshold estimate is plotted on the x-axis, while slope on the y-axis. The solid red line represents the least-squares fitted regression line.

Table A.2

Correlation Between the Threshold and Slope Estimates of the PF Fitting Results.

	LYS	P1	P2	P3	P4	P5	P6	P7	P8
Threshold/Slope	-.25	-.35	-.07	-.51	-.34	-.11	.24	-.50	-.04
p-value	0.186	0.146	0.424	0.021*	0.089	0.345	0.197	0.024*	0.449
N	15	11	9	16	17	15	15	16	13

Note. Each column represents values of one participant. The first row shows the correlation coefficient, while the second row the *p*-value between the threshold estimates of the two methods. The last row shows the number of data points. The * symbol indicates significant *p*-values ($p < 0.025$).

Reanalysis of combined CW and CCW trial data using PF fitting process

Another way of examining the data in the current study is by combining the CW and CCW trials together and by fitting PF functions to the combined data set. To do so, we took the raw trial data (provided in Supplementary File S3) of each participant of the three oriented-adapter conditions (pedestal, annulus and disk adapter with five adapter orientation levels) in Experiment 1. We pooled all trials of the same adapter condition across different runs together. The CW trials were assigned with negative orientation values and we calculated the proportion of CCW response for each target (both CW and CCW) orientation. Then we again used the Palamedes toolbox function (PAL_PFML_Fit.m) to fit a cumulative normal Gaussian PF to each adapter condition. Alpha (threshold) and beta (slope) were free parameters while gamma (guessing rate) and lambda (finger error rate) were set as fixed parameter with the value 0.01. Thus, the threshold represents about 50% CCW response rate, i.e. the subjective verticality of the test stimulus in each condition.

Figure A.5 below shows the averaged PF fitting parameters of all observers. The data are color-coded in the same manner as the Figure 2.2 in the main manuscript. The left panel shows the bias (alpha), while the right panel the JND (the inverse of slope/beta value). The bias estimate is very similar to the result of orientation shift in Figure 2.2a of the main manuscript, except that the bias values are lower. This was well expected since in the original PSI method, we estimated the 86% CCW rate. The JNDs of the pedestal condition (especially the 0 to 22.5°) are higher than the other two adapter type conditions. We suspected that the higher variability of data (larger standard error) in the pedestal condition of most participants leads to such results. Such variability is captured by JND, which represents the unreliability in the data.

Figure A.5

The Averaged PF Fitting Results of Combined CW and CCW Trials of Nine Participants in the Main Experiment.
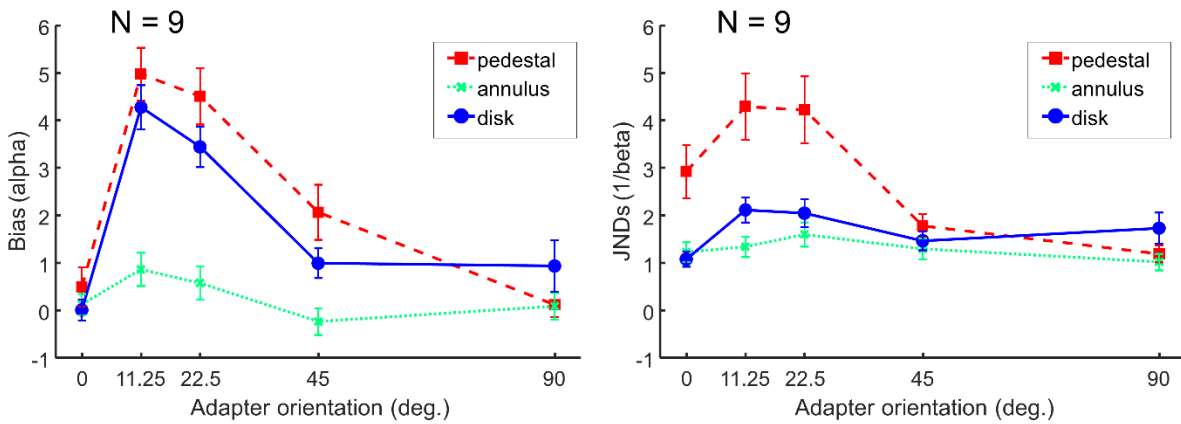
Note. In the left panel, the bias (alpha) is plotted against the adapter orientation. In the right panel, the JND is plotted against the adapter orientation. The error bars correspond to ±1 standard error of the mean.

B. Study 2 Supplementary materials

This file contains the TAE data (50% CCW response points) and fitting results of all participants. Figure B.1 shows the TAE data of each observer in two views, as is the case in the Figure 3.2 of the main manuscript. Readers can find the model fitting results of each observer in Figure B.2 and B.3. Figure B.4 represents the data of three conditions: the center, the disk and the same C&S adapter from the current study and the previous study (Lin, Chen, & Greenlee, 2020).

Orientation-specific lateral modulation

Figure B.1

The Data of the Individual Observer.
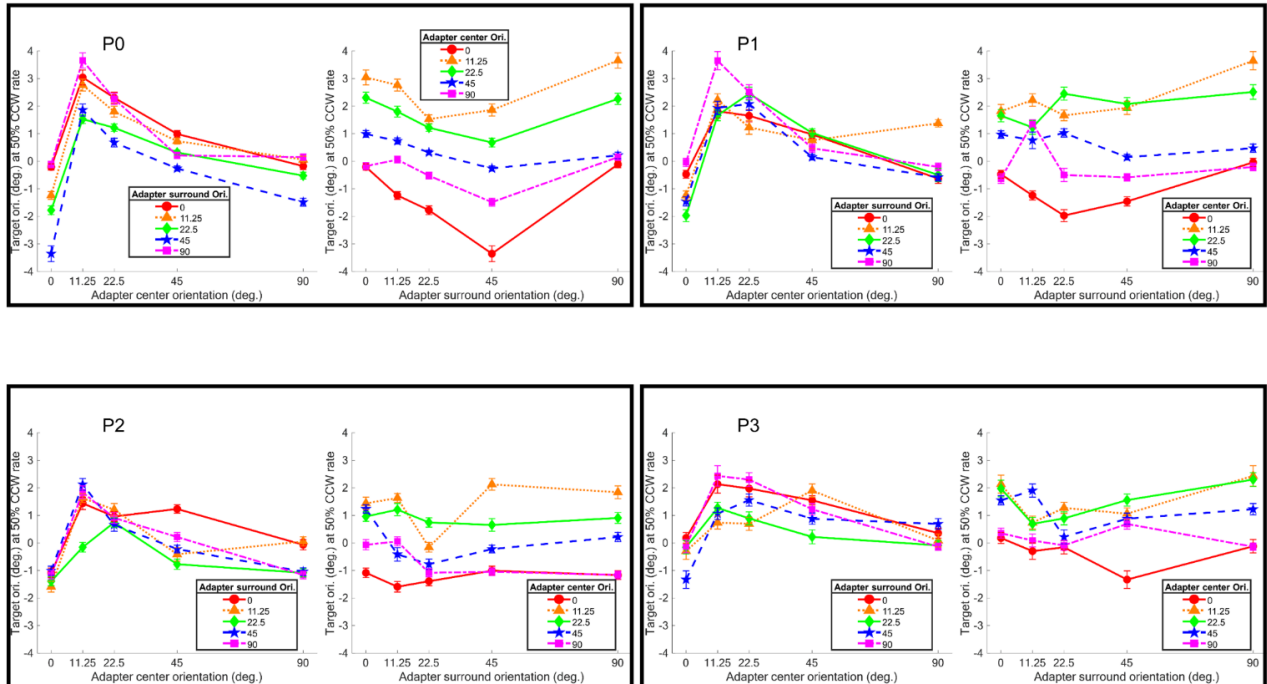
*Note.* Each subplot (labeled with participant's initial) presents the data set of one participant. In each subplot, the left panel shows the TAE plotted against the adapter center, whereas the right panel the TAE against the adapter surround. The error bars are ±1 standard error of measurement. See the **Results** section of the main manuscript and Figure 3.2 for further details.

Model fitting results of individual participants

Figure B.2

Model Predictions of Individual Observer Data
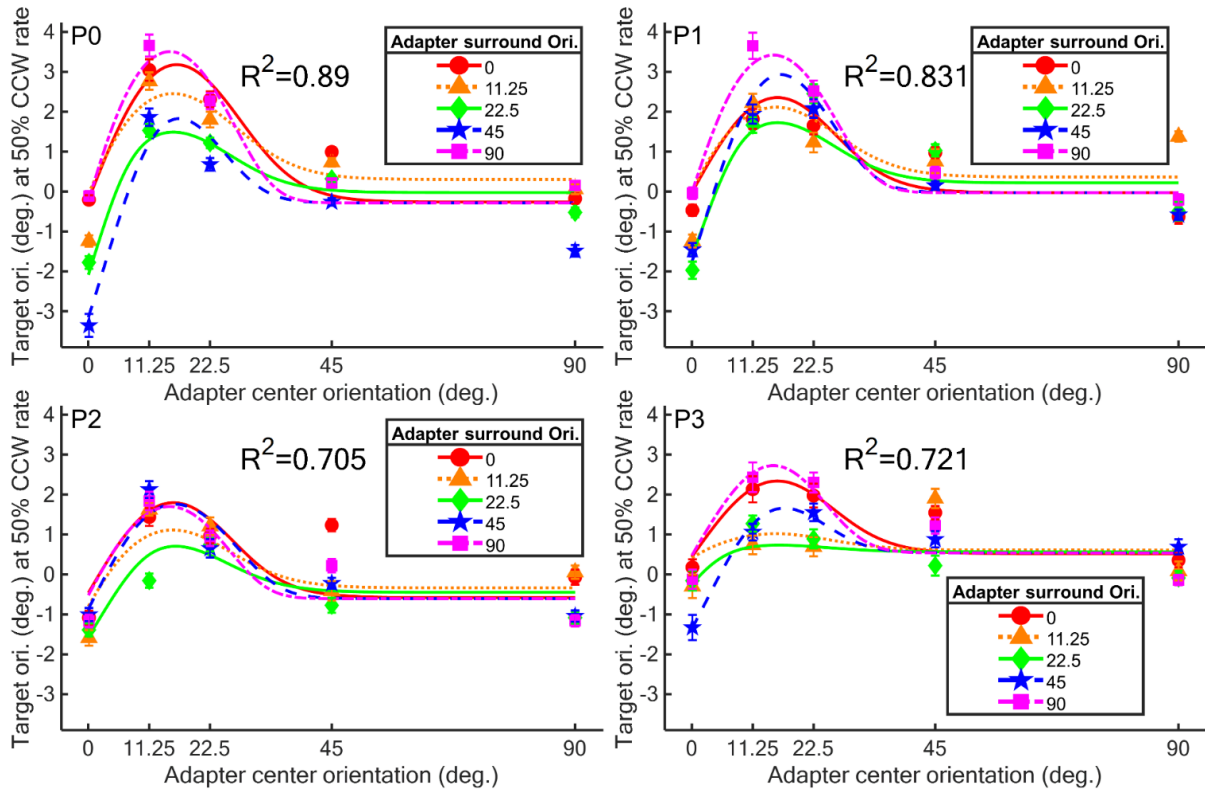
Note. This figure demonstrates the fitting results of each participant. Each panel shows the model predictions (in colored-smoothed curves) and the TAE data (the colored markers). Different colors represent different adapter surround orientation.

Figure B.3

Fitting parameters Ke and Ki
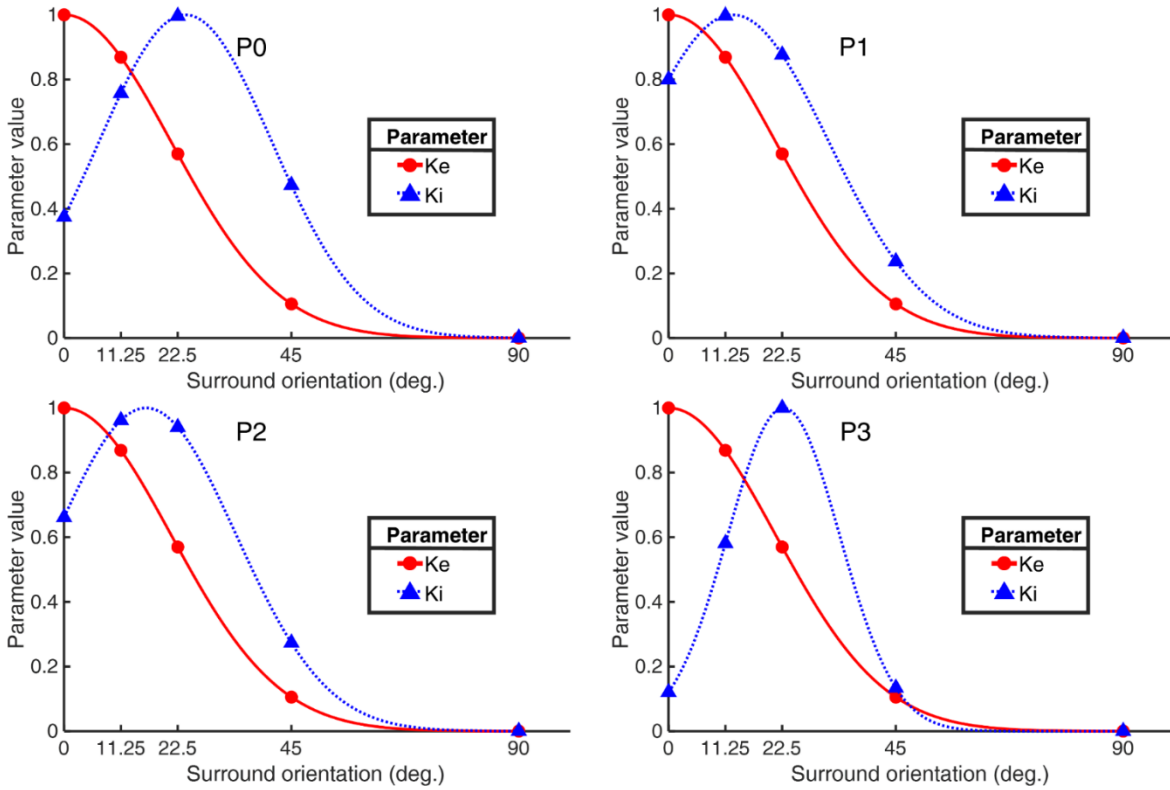
Note. This figure shows fitting parameters *Ke* and *Ki* of each observer. *Ke* (red circles and solid curve) and *Ki* (blue triangles and dashed curve) are plotted against surround orientation. Colored symbols represent the surround orientations used in the experiment.

Replication of the lateral inhibition

Figure B.4

Comparison Between Data in the Study 2 and the Study 1 of Individual Observers.
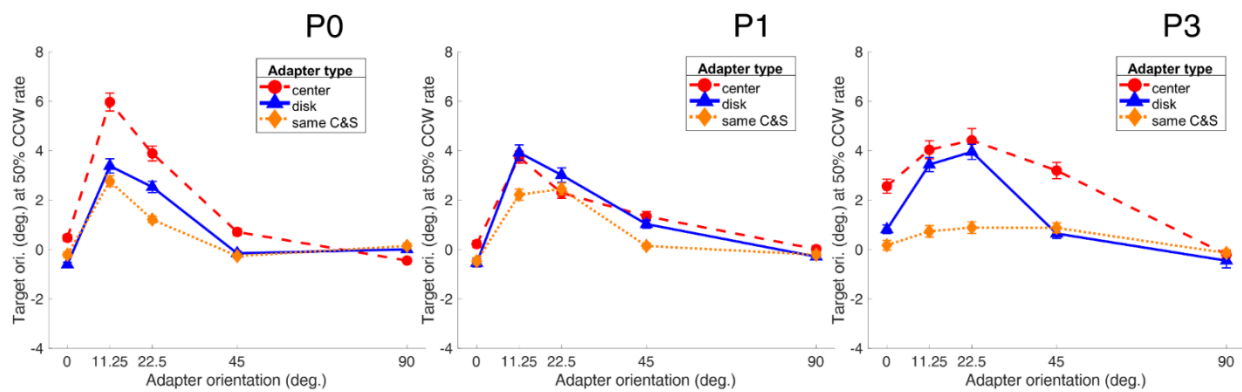
Note. Different colored curves and markers represent different adapter conditions. The error bars are ±1 standard error of measurement. See Figure 3.5 in the main manuscript and **Results** section of Chapter 3 for a more detailed description.

Table B.1

List of best fitting parameters and goodness of fit (R^2) of the current model on the averaged and individual TAE data.

Observer		MEAN	P0	P1	P2	P3
PARAMETER						
Se/Se_c		100.00	100.00	100.00	100.00	100.00
Se_s		100.00	100.00	100.00	100.00	100.00
Si/Si_c		0.20	0.20	0.20	0.20	0.20
Si_s		**17.31**	**49.55**	**17.77**	**8.62**	**44.73**
z		**0.02**	**0.05**	**0.02**	**0.07**	**0.03**
p		**2.88**	**3.02**	**3.09**	**3.21**	**2.79**
q		**1.19**	**1.18**	**1.28**	**1.63**	**1.32**
σ		18.01	18.01	18.01	18.01	18.01
Ke	$\theta_{excitatory}$	0.00	0.00	0.00	0.00	0.00
	$\sigma_{excitatory}$	30.00	30.00	30.00	30.00	30.00
Ki	$\theta_{inhibitory}$	**18.45**	**24.02**	**12.72**	**16.23**	**22.79**
	$\sigma_{inhibitory}$	**24.46**	**24.24**	**26.91**	**25.25**	**15.63**
m		**0.28**	**0.73**	**0.07**	**1.33**	**-1.09**
R^2		0.867	0.890	0.831	0.705	0.721
$RMSE$		0.43	0.53	0.57	0.60	0.49
MSE		0.38	0.16	0.20	0.18	0.23
number of free parameters		**7**(13)	**7**(13)	**7**(13)	**7**(13)	**7**(13)

Note. Free parameters and parameter values are marked in bold. Parameter σ was set as 18.01 to maintain the channel tuning FWHM as 30 degrees. The column **MEAN** represents the fitting parameters of the averaged data across the four participants.

C. Study 3 Supplementary materials

We summarize the BCEA data of each stimulus condition, including the sizes and positions, in Table C.1, of the six participants who we recorded eye tracking data from. In Figure 4.6 of the main manuscript, we show the fixation density maps as well as the BCEA ellipses of the four conditions.

The fixation density maps shown in Figure 4.6 in the main manuscript were created by dividing the whole stimulus screen into numerous cells. For the out-scanner control experiment where the resolution was 1280×1024, each cell was 16×16 square pixel large, resulting in 80 cells on the x-axis and 64 cells on the y-axis. For the in-scanner eye tracking recording where the resolution was 800×600, each cell was 10×10 square pixel, leading to 80 cells on the x-axis and 60 on the y-axis. We then counted the frequency of eye position located in each cell and divided each cell frequency by the highest frequency of all cells to calculate the eye position density. We overlayed such fixation density map on top of the stimulus.

As for the BCEA ellipses, we performed principle component analysis to recover the BCEA ellipses of all conditions (Niehorster et al., 2020). When k in the equation (3) in the main manuscript is equal to 1, the ellipse covers 63.2% of the fixation points, and the eigenvalues in the major and minor eigenvectors represent the squared lengths of the two axes. We plotted the ellipses of different conditions on the right plot in each panel in the following figures.

In our data, although there was some individual difference in terms of the density maps and BCEA ellipses, within each participant the fixation distribution and positions did not differ across conditions.

Table C.1

A Summary of the BCEA Analysis of Fixation Stability Across the Participants (n = 6).

	Conditions	Center	Full-Field	Filling-in	No Filling-in
Observer	BCEA parameter				
P1[a]	Size (in squared degree)	0.98	1.02	1.03	0.91
	Center x, y position (in degree, relative to the fixation point at 0,0)	0.46, 0.72	0.46, 0.44	0.43, 0.61	0.45, 0.64
P2[a]	Size (in squared degree)	0.49	0.35	0.41	0.58
	Center x, y position (in degree, relative to the fixation point at 0,0)	0.06, 0.06	0.10, 0.02	-0.10, 0.13	-0.10, 0.08
P3[b]	Size (in squared degree)	23.99	21.51	15.66	16.55
	Center x, y position (in degree, relative to the fixation point at 0,0)	-6.58, 0.26	-6.26, -0.12	-6.57, 0.45	-6.76, 0.37
P4[b]	Size (in squared degree)	27.06	18.23	15.66	16.55

	Center x, y position (in degree, relative to the fixation point at 0,0)	0.04, 2.38	0.24, 2.28	0.03, 2.57	-0.10, 2.44
P5[b]	Size (in squared degree)	39.69	39.49	36.40	38.14
	Center x position (in degree, relative to the fixation point at 0,0)	-3.49, 3.98	-3.49, 4.01	-3.47, 4.60	-3.69, 4.74
P6[b]	Size (in squared degree)	7.42	7.93	3.89	6.87
	Center x, y position (in degree, relative to the fixation point at 0,0)	-0.56, 4.20	-0.54, 4.25	-0.51, 4.27	-0.66, 4.28

Note. Each stimulus condition has one BCEA estimate that includes a size estimate and a center position of the BCEA ellipse. a. Data recorded with the Eyelink 1000 eye tracker in the out-of-scanner control experiment; b. Data recorded with the MRI-safe ViewPoint eye tracker during the fMRI experiment.